

# **Deleted in Liver Cancer 3 (DLC3) in the regulation of junctional Rho signaling and cell polarity**

Von der Fakultät Energie-, Verfahrens- und Biotechnik der Universität Stuttgart zur Erlangung der Würde eines Doktors der Naturwissenschaften (Dr. rer. nat.) genehmigte Abhandlung

Vorgelegt von

**Janina Hendrick**

aus Villingen-Schwenningen

Hauptberichter: Prof. Dr. Monilola Olayioye

Mitberichter: Prof. Dr. Thomas Kufer

Tag der mündlichen Prüfung: 20.12.2016

Institut für Zellbiologie und Immunologie  
Universität Stuttgart

2016



## Table of content

List of figures .....	6
List of tables .....	8
Abbreviations.....	9
Summary.....	12
Zusammenfassung .....	13
1. Introduction.....	15
1.1 The family of Rho GTPases .....	15
1.1.1 Cellular functions of Rho GTPases.....	15
1.1.2 Rho GTPases in tumor development and progression .....	16
1.1.3 Rho regulation by GEFs and GAPs .....	18
1.2 Epithelial cell polarity.....	19
1.2.1 Establishment of apical-basolateral cell polarity .....	19
1.2.2 The basolateral polarity protein Scribble.....	22
1.2.3 Cooperation of polarity proteins and Rho GTPases.....	24
1.2.4 Front-rear polarization of migratory cells .....	25
1.3 The DLC family of RhoGAP proteins .....	27
1.3.1 DLC proteins as candidate tumor suppressors .....	27
1.3.2 Multi-domain structure of DLC proteins .....	29
1.3.3 DLC proteins function at distinct subcellular sites .....	32
1.3.4 Cellular functions of the DLC3 isoform .....	35
1.4 Aims of the thesis.....	36
2. Material and methods .....	37
2.1 Material .....	37
2.1.1 Chemicals and reagents.....	37
2.1.2 Equipment.....	39
2.1.3 Consumables .....	39
2.1.4 Buffers and solutions.....	40
2.1.5 Human cell lines.....	41

## Table of content

---

2.1.6 Cell culture reagents and media.....	41
2.1.7 Plasmids .....	42
2.1.8 Antibodies and fluorescent dyes .....	43
2.1.9 Kits .....	45
2.1.10 Enzymes.....	45
2.1.11 Small interfering RNA (siRNA) .....	45
2.2 Methods.....	46
2.2.1 Cloning strategies .....	46
2.2.2 Cell culture and transfection.....	48
2.2.3 NanoLC-MS/MS analysis and MS data processing.....	50
2.2.4 Cell lysis, cellular fractionation and immunoprecipitation.....	51
2.2.5 SDS-PAGE and immunoblotting .....	52
2.2.6 Bacterial expression of GST proteins.....	52
2.2.7 Far-Western blotting and pull-downs.....	52
2.2.8 Immunofluorescence microscopy.....	53
2.2.9 RNA isolation and quantitative PCR.....	53
2.2.10 <i>In situ</i> proximity ligation assay (PLA).....	54
2.2.11 Cell disaggregation assay .....	54
2.2.12 Scratch assay .....	54
2.2.13 Statistical analysis.....	55
3. Results .....	56
3.1 Identification of DLC3 protein interaction partners.....	56
3.2 DLC3 interacts with the basolateral polarity protein Scribble.....	59
3.3 DLC3 localization is specified by its PDZL motif and Scribble .....	63
3.4 DLC3 regulates RhoA-ROCK signaling to maintain cell-cell contacts and Scribble localization.....	66
3.5 A targeted GAP domain rescues adherens junction destabilization upon DLC3 knockdown .....	70
3.6 DLC3 localization at the leading edge depends on Scribble and is required for local Rho-ROCK regulation .....	72

## Table of content

---

3.7 The PDZL motif determines DLC3 localization at cell junctions and basolateral membranes in polarized Caco-2 cells .....	74
3.8 DLC3 and Scribble are required for polarization and lumen formation of Caco-2 cysts in 3D culture .....	79
4. Discussion .....	82
4.1 The DLC3-Scribble complex regulates Rho signaling at adherens junctions .....	82
4.2 DLC3 and Scribble in the establishment of epithelial polarity .....	84
4.3 A novel function of DLC3 at the leading edge .....	86
4.4 PDZ ligand binding – a mechanism for DLC3 recruitment in different contexts? .....	89
4.5 Molecular mechanisms to spatiotemporally control DLC3 and its protein interactions .....	91
4.6 Conclusions and outlook .....	94
Supplements .....	95
References .....	106
Publications .....	118
Acknowledgements .....	120
Eidesstattliche Erklärung .....	121

## List of figures

Figure 1: The role of Rho GTPases during tumor initiation and progression. ....	17
Figure 2: Regulation of Rho GTPases by GEFs and GAPs. ....	18
Figure 3: Polarized organization of epithelial cells. ....	21
Figure 4: Establishment of front-rear polarity in migratory cells. ....	27
Figure 5: Multi-domain organization of DLC proteins. ....	30
Figure 6: Subcellular localization of DLC1, DLC2 and DLC3. ....	34
Figure 7: Workflow of affinity purification and mass spectrometry analysis to identify DLC3 protein binding partners. ....	56
Figure 8: DLC3 interacts with the polarity protein Scribble. ....	59
Figure 9: Scribble is an isoform-specific binding partner of DLC3. ....	60
Figure 10: DLC3 directly interacts with Scribble via a C-terminal PDZ ligand motif. ....	61
Figure 11: DLC3 interacts with Scribble <i>in situ</i> at cell-cell adhesions. ....	62
Figure 12: DLC3 accumulation at cell-cell contacts depends on Scribble. ....	63
Figure 13: The PDZL motif controls DLC3 localization at cell junctions. ....	65
Figure 14: DLC3 depletion enhances RhoA activity at cell-cell adhesions. ....	66
Figure 15: Increased junctional pMLC levels in DLC3-knockdown cells. ....	67
Figure 16: ROCK inhibition rescues the cell adhesion defect caused by DLC3 depletion. ....	68
Figure 17: Scribble localization and cell junction integrity depend on DLC3 as a regulator of Rho-ROCK activity. ....	69
Figure 18: Targeting of the DLC3 GAP domain to cell-cell contacts by Scribble-LRR domains rescues adherens junction destabilization upon DLC3 knockdown. ....	71
Figure 19: DLC3 localization at the leading edge of migrating cells depends on Scribble. ....	72
Figure 20: DLC3 and Scribble knockdown cause RhoA accumulation and activation at the wound edge. ....	73
Figure 21: Increased pMLC levels at the cellular front of DLC3- and Scribble-depleted cells. ....	74
Figure 22: DLC3 and Scribble interact in Caco-2 cells. ....	75
Figure 23: The PDZ ligand motif determines junctional accumulation and membrane association of DLC3 in Caco-2 cells. ....	76
Figure 24: Basolateral DLC3 localization in polarized Caco-2 cysts is controlled by its PDZL motif. ....	77
Figure 25: Expression of GAP-active DLC3 disrupts the polarized morphology of established Caco-2 cysts. ....	78

## List of figures

---

Figure 26: DLC3 and Scribble depletion impair apical-basolateral polarization at the two-cell stage during Caco-2 cyst development.....	79
Figure 27: DLC3 and Scribble knockdown cause aberrant morphogenesis of Caco-2 cysts. ....	81

## List of tables

Table 1: List of chemicals and reagents used in this thesis. ....	37
Table 2: List of equipment used in this thesis. ....	39
Table 3: List of consumables used in this thesis. ....	39
Table 4: List of buffers and solutions used in this thesis. ....	40
Table 5: List of cell lines used in this thesis. ....	41
Table 6: List of cell culture reagents and media used in this thesis. ....	41
Table 7: List of plasmid vectors used in this thesis. ....	42
Table 8: List of primary antibodies used for immunoblotting and immunofluorescence. ...	43
Table 9: List of secondary antibodies used for immunoblotting and immunofluorescence. .....	44
Table 10: Fluorescent dyes used for immunofluorescence. ....	44
Table 11: Kits used in this thesis. ....	45
Table 12: Enzymes used for cloning. ....	45
Table 13: DLC3 binding partners involved in endocytic trafficking, cell signaling and with an adaptor or scaffold function. ....	57
Table 14: Cell junction-associated DLC3 binding partners according to GOCC database annotation. ....	58
Table S1: DLC3 protein interaction partners identified by mass spectrometry analysis. ..	95

## Abbreviations

AJ	adherens junction
AKT	protein kinase B
APS	ammonium persulfate
BSA	bovine serum albumin
Cdc42	cell division cycle 42
CTEN	C-terminal tensin-like
cv-c	crossveinless-c
DAPI	4',6-diamidin-2-phenylindol
Dia	orthologs of <i>Drosophila melanogaster</i> diaphanous protein
DLC (1-3)	deleted in liver cancer
Dlg	discs large
DMSO	dimethyl sulfoxide
DNA	deoxyribonucleic acid
DTT	dithiothreitol
ECL	enhanced chemiluminescence
ECM	extracellular matrix
EDTA	ethylene diamine tetraacetic acid
EF1A1	eukaryotic elongation factor 1A1
EGF	epidermal growth factor
EGFR	epidermal growth factor receptor
EMT	epithelial-to-mesenchymal transition
ERC	endocytic recycling compartment
ERK	extracellular signal-regulated kinase
FA	focal adhesion
FACS	fluorescence-activated cell sorting
FAK	focal adhesion kinase
FCS	fetal calf serum
FL	full-length
FRET	fluorescence resonance energy transfer
GAP	GTPase-activating protein
GDI	guanine nucleotide dissociation inhibitor
GDP	guanosine diphosphate
GEF	guanine nucleotide exchange factor
GFP	green fluorescent protein
GST	glutathione S-transferase

## Abbreviations

---

GTP	guanosine triphosphate
HGF	hepatocyte growth factor
HCC	hepatocellular carcinoma
HRP	horseradish peroxidase
iBAQ	intensity based absolute quantification
IF	immunofluorescence
IP	immunoprecipitation
IPTG	isopropyl $\beta$ -D-1-thiogalactopyranoside
IQGAP	IQ motif-containing GTPase-activating protein 1
JAM	junction adhesion molecule
LB	Luria-Bertani
LC-MS/MS	liquid chromatography-tandem mass spectrometry
Lgl	lethal giant larvae
LOH	loss of heterozygosity
LRR	leucine-rich repeat
mAb	monoclonal antibody
MLC	myosin light chain
NaDoc	sodium deoxycholate
NLS	nuclear localization signal
ns	not significant
NSCLC	non-small cell lung cancer
pAb	polyclonal antibody
PAGE	polyacrylamide gel electrophoresis
Pals	protein-associated with Lin seven
Par	partitioning defective
PATJ	Pals1-associated tight junction protein
PBR	polybasic region
PBS	phosphate buffered saline
PCR	polymerase chain reaction
PDZ	PSD-95, discs large and ZO-1 domain
PDZL	PDZ ligand motif
PFA	paraformaldehyde
PI	phosphatidylinositol
PI3K	phosphatidylinositol 3-kinase
PIP <sub>2</sub>	phosphatidylinositol-4,5-bisphosphate
PIP <sub>3</sub>	phosphatidylinositol-3,4,5-trisphosphate
Pix	p21-activated kinase interacting exchange factor

## Abbreviations

---

aPKC	atypical protein kinase C
PLA	proximity ligation assay
PLC $\delta$ 1	phospholipase C $\delta$ 1
PMSF	phenylmethylsulfonyl fluoride
PTEN	phosphatase and tensin homolog
PVDF	polyvinylidene difluoride
Rac	Ras-related C3 botulinum toxin substrate
Ras	rat sarcoma
RhoA/B/C	Ras homology protein A/B/C
RhoGAP	GTPase-activating protein for Rho proteins
Rho proteins	Rho GTPase proteins (e.g. RhoA, Rac1 and Cdc42)
RIPA	radioimmunoprecipitation assay buffer
RNA	ribonucleic acid
RNAi	RNA interference
ROCK	Rho-associated, coiled-coil containing kinase
RPMI	medium named after the Roswell Park Memorial Institute
RT	room temperature
SAM	sterile $\alpha$ motif
SDS	sodium dodecyl sulfate
s.e.m.	standard error of the mean
SH	Src homology
siRNA	small interfering RNA
SNX27	sorting nexin 27
StAR	steroidogenic acute regulatory
STARD	StAR-related lipid transfer domain
START	StAR-related lipid transfer
TAE	tris-acetate-EDTA
TEMED	N,N,N',N'-tetramethyl ethyldiamine
TfnR	transferrin receptor
Tiam	T-cell lymphoma invasion and metastasis-inducing protein
TJ	tight junctions
Tris	tris-hydroxymethyl aminomethane
v/v	volume/volume
WB	Western Blot
w/v	weight/volume
WT	wild type
ZO	zonula occludens

## Summary

Apicobasal cell polarity is essential for normal epithelial function and tissue integrity and established by several polarity proteins. Cell polarization, including the formation and maintenance of cell-cell contacts, also requires spatially restricted cytoskeleton remodeling. Small Rho GTPases function as key regulators of cytoskeleton dynamics and are thus involved in fundamental cellular processes like cell polarity and cell-cell adhesion. However, the spatial control of cellular Rho signaling by its regulators, specific guanine nucleotide exchange factors (GEF) and GTPase-activating proteins (GAP), is still poorly understood. The deleted in liver cancer (DLC) proteins represent a family of RhoGAPs that is frequently downregulated in different types of cancer and comprises three structurally related family members, DLC1/2/3. There is growing evidence that the different DLC proteins also possess non-redundant functions and are regulated by isoform-specific mechanisms based on their distinct subcellular localizations. The still poorly characterized DLC3 isoform was reported to localize to adherens junctions and Rab8-positive membrane tubules, besides its association with focal adhesions which is common to all DLC isoforms. Considering that the DLC3 interactome is still largely unknown, it is unclear how DLC3 is recruited to specific subcellular sites to execute its functions.

In this study, DLC3 protein binding partners were identified using a proteomic approach. By this means, the basolateral polarity protein Scribble was discovered as the first isoform-specific scaffold for DLC3 at adherens junctions. The interaction was mapped to the PDZ domains of Scribble and a unique PDZ ligand (PDZL) motif in DLC3 and both Scribble depletion and PDZL deletion abrogated DLC3 junctional localization. Using a RhoA biosensor and a targeted GAP domain, convincing evidence was provided for DLC3 as local regulator of RhoA-ROCK signaling at and Scribble localization to cell-cell adhesions controlling E-cadherin function and junctional integrity. In addition to their role at adherens junctions, DLC3 and Scribble were shown to restrict RhoA-ROCK signaling at the leading edge of cells that polarize during directed cell migration. In a three-dimensional model system of cyst development, DLC3 and Scribble depletion furthermore impaired epithelial morphogenesis and lumen formation, emphasizing the relevance of both proteins for the establishment of cell polarity. Taken together, these findings uncover a new control mechanism for spatial Rho regulation that involves Scribble-mediated positioning of DLC3's GAP activity at cell junctions in polarized epithelial cells.

## Zusammenfassung

Apikobasale Zellpolarität ist unerlässlich für die normale Funktion von Epithelien und für Gewebsintegrität und wird durch etliche Polaritätsproteine aufgebaut. Zellpolarisierung, einschließlich der Ausbildung und Aufrechterhaltung von Zellkontakten, erfordert auch eine räumlich begrenzte Remodellierung des Zytoskeletts. Kleine Rho-GTPasen fungieren als Schlüsselregulatoren des Zytoskeletumbaus und sind daher involviert in grundlegende, zelluläre Prozesse wie Zellpolarität und Zell-Zell-Adhäsion. Allerdings ist die räumliche Kontrolle der Rho-Signalgebung in der Zelle durch ihre Regulatoren, spezifische GEF- (*guanine nucleotide exchange factors*) und GAP-Proteine (*GTPase-activating proteins*), noch unzureichend verstanden. Die DLC-Proteine (*deleted in liver cancer*) stellen eine RhoGAP-Proteinfamilie dar, welche in verschiedenen Krebsarten häufig dereguliert ist und drei strukturell verwandte Familienmitglieder umfasst, DLC1/2/3. Es gibt vermehrt wissenschaftliche Belege dafür, dass die unterschiedlichen DLC-Proteine auch nicht-redundante Funktionen ausüben und durch isoform-spezifische Mechanismen kontrolliert werden aufgrund ihrer unterschiedlichen subzellulären Lokalisationen. Für die noch unzulänglich charakterisierte DLC3-Isoform wurde eine Lokalisation an *adherens junctions* und Rab8-positiven, tubulären Strukturen festgestellt, neben ihrer Assoziation mit fokalen Adhäsionskontakten, welche alle drei DLC-Proteine miteinander gemein haben. Da das DLC3-Interaktom noch weitestgehend unbekannt ist, ist es unklar, wie DLC3 an spezifische subzelluläre Orte rekrutiert wird, um dort seine Funktionen auszuführen.

In dieser Studie wurden mit Hilfe eines proteomischen Ansatzes DLC3-Proteinbindungspartner identifiziert. Auf diese Weise wurde das basolaterale Polaritätsprotein Scribble als erstes isoform-spezifisches Gerüstprotein für DLC3 an *adherens junctions* entdeckt. Die Interaktion beruht auf den Scribble-PDZ-Domänen und einem einzigartigen PDZ-Bindemotiv in DLC3 und sowohl Scribble-Verlust als auch die Deletion des PDZ-Bindemotivs hoben die Lokalisation von DLC3 am Zellkontakt auf. Unter Verwendung eines RhoA-Biosensors und einer zielgerichteten GAP-Domäne wurden überzeugende Nachweise für DLC3 als lokalen Regulator der RhoA-ROCK-Signalgebung und Scribble-Lokalisation am Zellkontakt geliefert, welche die Funktion von E-Cadherin und Intaktheit der Zelladhäsionen kontrollieren. Zusätzlich zu ihrer Rolle an *adherens junctions* wurde gezeigt, dass DLC3 und Scribble RhoA-ROCK-Signaling am Leitsaum von Zellen einschränken, die während der gerichteten Zellmigration polarisieren. DLC3- und Scribble-Knockdown in einem 3D-Modell der Zystenbildung verhinderten außerdem epitheliale Morphogenese und Lumenbildung, was die Bedeutung beider

Proteine bei der Ausbildung von Zellpolarität hervorhebt. Zusammengenommen decken diese Ergebnisse einen neuen Kontrollmechanismus für lokale Rho-Regulation auf, welcher die genaue Positionierung der DLC3-GAP-Aktivität an Zellkontakten in polarisierten Epithelzellen durch Scribble beinhaltet.

# 1. Introduction

## 1.1 The family of Rho GTPases

### 1.1.1 Cellular functions of Rho GTPases

Rho GTPases function as molecular switches controlling a wide range of signal transduction pathways in the cell. They integrate external stimuli by linking surface receptors to cytoskeleton dynamics. Thereby, they serve as key regulators of the actin and microtubule cytoskeleton which is the structural framework that determines cell morphology, polarity and the dynamic properties required for cell movement and division. Thus, Rho proteins are important for the control of numerous biological processes including cell adhesion, differentiation, migration, vesicular trafficking, cell cycle progression, cytokinesis and gene transcription (Hall, 1998). Rho GTPases represent a family within the superfamily of Ras-related small GTPases comprising 8 subfamilies and are highly conserved from lower eukaryotes to mammals. They act as binary switches cycling between an active GTP-bound and an inactive GDP-bound state and are activated by surface receptors including receptor tyrosine kinases, integrins, cadherins, G protein-coupled receptors and cytokine receptors (Bos et al., 2007). In their active form, Rho proteins activate more than 60 downstream effectors identified thus far, for example different serine/threonine kinases, tyrosine kinases, lipid kinases, actin regulators and scaffold proteins. In this way, they trigger signaling cascades and modulate local actin and microtubule dynamics to induce a wide range of cellular responses (Jaffe and Hall, 2005).

More than twenty Rho proteins are encoded in the human genome including RhoA, Rac and Cdc42 as the best characterized members. Activation of the different Rho family members leads to contrasting effects in actin organization. RhoA activation is mainly responsible for actin-myosin contraction. On the one hand, it promotes stress fiber formation by bundling of actin filaments with myosin filaments. On the other hand, active RhoA mediates clustering of integrins and integrin-associated proteins forming focal adhesions (Hall, 1998). Rac activation, by contrast, induces actin polymerization in the cell periphery and the formation of membrane ruffles and lamellipodia, whereas Cdc42 activity at the inner plasma membrane is required for the generation of filopodial structures (Hall, 1998). These complex alterations in actin structure, controlled by different Rho family members, are realized through activation of numerous downstream effectors. Cdc42 and Rac, for example, activate Wiskott-Aldrich syndrome family proteins (WASp, WAVE and WASH) and the actin-related protein 2/3 (Arp2/3) complex to induce actin nucleation and polymerization. Rac further activates filamins whose cross-linking property is required for

actin branching and net assembly in lamellipodia. However, Rac also antagonizes RhoA by inhibiting the contractile activity of myosin motor proteins. By contrast, following RhoA activation, parallel actin bundles are built by formin proteins, like diaphanous-related formin (Dia), to increase the amount of cellular stress fibers. In addition, RhoA activates Rho-associated protein kinase (ROCK) to stabilize actin filaments and enhance phosphorylation of myosin light chain (MLC), which in turn promotes contractile myosin activity and builds up tension within the cell (Jaffe and Hall, 2005; Ridley, 2006).

These cytoskeletal changes are essential for many fundamental cellular processes and have to be coordinated tightly. For instance, Rho mediated cytoskeleton dynamics determine cell morphology and the establishment and maintenance of epithelial cell polarity (described in section 1.2.3). Moreover, directed cell migration requires polarization and remodeling of the actin network based on external cues. This includes actin polymerization and elongation of filaments at the front of the cell and actin-myosin contraction at the rear as driving forces of migration (see section 1.2.4) (Etienne-Manneville and Hall, 2002; Jaffe and Hall, 2005). Rho GTPases also modulate cell cycle progression by controlling the activation of cyclin-dependent kinases in G1 phase and the structure of the actin and microtubule cytoskeleton during M phase. In addition, RhoA plays an important role during cytokinesis, when Rho effector proteins accumulate at the cleavage furrow between two daughter cells to form a contractile actin-myosin ring. Besides their function in regulating cytoskeleton dynamics, Rho proteins have been described to affect different signal transduction pathways leading to alterations in gene expression (Etienne-Manneville and Hall, 2002; Jaffe and Hall, 2005). In general, an appropriate balance of Rho GTPase activity has to be achieved to allow the correct execution of all these cellular processes and to prevent cell transformation and disease.

### **1.1.2 Rho GTPases in tumor development and progression**

Associated with their involvement in many important cellular pathways, deregulated activity of Rho GTPases is observed during malignant cell transformation. Thus, Rho proteins contribute to the establishment of the so called “hallmarks of cancer” specified by Hanahan and Weinberg in 2000. These capabilities acquired by cancer cells include replicative immortality, insensitivity to growth repressors, sustaining growth signaling, evading cell death, inducing angiogenesis and promoting tissue invasion and metastasis (Hanahan and Weinberg, 2000). Elevated Rho activity is associated with tumor development and progression. However, its major cause seems to be altered gene expression or function of Rho regulators, rather than activating mutations in the Rho

GTPases themselves (Orgaz et al., 2014; Sahai and Marshall, 2002a). In principle, Rho GTPases have been reported to be involved in most steps of cancer initiation and progression (Fig. 1).

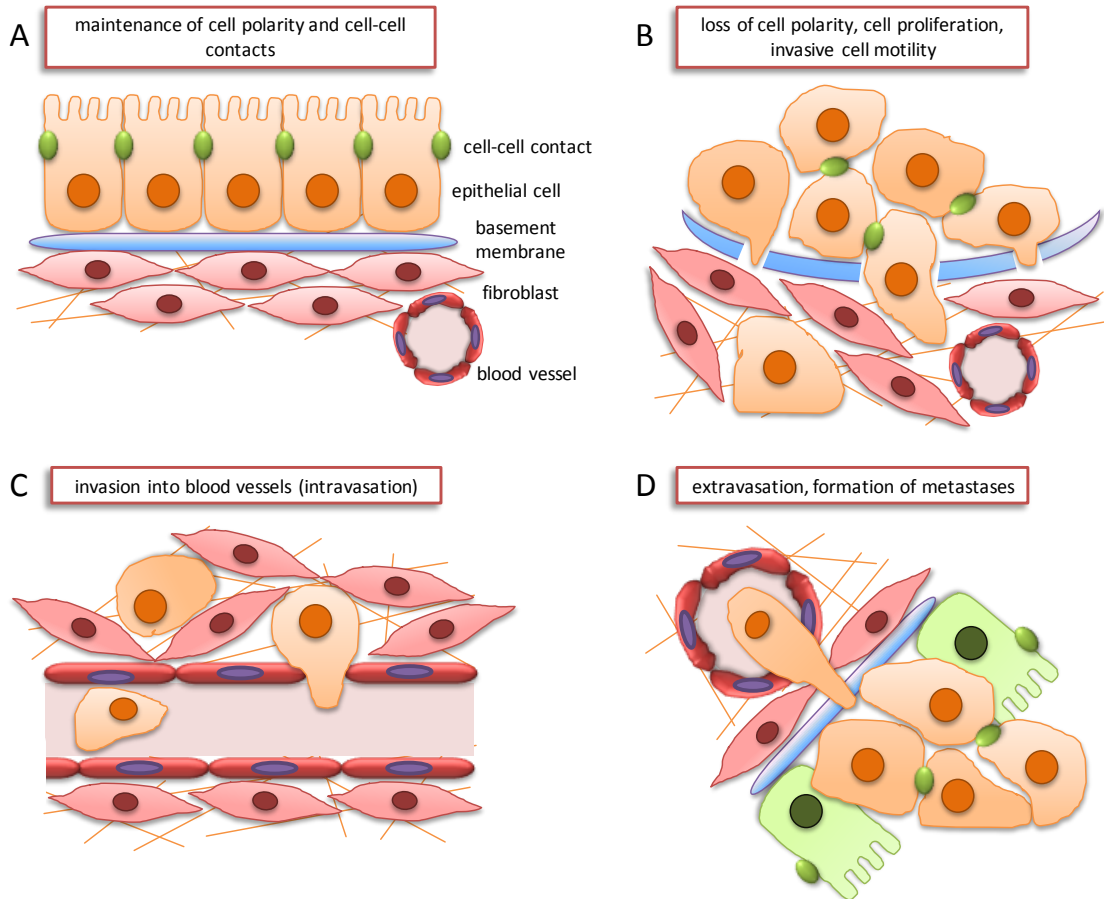


**Figure 1: The role of Rho GTPases during tumor initiation and progression.** The single steps of cancer development are depicted. Polarized epithelial cells (A) transform into highly proliferative and invasive cancer cells (B) that invade into tissues and blood vessels (C) and form metastases (D). Processes regulated by Rho GTPases are designated. Modified from Noll et al., 2016.

In normal epithelia, they control tissue integrity by contributing to the establishment and maintenance of apical-basal cell polarity and intact cell junctions. However, during tumor development, epithelial cell polarity is lost and cell-cell contacts are destabilized. Deregulated Rho activity promotes the conversion of cells towards a motile phenotype during a process termed epithelial-to-mesenchymal transition (EMT) (Sahai and Marshall, 2002a; Vega and Ridley, 2008). In addition, some Rho GTPases contribute to uncontrolled cell proliferation and tumor growth by regulating gene transcription and accelerating cell cycle progression. During tumor progression, all important Rho family members are involved in cell migration and invasion into tissues and blood vessels, which is a prerequisite for tumor spreading and metastasis formation (Sahai and Marshall,

2002a; Vega and Ridley, 2008). Consequently, to prevent aberrant Rho signaling and ensure normal cellular functions, the activity of Rho GTPases has to be tightly controlled in the cell.

### 1.1.3 Rho regulation by GEFs and GAPs

The spatiotemporal activation of Rho GTPases is controlled by guanine nucleotide exchange factors (GEFs) and GTPase-activating proteins (GAPs). These are signaling nodes that receive multiple input signals to modulate the amplitude and duration of GTPase activity and trigger appropriate downstream responses. Until today, more than 80 GEF and 70 GAP proteins have been discovered in the control of the 20 known Rho GTPases, emphasizing the requirement for precise Rho regulation in different cellular contexts (Vigil et al., 2010). In particular, GEFs exchange Rho-bound GDP for GTP to activate the GTPase and induce signaling of downstream effectors. By contrast, GAPs enhance the low intrinsic GTPase-activity of Rho proteins by providing an essential catalytic group for GTP hydrolysis to return them into the inactive state and terminate the signal (Fig. 2). Rho GTPases are targeted to cell membranes by lipid modifications (prenylation or palmitoylation) at their C-termini influencing their interaction with specific GEFs and effectors to promote downstream signaling. Restriction of Rho activity is additionally mediated by guanine nucleotide dissociation inhibitors (GDIs) which prohibit GDP release or mask the C-terminal lipid anchor to sequester the GTPase in the cytoplasm and prevent its activation (Fig. 2) (Bos et al., 2007).

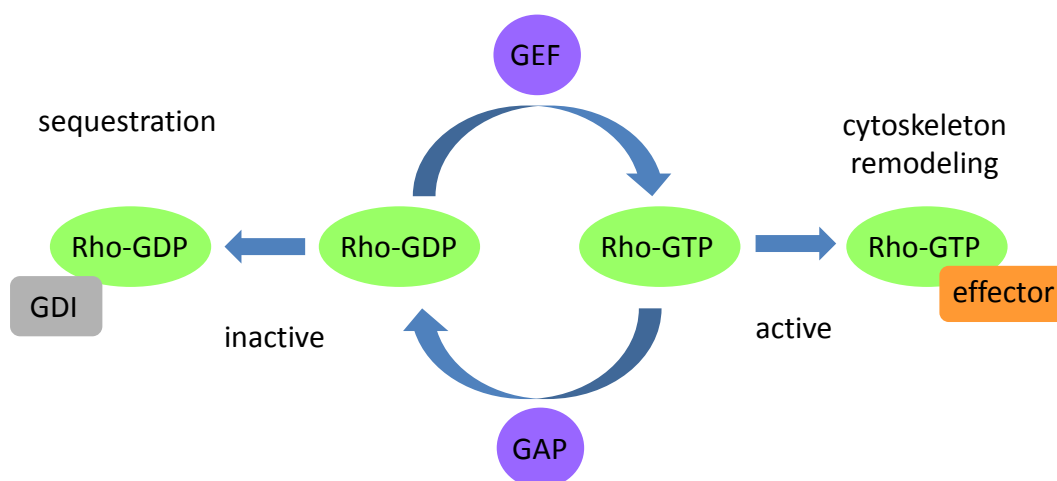


**Figure 2: Regulation of Rho GTPases by GEFs and GAPs.** Schematic representation of the Rho activation cycle regulated by guanine nucleotide exchange factors (GEF), GTPase-activating proteins (GAP) and guanine nucleotide dissociation inhibitors (GDI).

In terms of domain organization, RhoGEFs contain conserved tandem Dbl homology (DH)–pleckstrin homology (PH) or dedicator of cytokinesis (DOCK) domains, whereas RhoGAPs have conserved GAP domains. However, it is still poorly understood how the specificity of GEFs and GAPs for certain Rho GTPases is achieved, which is in some cases very broad, whereas other Rho regulators control only one specific GTPase (Bos et al., 2007). GEF and GAP proteins often display a multi-domain organization representing platforms whose localization, specificity and activity seem to be controlled by various means (Hodge and Ridley, 2016). Although the precise regulatory mechanisms for the Rho regulators themselves are just at the beginning to be understood, a complex network of control events seems to be essential for balanced Rho activity and appropriate signaling outputs. Due to their multi-domain structure, GEF and GAP proteins additionally possess functions independent of Rho regulation and serve as scaffolds mediating the cooperation with other signaling pathways (Vigil et al., 2010). For instance, IQGAP is a scaffold protein with a permanent inactive RasGAP domain, but it still regulates cytoskeleton dynamics, calcium signaling and cell adhesion through other domains (White et al., 2012). Taken together, the large variety of RhoGEF and RhoGAP proteins ensures the proper modulation of Rho signaling in time and space. However, deregulated expression and altered activity of Rho regulators caused by somatic mutations, epigenetic changes or post-translational modifications are associated with tumorigenesis (Vega and Ridley, 2008). Consequently, GEF and GAP proteins represent potential targets for cancer therapy whose regulation and function remain to be investigated more precisely.

## **1.2 Epithelial cell polarity**

### **1.2.1 Establishment of apical-basolateral cell polarity**

Apical-basolateral polarity is a characteristic of highly organized epithelial tissues. Cell polarity is defined as the asymmetric distribution of proteins and lipids in the cell separating the plasma membrane into discrete compartments. Apical membranes facing the lumen, for example of a duct, are covered with extracellular fluid, whereas the basolateral domain is anchored to the basement membrane on underlying tissues and attached to adjacent cells. Epithelial polarity is crucial for the spatial organization of intracellular signaling pathways. It allows the differential interpretation of cues from the surrounding environment to trigger adequate downstream signaling and control cell proliferation, differentiation and motility, (Halaoui and McCaffrey, 2015; Iden and Collard, 2008). Loss of polarity is a prerequisite and characteristic of cancer at the same time and occurs at a very early stage during the multi-step process of cancer development. Most

cancers are formed from epithelia in which disruption of apical-basolateral polarity and cell-cell adhesions leads to tissue disorganization, epithelial-to-mesenchymal transition (EMT) and eventually to metastasis (Ellenbroek et al., 2012; Halaoui and McCaffrey, 2015).

The specification of apical and basolateral membrane domains is, on the one hand, mediated by cell-cell adhesions including adherens junctions (AJ) and tight junctions (TJ). On the other hand, polarity protein complexes are responsible for controlling polarity signaling and epithelial homeostasis (Fig. 3) (Ellenbroek et al., 2012). The major function of adherens junctions, in addition to their role in defining an apical-basal axis, is to form strong adhesive structures between adjacent cells. By linking cell adhesions to the cytoskeleton, adherens junctions make cells resistant to external forces and preserve tissue integrity (Baum and Georgiou, 2011). Adherens junctions are built of  $\text{Ca}^{2+}$ -dependent, homophilic interactions of epithelial cadherins (E-cadherin) on adjacent cells. E-cadherins are transmembrane proteins characterized by long extracellular domains and cytoplasmic parts connected to cytoplasmic plaque proteins and the actin network. In particular, the Armadillo repeat protein  $\beta$ -catenin binds to the cytoplasmic tail of E-cadherins, while p120-catenin and  $\alpha$ -catenin further stabilize the structure and connect it to actin bundles and actin-associated proteins. Thus, mature adherens junctions represent large protein complexes of densely clustered E-cadherin molecules specifying the basolateral membrane domain (Baum and Georgiou, 2011; Takeichi, 2014). Tight junctions, by contrast, serve as permeability barriers separating fluid of the apical and basolateral compartment. Thereby, they contribute to the asymmetric distribution of molecules and spatial organization of signaling pathways (Quiros and Nusrat, 2014). Tight junctions look like sealing strands which stick together the plasma membranes of adjacent cells. They are composed of transmembrane proteins like claudins and occludins that undergo interactions with scaffolds like the zonula occludens (ZO) proteins. These scaffolds are platforms for large protein networks that organize the structure of tight junctions, link them to the actin cytoskeleton and determine apical surface identity (Mack and Georgiou, 2014; Quiros and Nusrat, 2014).

Moreover, three different polarity protein complexes exist to control polarity signaling and maintain epithelial cell polarity. The partitioning defective (Par) and the Crumbs complex define the apical membrane compartment, whereas the Scribble complex preserves basolateral membrane identity (Fig. 3). These polarity complexes are conserved in many cell types and species. The Par complex, which has been discovered in *Caenorhabditis elegans* first, consists of Par3, Par6 and atypical protein kinase C (aPKC). Par3 is a multi-

domain scaffold protein associated with tight junctions through interaction with junction adhesion molecule A (JAM-A). Phosphorylation by aPKC is required for the stable association of Par3 with tight junctions. In addition, Par3 binds to Par6, an adaptor that is permanently bound to aPKC, to stabilize Par6 and prevent its degradation (Assémat et al., 2008; Ellenbroek et al., 2012). The Crumbs complex was first described in *Drosophila* and is constituted of the transmembrane protein Crumbs3 which interacts with protein-associated with Lin seven 1 (Pals1) and Pals1-associated tight junction protein (PATJ). The sophisticated regulation of epithelial polarity includes interplays between polarity proteins of different complexes. For example, Par6 also binds to Crumbs3 and aPKC phosphorylates Crumbs3, which is a requirement for stable membrane association of PATJ and aPKC (Assémat et al., 2008; Halaoui and McCaffrey, 2015).

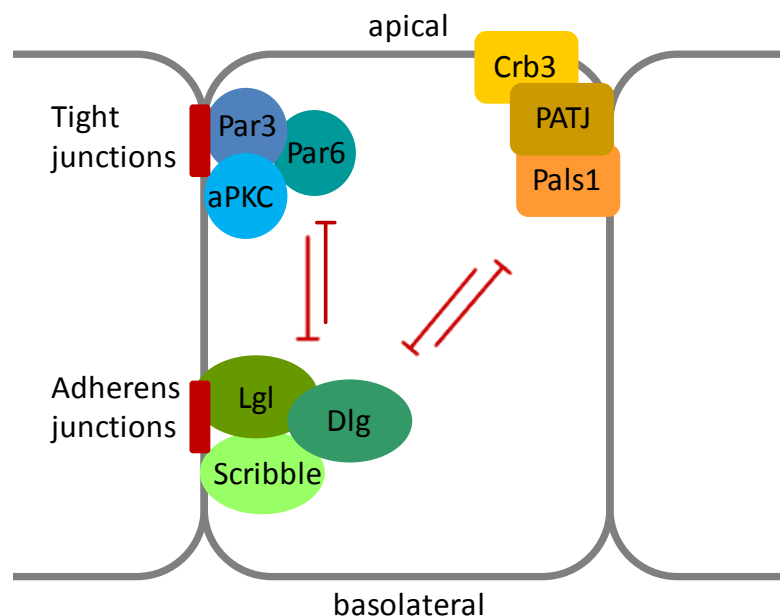


**Figure 3: Polarized organization of epithelial cells.** Specification of apical and basolateral membrane compartments by tight and adherens junctions and polarity protein complexes. Apical localization of the partitioning defective homolog (Par) and Crumbs (Crb3) complexes and basolateral restriction of the Scribble complex are shown. Dlg = discs large homolog, Lgl = lethal giant larvae, aPKC= atypical protein kinase C, Pals = protein associated with Lin-7, PATJ = Pals1-associated tight junction protein. Based on Ellenbroek et al., 2012.

In general, the apical Par and Crumbs complexes function in a mutually exclusive fashion with the basolateral Scribble complex. The Scribble complex was also identified in *Drosophila* for the first time and is composed of Scribble (Scrib), discs large (Dlg) and lethal giant larvae (Lgl) (described in section 1.2.2). It controls the maintenance of epithelial polarity by restriction of basolateral protein localization. Another interplay between the different polarity complexes is the phosphorylation of Lgl by aPKC, which

excludes Lgl from apical membranes and helps to preserve apical membrane identity (Ellenbroek et al., 2012). Additionally to their interactions with each other, the three polarity complexes bind to cytoskeleton-associated proteins, for example myosin II, 14-3-3 and YMO1 (Hurd et al., 2003; Laprise et al., 2006; Strand D, 1995). In this way, they directly modulate actin cytoskeleton dynamics to control cell morphology and polarity (Assémat et al., 2008). However, disturbance of these highly coordinated mechanisms to establish and maintain epithelial polarity has severe consequences. Considering that the key function of polarity proteins is the spatial organization of signal transduction components, mutations affecting the localization or protein interactions of polarity proteins can have drastic impacts on downstream signaling events. In line with this, altered expression of polarity proteins and aberrant polarity signaling have been reported to contribute to cancer progression (Halaoui and McCaffrey, 2015).

### **1.2.2 The basolateral polarity protein Scribble**

The Scribble polarity protein, in complex with Dlg and Lgl, is crucial for epithelial cell polarity. In *Drosophila*, Scribble is required during embryonic development, for example for the polarization of wing imaginal disc and follicular epithelia. The name “Scribble” originates from the finding that mutations in *Drosophila Scribble* resulted in animals with corrugated cuticular surfaces due to disorganization of the underlying epithelial cells (Bilder and Perrimon, 2000; Humbert et al., 2008). In mammalian tissues, Scribble plays an important role in polarization and development as well. *Scribble* knockout mice have a lethal phenotype because of severe neural tube closure defects. They further display failures in eyelid closure and abdominal wall closure and curly tails, characteristics also observed in the *Scribble* point mutation models *Circletail* and *rumz* (Murdoch et al., 2003; Pearson et al., 2011; Zarbališ et al., 2004). In addition, Scribble was shown to be important for normal mammary gland morphogenesis by mammary fat pad transplantation studies and in a conditional mouse model of *Scribble* loss (Godde et al., 2014; Zhan et al., 2008). While Scribble is essential for the maintenance of apical-basolateral polarity in *Drosophila*, its major function in mammalian cells appears to be within the planar polarity pathway. In particular, Scribble was reported to interact with the planar polarity protein Vangl2 and *Scribble* mutations led to a significant disruption of stereociliary bundle polarization in murine cochlea as a consequence of impaired planar cell polarity (Kallay et al., 2006; Montcouquiol et al., 2003). Moreover, Scribble functions as a tumor suppressor in *Drosophila* and mammalian cells and its loss cooperates with oncogenic Ras signaling in cell transformation and invasion (Bilder and Perrimon, 2000; Dow et al., 2003; Dow et al., 2008; Pagliarini and Xu, 2003). The polarity protein is involved in the control of

proliferation, for example by regulating ERK activation and nuclear translocation (Dow et al., 2008; Elsum et al., 2013; Nagasaka et al., 2010). The finding that Scribble represents a target of human papillomavirus (HPV) oncoproteins for ubiquitin-mediated degradation, further emphasizes its role as a tumor suppressor that is downregulated in cancer (Nakagawa and Huibregtse, 2000).

Scribble is a multi-domain scaffold protein containing 16 leucine-rich repeats (LRRs) and four PSD-95, discs large and ZO-1 (PDZ) domains. The LRR domains target the protein to basolateral membranes and are crucial for the development and maintenance of epithelial polarity and proliferation control (Navarro et al., 2005; Zeitler et al., 2004). Its PDZ domains, by contrast, act as protein interaction platforms and are required for the scaffolding functions of Scribble. Loss of Scribble has been reported in lobular breast cancer and colorectal cancer and is associated with disorganized tissue architecture including abnormal localization of E-cadherin (Gardioli et al., 2006; Navarro et al., 2005). This is partially attributed to the role of Scribble in controlling adherens junction integrity and E-cadherin internalization. Particularly, Scribble was shown to stabilize the interaction of E-cadherin and p120-catenin at adherens junctions to prevent E-cadherin endocytosis and mistrafficking to the Golgi (Lohia et al., 2012; Qin et al., 2005). The scaffolding functions of Scribble are, for example, important for PDZ-mediated recruitment of the RacGEF  $\beta$ -Pix to adherens junctions to form a signaling complex with PAK2 regulating epithelial morphogenesis (Frank et al., 2012). Moreover, the Scribble- $\beta$ -Pix interaction is required for Myc-induced apoptosis during lumen formation of MCF10A breast epithelial cells in 3D-cultures (Zhan et al., 2008). In addition to its role at adherens junctions, Scribble functions at the leading edge during directed cell migration where it is required for polarization of the cellular front and lamellipodia formation. This cellular function of Scribble can be explained mechanistically also by its interaction with  $\beta$ -Pix promoting Rac and Cdc42 activation at the leading edge (Dow et al., 2006; Nola et al., 2008; Osmani et al., 2006).

Correct membrane localization of Scribble is essential for its functions and mislocalization of Scribble by a point mutation in the LRR domains impairing its membrane association was shown to inhibit polarized morphogenesis of MCF10A acini (Zhan et al., 2008). Recently, different posttranslational modifications regulating the precise subcellular localization of Scribble were identified. On the one hand, the phosphorylation state of Scribble seems to determine its localization at adherens junctions and its interaction with E-cadherin/catenin complexes (Yoshihara et al., 2011). On the other hand, modification of Scribble by palmitoylation was reported to control its membrane association (Chen et al.,

2016). The observation that mislocalized Scribble failed to inhibit Ras-induced cell invasion of MCF10A cells further confirms that correct membrane localization of Scribble is a prerequisite for its tumor suppressive functions. However, the cells still retained the ability to suppress Ras-induced anchorage-independent growth indicating that some, but not all properties of Scribble depend on its localization (Elsom and Humbert, 2013). Taken together, due to its diverse scaffolding functions, Scribble is involved in a complex, context-dependent regulatory network to preserve epithelial polarity and growth control.

### **1.2.3 Cooperation of polarity proteins and Rho GTPases**

Establishment of epithelial polarity is achieved by the cooperation of polarity proteins and Rho GTPases. To this end, polarity proteins serve as scaffolds which modulate the precise localization and activation of Rho GTPases and their GEF and GAP proteins. Accurately tuned Rho signaling coordinates local cytoskeleton remodeling, protein-protein interactions and polarized vesicular trafficking, which are requirements for apical-basal polarization and normal epithelial morphogenesis (Mack and Georgiou, 2014; Ngok et al., 2014). Although Rho, Rac and Cdc42 have all been shown to be important for cell junction formation and integrity, their activities have to be carefully balanced in a spatial and temporal manner. In general, Rac-induced lamellipodia formation is required during the initial phase of junction formation and cooperates with Rho-mediated actomyosin contractility during the assembly and expansion of adherens junctions. In addition, Cdc42 was reported to be involved in apical-basal polarization and polarized transport and is especially required for the establishment of acini lumen in three-dimensional cultures (Citi et al., 2014; Ngok et al., 2014).

It is well established that antagonistic Rac and RhoA activity gradients exist along the apical-basal axis of epithelial cells which are essential for junction formation and to preserve apical and basolateral membrane identities (Mack and Georgiou, 2014). Rac activity, for example, is controlled by the GEF protein Tiam, a well-known regulator of cell adhesion and polarity. Tiam itself is inhibited by association with the apical Par complex component Par3, whereas basolateral recruitment by the scaffold  $\beta$ 2-syntrophin leads to Tiam activation (Mack et al., 2012; Mertens et al., 2005; Nishimura et al., 2005). Thus, Rac regulation by Tiam contributes to the formation of an apical-basal Rac activity gradient. Furthermore, during the maturation of adherens junctions active Rac promotes the association of p190RhoGAPa with cadherin-bound p120-catenin, thereby suppressing basolateral Rho activation (Noren et al., 2003; Wildenberg et al., 2006). Owing to this negative crosstalk, RhoA activity is restricted towards apical junctions. However, in recent

times, the development of genetically encoded Rho biosensors allowed the analysis of spatiotemporal Rho activation in more detail. Such studies revealed, for example, that RhoA is also active in the cell periphery of contacting cells during the initial phase of cell-cell adhesion, emphasizing the complexity of Rho regulation in polarized cells (Yamada and Nelson, 2007). Recently, p114RhoGEF was identified as the first junction-associated regulator of RhoA signaling at the apical membrane domain regulating adhesion assembly and epithelial morphogenesis (Terry et al., 2011). Further studies elucidated that p114RhoGEF associated with apical PATJ, a component of the Crumbs complex, and confirmed that this complex contributes to apical membrane specification through RhoA signaling (Nakajima and Tanoue, 2011). In addition, the Crumbs complex is involved in the exclusion of apical Rac and Cdc42 activation. In particular, the Rac/Cdc42GAP protein Rich1 is targeted to Crumbs by the junction-associated protein Angiomotin (Amot) to balance Rac and Cdc42 activities and preserve tight junction stability (Wells et al., 2006).

Moreover, further examples for the crosstalk of polarity proteins with Rho GTPases and their regulators have been uncovered. On the one hand, the RhoGEF Ect2 was shown to function at the zonula adherens where it regulates RhoA-mediated actomyosin remodeling and junction integrity (Ratheesh et al., 2012). On the other hand, Ect2 was also identified to control Cdc42 activity and its targeting to Par6, promoting aPKC activation and tight junction formation (Zihni et al., 2014). Further RhoGEFs have been reported to localize to the apical membrane to induce RhoA signaling and control cell adhesion including TEM4 and the ZO-1-associated GEF ARHGEF11 (Itoh et al., 2012; Ngok et al., 2013). In summary, a complex cooperation network of polarity proteins and Rho GTPases seems to be required to organize epithelial architecture which is only beginning to be understood. Especially, the interplay of the basolateral Scribble complex with Rho proteins has been insufficiently studied, since the focus of research was mainly on the apical polarity complexes. Thus, there are still many open questions as to how Rho regulators, and particularly junction-associated RhoGAP proteins, function in epithelial polarity and by which molecular mechanisms they themselves are regulated.

#### **1.2.4 Front-rear polarization of migratory cells**

Front-rear polarization of cells is crucial for directed cell migration, for example during development and tissue morphogenesis, but also in the context of pathologies like cancer. Various different external stimuli induce the transition from apical-basolateral to front-rear polarity including growth factors and the extracellular matrix. The establishment of a leading edge at the front and a retracting tail at the rear of the cell requires global changes

in the organization of the cytoskeleton, protein trafficking and signaling pathways. These changes are once again coordinated by the interplay of Rho GTPases and cell polarity proteins (Fig. 4) (Iden and Collard, 2008; Nelson, 2009). In general, spatial activation of Rac and Cdc42 at the leading edge allows forward movement by the formation of membrane protrusions, disassembly of integrin-mediated contacts and the polarization of the cytoskeleton towards the front of the cell. By contrast, at the trailing edge, RhoA-driven actomyosin contraction causes detachment of the cell from the extracellular matrix (ECM) and membrane retraction (Ridley et al., 2003). However, the situation seems to be more complex, since in recent studies RhoA activation at the leading edge was reported also in the very initial phase of protrusion formation where it promoted actin filament assembly through Dia (Palazzo et al., 2001).

Polarity protein complexes are typically located at the cellular front of migrating cells where they activate Rac and Cdc42, as shown for example for Scribble through recruitment of the GEF protein  $\beta$ -Pix (Audebert et al., 2004). Additionally, Cdc42 and Rac activation at the leading edge is induced by integrin interactions with the ECM (Etienne-Manneville and Hall, 2001). Several substrates of the Par complex component aPKC are important for front-rear polarization (Fig. 4). On the one hand, the RacGEF Tiam is a substrate of aPKC (Nishimura et al., 2005; Pegtel et al., 2007). On the other hand, glycogen synthase kinase-3 $\beta$  (GSK3 $\beta$ ) is inactivated upon aPKC-mediated phosphorylation, leading to microtubule stabilization by the GSK3 $\beta$  target APC and its interaction with the Scribble complex protein Dlg at the leading edge (Etienne-Manneville et al., 2005; Zumbunn et al., 2001). In particular, the polarized orientation of microtubules and correct positioning of the centrosome, the microtubule organizing center, are prerequisites for directed cell migration (Fig. 4) (Nelson, 2009). aPKC-mediated GSK3 $\beta$  inhibition further maintains the RhoGAP p190RhoGAP in its active state to suppress RhoA activity at the cellular front (Jiang et al., 2008).

Moreover, front-rear polarity is regulated by polarized vesicular trafficking including the redistribution of integrins from the rear to the front of the cell, which is controlled, for example, by aPKC and the endocytic adaptor protein Numb (Nishimura and Kaibuchi, 2007). The Scribble complex component Lgl was also described to be important for polarized protein delivery and vesicle fusion at the leading edge (Klezovitch et al., 2004; Muösch et al., 2002). Finally, establishment of front-rear polarity is characterized by asymmetric phosphatidylinositol distribution including enrichment of phosphatidylinositol-3,4,5-trisphosphate (PIP<sub>3</sub>) at the leading edge. This might be explained by a positive feedback loop of Cdc42 and PI3K that promotes high PIP<sub>3</sub> levels and excludes the

phosphatase PTEN at the cellular front (Raftopoulou and Hall, 2004; Ridley et al., 2003). Thus, front-rear polarization, similar to apical-basolateral polarity, requires a highly coordinated crosstalk of different Rho GTPases and polarity proteins to ensure locally defined signaling and cytoskeleton remodeling events.

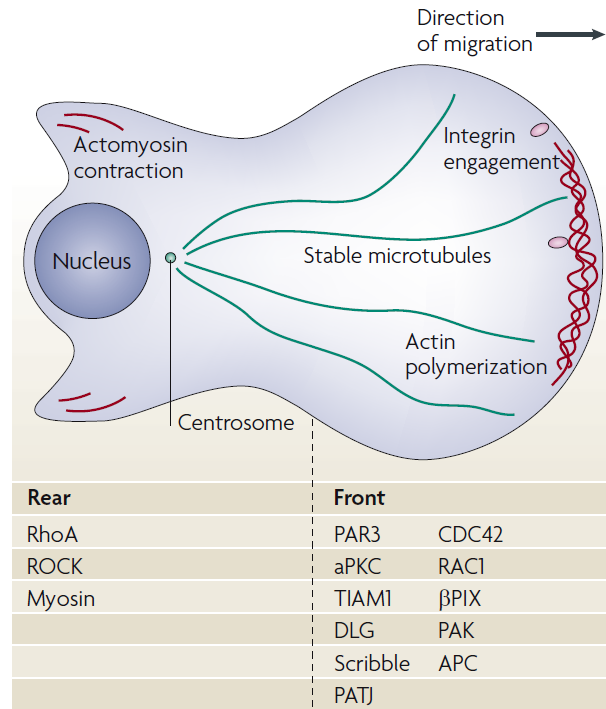


**Figure 4: Establishment of front-rear polarity in migratory cells.** Actin and microtubule cytoskeleton dynamics required for front-rear polarization are illustrated. Rho GTPases and polarity proteins involved in the formation of a leading edge at the front and a retracting tail at the rear of migratory cells are listed according their site of action. Taken from Iden and Collard, 2008.

### 1.3 The DLC family of RhoGAP proteins

#### 1.3.1 DLC proteins as candidate tumor suppressors

The deleted in liver cancer (DLC) proteins constitute a family of RhoGAPs which is often downregulated in cancer. In particular, loss of DLC expression is the most frequent change observed among RhoGAP proteins and in some human cancers the family member DLC1 is downregulated with the same frequency as the established tumor suppressor p53 (P. Kandpal, 2006; Xue et al., 2008). DLC proteins are found in all multi-cellular organisms. In *Drosophila*, one DLC-like protein exists, RhoGAP88C, which is essential for viability. Nonlethal mutations in the gene encoding RhoGAP88C have prominent phenotypes including loss of the wing crossvein due to which the gene was termed *crossveinless-c* (*cv-c*) (Denholm et al., 2005; Durkin et al., 2007b). RhoGAP88C is important for restricting Rho signaling and controlling cytoskeletal dynamics during

*Drosophila* morphogenesis, for example during development and epithelial invagination of the fly's trachea (Brodu and Casanova, 2006; Denholm et al., 2005). In humans, three DLC family members emerged through gene duplication, DLC1, DLC2 and DLC3, which are structurally similar and partially overlap, but also differ in their subcellular localization (Braun and Olayioye, 2015).

DLC1, the best studied family member, was first discovered in 1998 as candidate tumor suppressor which is lost in primary hepatocellular carcinoma (HCC) and HCC-derived cell lines (Yuan et al., 1998). Later it was shown that p122RhoGAP, originally identified as a phospholipase C $\delta$ 1 (PLC $\delta$ 1)-interacting protein in rat brain (Homma and Emori, 1995), represents the rat orthologue of human DLC1. This is an example for the existence of DLC orthologues in other vertebrates, which is the case for each of the three DLC proteins. Apart from HCC, DLC1 expression is lost in numerous types of cancer, including breast, colorectal, lung, ovarian and prostate cancer. Deregulated DLC1 levels are caused by deletion of the *DLC1* locus, mapped to chromosome 8 (8p21.3-22), or epigenetic gene inactivation by promotor hypermethylation (Durkin et al., 2007b). Reconstitution of DLC1 expression in tumor cell lines lacking endogenous DLC1 inhibited cell proliferation and tumor development in the mouse model, supporting its function as candidate tumor suppressor (Yuan et al., 2003). Moreover, stable expression of DLC1 in human liver and breast cancer cell lines reduced the migration and invasion properties of these cells (Goodison et al., 2005; Wong et al., 2005). Finally, the role of DLC1 as a tumor suppressor was clearly proven in a new mouse model of liver cancer (Xue et al., 2008). Investigations of the cellular effects of DLC1 depletion by RNA-interference revealed enhanced stress fiber and focal adhesion formation in breast cancer cells associated with increased cell migration. Conversion of cells towards this motile phenotype was induced by aberrant Rho signaling and activation of the Rho effector protein Dia1 (Holeiter et al., 2008). In general, DLC1 displays a broad tissue distribution with high expression levels in lung and ovary and moderate abundance in kidney, spleen, intestine and thyroid. Four different transcript variants have been reported for the *DLC1* locus, but their relative abundance, tissue distribution and biological functions remain to be determined (Ko et al., 2010; Lukasik et al., 2011). The finding that *DLC1* knockout causes a lethal phenotype in mice due to severe neural tube, brain and cardiac defects (Durkin et al., 2005; Sabbir et al., 2010), points out the relevance of DLC1 in embryonic development and tissue morphogenesis.

The *DLC2* gene was discovered in a loss of heterozygosity (LOH) region on chromosome 13 (13q12.3) where other tumor suppressors like BRCA2 are encoded. Four

transcript variants of *DLC2* have been described and similar to *DLC1*, *DLC2* is widely expressed in normal tissues with high abundance in liver, heart and brain (Ching et al., 2003; Ullmannova and Popescu, 2006). In contrast to *DLC1*, the *DLC2* knockout mouse is viable (Lin et al., 2010; Yau et al., 2009). Moreover, *DLC2* expression was reported to be lost or downregulated in various human cancers and tumor-derived cell lines, classifying the protein as a candidate tumor suppressor (Ching et al., 2003; Ullmannova and Popescu, 2006). This was further confirmed by the observation that *DLC2* overexpression suppressed the growth of MCF7 breast cancer cells and inhibited proliferation, motility and anchorage-independent growth in the human hepatoma cell line HepG2 (Leung et al., 2005; Nagaraja and Kandpal, 2004).

The still poorly characterized *DLC3* protein is encoded on the X chromosome (Xq13). First evidence for *DLC3* was found in 1996, when its cDNA was isolated from a human myeloid cell line library (Nagase et al., 1996). Two *DLC3* isoforms are described, *DLC3 $\alpha$*  and *DLC3 $\beta$* , the former shares 44% sequence identity with *DLC1* and 52% with *DLC2*. *DLC3* expression is also detected in a broad range of human tissues with highest levels in lung, kidney and placenta. Similar to its family members, reduced *DLC3* expression levels were observed in many different types of cancer (Durkin et al., 2007a). Overexpression studies in HeLa cells revealed that *DLC3* alters cell morphology by reducing actin stress fibers in a GAP-dependent manner (Kawai et al., 2007). In addition, expression of *DLC3* in human breast and prostate cancer cell lines inhibited proliferation, colony formation and growth in soft agar, proposing also a potential tumor suppressor function for the third *DLC* family member (Durkin et al., 2007a).

### **1.3.2 Multi-domain structure of *DLC* proteins**

The three *DLC* proteins have a conserved structural organization that includes three functional protein domains, a catalytic RhoGAP domain, a sterile  $\alpha$ -motif domain (SAM) and a StAR (steroidogenic acute regulatory protein)-related lipid transfer domain (START) (Fig. 5). This multi-domain structure allows *DLC* proteins to be regulated in various ways by serving as a platform for protein interactions. Consequently, the different domains contribute to specify the subcellular localization of the RhoGAPs, which is a prerequisite for spatially restricted Rho regulation (Braun and Olayioye, 2015; Lukasik et al., 2011). The SAM domain is located at the N-terminus of *DLC* proteins and comprises around 70 amino acids. Isoforms lacking the SAM domain have been described for *DLC2* and *DLC3* (Ching et al., 2003; Durkin et al., 2007a). SAM domains are commonly found in transcription factors and signaling proteins, they form oligomers or other protein

interactions and certain SAM domains have even been reported to bind to DNA, RNA and lipid molecules (Li et al., 2007; Qiao and Bowie, 2005). In DLC proteins, the role of the SAM domain is not established yet. However, there is evidence that it is involved in regulating DLC localization by serving as a binding site for protein interactions (see section 1.3.3). Moreover, the SAM domain appears to control GAP activity, since DLC1 was described to be more active upon SAM deletion (Kim et al., 2008). In this context, an autoinhibitory mechanism regulating DLC1's GAP activity is discussed based on intramolecular interactions involving the SAM domain.

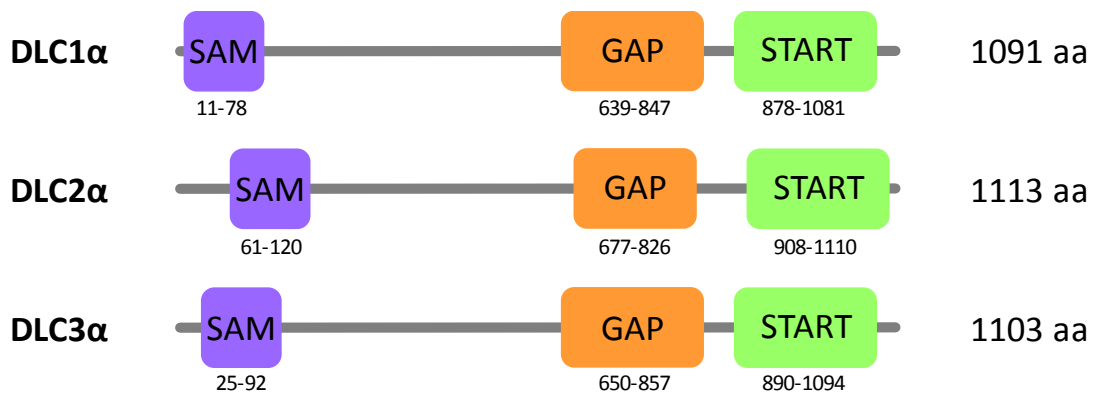


**Figure 5: Multi-domain organization of DLC proteins.** Schematic representation of the three functional domains contained in DLC proteins including a sterile  $\alpha$ -motif (SAM) domain, a catalytic RhoGAP domain and a StAR (steroidogenic acute regulatory protein)-related lipid transfer domain (START). Based on Lukasik et al., 2011.

The RhoGAP domain encompasses about 150-200 amino acids and is the most highly conserved region among the three DLC family members with about 70% sequence identity. All DLC proteins contain a conserved arginine residue (DLC1: R677, DLC2: R699, DLC3: 688) which is crucial for their catalytic GAP activity. This so-called arginine finger stabilizes the transition state during GTP hydrolysis by introducing a positive charge into the catalytic site of the GTPase. Additionally, another two conserved amino acids, a lysine and a second arginine residue within the GAP domain, are essential for the DLC's enzymatic activity (Braun and Olayioye, 2015; Durkin et al., 2007b). In accordance with their GAP domain conservation, all DLC isoforms have been shown to regulate RhoA activity, but displayed only weak or no GAP activity towards Cdc42 and Rac, respectively, at least in *in vitro* studies (Ching et al., 2003; Holeiter et al., 2012; Holeiter et al., 2008; Kawai et al., 2007; Wong et al., 2003). Furthermore, DLC1 has been reported to control RhoB and RhoC activity *in vitro*, which are isoforms closely related to RhoA (Healy et al., 2008). Due to their GAP activity, overexpression of DLC proteins is characterized by a

prominent phenotype, including loss of actin stress fibers, a round cell shape and elongated protrusions (Ching et al., 2003; Kawai et al., 2007; Wong et al., 2005). Considering that DLC depletion also has drastic consequences on cell morphology and function, optimal DLC expression levels and a tight balance of their activity seem to be crucial for normal cellular performance.

The C-terminal START domain of around 210 amino acids length is responsible for the nomenclature of the DLC proteins which are also named StarD12 (DLC1), StarD13 (DLC2) and StarD8 (DLC3). In humans, 15 START domain-containing proteins have been identified which are typically involved in lipid transport and metabolism (Alpy and Tomasetto, 2005; Wirtz, 2006). START domains function as lipid binding pockets transferring single lipid molecules from one membrane compartment to another, while protecting them from the hydrophilic cytosolic environment. However, potential lipid ligands for the DLC START domains are unknown so far and it still has to be investigated whether DLC proteins are involved in lipid transport or rather in lipid signaling. Moreover, DLC2 has been reported to locate to mitochondria in dependence of its START domain (Ng et al., 2006). Considering that other START domain proteins play a role in mitochondrial metabolism (Alpy and Tomasetto, 2005), the involvement of DLC2 in such processes remains to be determined.

Between the SAM and the RhoGAP domain, there is an unstructured region which is the sequence with the least conservation among the three DLC proteins. However, within this region there are several short stretches with higher sequence similarity, for example a consensus LD motif (position 469-476 in DLC1). LD motifs are also found in paxillin and other signaling molecules and mediate their binding to focal adhesion-associated proteins, a mechanism that also determines DLC localization (Brown et al., 1998; Li et al., 2011). Furthermore, serine-rich sequences have been identified within the unstructured region serving as potential phosphorylation sites by serine-threonine kinases to regulate DLC localization and function (Durkin et al., 2007b). Another possible mechanism to control DLC proteins might rely on proline-rich sequences detected within the unstructured middle region which could bind to proline recognition domains, like SH3 domains or WW motifs, contained in many signaling molecules (Durkin et al., 2007b). In summary, the multi-domain structure allows for the regulation of the DLC proteins by various mechanisms and further implicates that they might also have GAP-independent, scaffolding functions (Barras and Widmann, 2013).

### 1.3.3 DLC proteins function at distinct subcellular sites

Partially overlapping but also distinct subcellular localizations have been reported for the three DLC proteins (Fig. 6) which seem to be regulated by differential protein interactions to allow for the spatiotemporal control of Rho activity in the cell (Braun and Olayioye, 2015). The best studied localization of DLC proteins is their association with focal adhesions (FA). Considering that DLC1 depletion is characterized by increased FA and stress fiber formation, while DLC1 overexpression has a GAP-dependent, opposite effect, DLC proteins seem to be strongly involved in Rho regulation during focal adhesion assembly (Holeiter et al., 2008; Wong et al., 2005). Focal adhesions are adhesive structures which connect integrins, as transmembrane receptors for extracellular matrix (ECM) ligands, with the actin cytoskeleton to control stress fiber formation, cell shape and motility. They are built of integrins, signaling molecules like focal adhesion kinase (FAK) and adaptor proteins including paxillin, vinculin and tensin proteins. Focal adhesions represent highly dynamic structures with a permanent turn-over and only some of the transient adhesive contacts mature into tensin-enriched, more stable focal adhesions (Geiger et al., 2001; Zaidel-Bar et al., 2004). First, the DLC rat homolog p122RhoGAP was reported to localize to focal adhesions where it interacts with vinculin (Kawai et al., 2004). Until today, association of all three human DLC proteins with focal adhesions was revealed (Fig. 6) and their interaction with tensin adaptors was investigated in detail (Cao et al., 2012; Kawai et al., 2007; Liao et al., 2007; Qian et al., 2007; Yam et al., 2006). DLC1 was shown to interact with each member of the tensin family through different binding modes. Binding to the Src homology 2 (SH2) and phosphotyrosine-binding (PTB) domains of tensin1 and CTEN is mediated by a binding motif in DLC1 located at position 440-445, whereas the interaction with tensin2 PTB involves a second, alternative DLC1 binding region (position 375-385) (Chan et al., 2009; Liao et al., 2007; Qian et al., 2007). Moreover, binding of tensin3 to the DLC1 SAM domain disrupted an autoinhibitory interaction between the SAM and GAP domains leading to DLC1 activation (Cao et al., 2012). As a consequence, DLC1-mediated RhoA inactivation was observed accompanied by decreased motility and growth of the cells. In addition, DLC2 and DLC3 were both shown to be recruited to focal adhesions by binding to tensin1 and tensin2 (Kawai et al., 2010; Kawai et al., 2007; Kawai et al., 2009; Qian et al., 2007). DLC1 and DLC3 further bind to talin through their LD-like motifs that share homology with the LD motifs of paxillin (Li et al., 2011). Thus, DLC localization at focal adhesions seems to be controlled by a variety of protein interactions. Furthermore, recruitment to focal adhesion was reported to be crucial for the tumor suppressor properties of DLC1. Although mutations disrupting the focal adhesion localization of DLC1 did not impair overall Rho inactivation, the biological

activity of DLC1 was obviously reduced as determined by migration and growth assays (Li et al., 2011; Liao et al., 2007; Qian et al., 2007). However, despite intensive studies on DLC interactions with focal adhesion proteins, further investigations are necessary to elucidate the role and localization of DLC proteins during focal adhesion maturation and dynamics.

Adherens junctions (AJ) represent another subcellular site where DLC1 and DLC3 are located (Fig. 6) (Holeiter et al., 2012; Tripathi et al., 2012). Previous findings concerning the association of DLC3 with adherens junctions are summarized in section 1.3.4. First studies that revealed a role for DLC1 at adherens junctions were performed by ectopic expression of E-cadherin in non-small cell lung cancer (NSCLC) cell lines. By this means, anchorage-independent growth and cell migration were decreased due to RhoA inhibition, a phenotype that could be rescued by DLC1 and p190RhoGAP depletion (Asnaghi et al., 2010). Later the exact mechanism by which DLC1 is recruited to adherens junctions was elucidated, which depends on  $\alpha$ -catenin binding targeting DLC1 to E-cadherin-mediated cell adhesions in a GAP-dependent manner (Tripathi et al., 2012). The DLC1- $\alpha$ -catenin interaction is essential for AJ stability and contributes to the tumor suppressive effect of DLC1 regarding the colony formation and invasion abilities of prostate cancer cells. Additionally, DLC1 was reported to increase E-cadherin expression via RhoA and RhoC inactivation, which strengthened cell aggregation and reduced cell invasion (Tripathi et al., 2014b).

Moreover, DLC1 was identified to act at membrane protrusions and the leading edge of migrating cells and DLC1 expression in fibroblasts particularly inhibited RhoA at the cellular front (Healy et al., 2008). By contrast, DLC1 depletion led to Dia1 enrichment at membrane protrusions of breast cancer cells during directed cell migration enhancing their wound closure ability (Holeiter et al., 2008). This supports the idea that Rho activation occurs not only at the retracting tail of migrating cells, but also in the initial phase of protrusion formation to induce actin polymerization at the leading edge (Palazzo et al., 2001). Another example of how DLC1 localization at the plasma membrane is controlled is provided by the SAM domain-mediated interaction with the elongation factor EF1A1, a regulator of microtubule and actin remodeling. DLC1 promoted membrane association of EF1A1 and thereby inhibited cell migration in a GAP-dependent manner (Zhong et al., 2009). Besides, it has been shown that DLC1 regulates Rho-ROCK signaling at the cell cortex of HCC cells. DLC1 expression was associated with low cortical phosphorylation levels of the ROCK target myosin light chain (MLC), which was the reason for reduced numbers of focal adhesions and stress fibers and for cell shrinkage (Wong et al., 2008).

Another DLC1-protein interaction proposed to play a role at the plasma membrane is the binding of the tumor suppressor PTEN to the SAM domain of DLC1 (Heering et al., 2009). The PTEN-DLC1 interaction seems to be important in the control of directed cell migration, possibly through PTEN-mediated dephosphorylation of FAK at the leading edge of migrating cells.

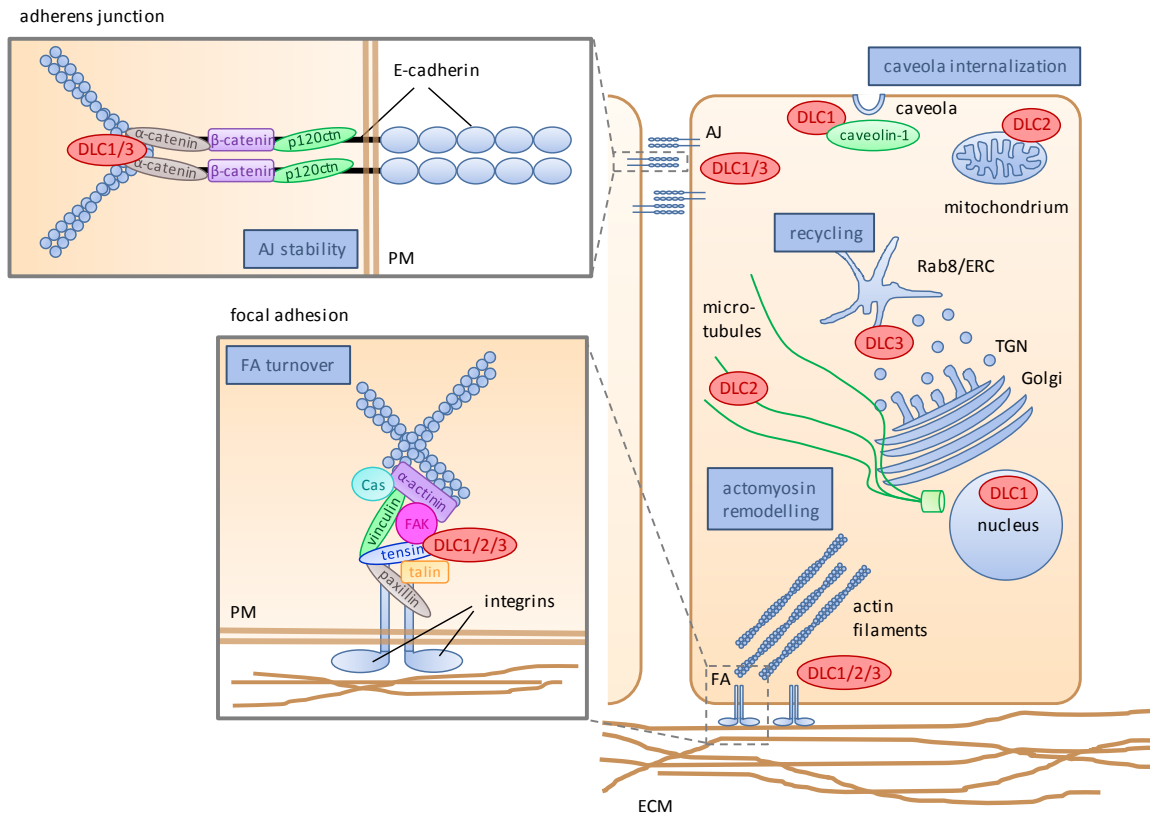


**Figure 6: Subcellular localization of DLC1, DLC2 and DLC3.** The different DLC isoforms and their localization at focal adhesions (FA), adherens junctions (AJ), the Rab8-positive endocytic recycling compartment (ERC), trans-Golgi network (TGN), nucleus, caveolae and mitochondria are depicted. Taken from Braun and Olayioye, 2015.

Further DLC1-protein interactions have been identified which regulate its subcellular localization. Nuclear translocation of DLC1, first discovered in NSCLC cells (Yuan et al., 2007), was impaired upon masking of a nuclear localization signal (NLS) by the adaptor protein 14-3-3 (Scholz et al., 2009). Moreover, Caveolin-1 recruits DLC1 to caveolae, which are invaginations of the plasma membrane that contain many receptors and signaling molecules. This targeting mechanism depends on a binding motif within the START domain of DLC1 and seems to influence its tumor suppressive properties *in vitro* and *in vivo* in a GAP-independent manner (Du et al., 2012; Yam et al., 2006). Finally, DLC1 function is controlled by binding to p120RasGAP, a negative regulator of Ras with ubiquitous expression patterns. P120RasGAP interacts with the arginine finger of the

DLC1-GAP domain decreasing its GAP activity towards RhoA and reducing its tumor suppressive properties (Jaiswal et al., 2014; Yang et al., 2009). Thus, DLC proteins function at different subcellular sites and seem to be regulated by a variety of protein interactions which still have to be uncovered in more detail.

#### **1.3.4 Cellular functions of the DLC3 isoform**

DLC3 is the least characterized member of the DLC family and apart from its localization at focal adhesions (Kawai et al., 2007), DLC3 was identified to localize to the Golgi apparatus and to Rab8-positive membrane tubules in HeLa cells (Braun et al., 2015). Its loss was associated with increased perinuclear RhoA activation and fragmentation of the Rab8- and Golgi-compartments. Furthermore, DLC3 was revealed to coordinate endocytic trafficking of transferrin and epidermal growth factor receptors (EGFR). In particular, DLC3 depletion impaired EGFR degradation and prolonged Akt signaling, which might account for the potential tumor suppressive properties of DLC3 (Braun et al., 2015). Thus, DLC3 was established as a regulator of endocytic transport and organelle integrity by spatially restricting perinuclear Rho activity. Moreover, the full-length DLC3 $\alpha$  isoform has been described to localize to cell-cell adhesions (Holeiter et al., 2012). DLC3 displayed a strong colocalization with E-cadherin and  $\beta$ -catenin at adherens junctions of MCF7 breast cancer cells and was detected at the basolateral membrane of polarized MCF10A acini (Holeiter et al., 2012). In addition, DLC3 depletion caused mislocalization of E-cadherin,  $\beta$ -catenin and p120-catenin at adherens junctions, which was associated with decreased cell aggregation and enhanced cell migration. ROCK inhibition rescued E-cadherin/ $\beta$ -catenin localization at cell adhesions, indicating that DLC3 acts as a regulator of Rho-ROCK signaling that is required for adherens junction integrity (Holeiter et al., 2012).

## 1.4 Aims of the thesis

Rho GTPases play a key role in the regulation of a variety of cytoskeleton-mediated cellular processes by functioning as molecular switches that integrate external stimuli and control appropriate downstream signaling. Studies in which subcellular Rho activation patterns were investigated by the use of genetically encoded biosensors revealed that Rho signaling has to be tightly controlled in time and space. However, the current knowledge about the molecular mechanisms regulating spatiotemporal Rho activation is still limited. Deleted in liver cancer (DLC) proteins represent an extraordinary family of Rho regulators that is deregulated in different types of cancer more frequently than any other RhoGAP protein. Due to their different subcellular localizations, the three DLC proteins are proposed to exert also non-redundant functions. The multi-domain structure of DLCs provides a platform for a variety of molecular control mechanisms which still have to be investigated, in particular with respect to isoform-specific regulation. Numerous DLC1 protein interaction partners controlling DLC1 localization and function have been identified. By contrast, the interactome of the still poorly studied DLC3 isoform remains to be characterized, since apart from FA-associated tensin and talin proteins, no DLC3 binding partners are known until today.

DLC3 has been reported to localize to adherens junctions and basolateral membranes in polarized cells where it controls E-cadherin localization and junction integrity. Thus, the main objective of this thesis was to identify DLC3 protein binding partners by a proteomic approach to gain insights into targeting of DLC3 to specific subcellular sites, especially to cell-cell adhesions. In particular, I aimed to validate and characterize the interaction of DLC3 and the basolateral polarity protein Scribble, one of the mass spectrometry candidates, using biochemical techniques. I further investigated the subcellular localization of DLC3 and Scribble in dependence of each other by immunofluorescence studies in 2D and 3D cell culture models. Moreover, a major aim of this thesis was to uncover the biological functions of the DLC3-Scribble interaction at adherens junctions and investigate the relevance of both proteins for epithelial cell polarization.

## 2. Material and methods

### 2.1 Material

#### 2.1.1 Chemicals and reagents

**Table 1: List of chemicals and reagents used in this thesis.**

<b>Chemicals and Reagents</b>	<b>Company</b>
Acrylamide (Rotiphorese Gel 30)	Carl Roth GmbH & Co., Karlsruhe, Germany
Agar	Carl Roth GmbH & Co., Karlsruhe, Germany
Agarose	Carl Roth GmbH & Co., Karlsruhe, Germany
Ammonium persulfate (APS)	Carl Roth GmbH & Co., Karlsruhe, Germany
Ampicillin	Sigma-Aldrich, St.Louis, USA
Anti-Flag M2 Affinity Gel	Sigma-Aldrich, St.Louis, USA
Blocking reagent	Roche Biosciences, Basel, Switzerland
$\beta$ -Mercaptoethanol	Sigma-Aldrich, St.Louis, USA
Bromphenol blue	Serva, Heidelberg
Complete Protease Inhibitor Cocktail (EDTA free)	Roche Biosciences, Basel, Switzerland
Dimethyl sulfoxide (DMSO)	Carl Roth GmbH & Co., Karlsruhe, Germany
Dithiothreitol (DTT)	Carl Roth GmbH & Co., Karlsruhe, Germany
DNA Orange	Sigma-Aldrich, St.Louis, USA
Ethanol	VWR, Darmstadt, Germany
Ethidium bromide	Roche Biosciences, Basel, Switzerland
Ethylenediaminetetraacetic acid (EDTA)	Carl Roth GmbH & Co., Karlsruhe, Germany
Fluoromount-G	Southern Biotech, Birmingham, USA
Gene Ruler 1 kb Ladder	Thermo Scientific, Waltham, USA
Glutathione beads	Pierce/Thermo, Rockford, USA
$\beta$ -Glycerophosphate	Sigma-Aldrich, St.Louis, USA
Glycine	Carl Roth GmbH & Co., Karlsruhe, Germany
Goat serum	Invitrogen, Karlsruhe, Germany
Hydrochloric acid (HCl)	Carl Roth GmbH & Co., Karlsruhe, Germany

## Material and methods

---

Chemicals and Reagents	Company
Isopropanol	Carl Roth GmbH & Co., Karlsruhe, Germany
Kanamycin	Carl Roth GmbH & Co., Karlsruhe, Germany
Magnesium chloride (MgCl <sub>2</sub> )	Carl Roth GmbH & Co., Karlsruhe, Germany
Methanol	Carl Roth GmbH & Co., Karlsruhe, Germany
NP-40 (Nonidet P40)	Sigma-Aldrich, St.Louis, USA
PageRuler - prestained protein ladder	Thermo Scientific, Waltham, USA
Paraformaldehyde (PFA)	Carl Roth GmbH & Co., Karlsruhe, Germany
Phenylmethylsulphonyl fluoride (PMSF)	Sigma-Aldrich, St.Louis, USA
Potassium chloride (KCl)	Carl Roth GmbH & Co., Karlsruhe, Germany
Protein G Sepharose beads	KPL, Gaithersburg, USA
N,N,N,N-Tetramethylethyldiamine (TEMED)	Carl Roth GmbH & Co., Karlsruhe, Germany
Sodium azide (NaN <sub>3</sub> )	Sigma-Aldrich, St.Louis, USA
Sodium chloride (NaCl)	Carl Roth GmbH & Co., Karlsruhe, Germany
Sodium dodecyl sulfate (SDS)	Carl Roth GmbH & Co., Karlsruhe, Germany
Sodium fluoride (NaF)	Carl Roth GmbH & Co., Karlsruhe, Germany
Sodium hydroxide (NaOH)	Carl Roth GmbH & Co., Karlsruhe, Germany
Sodium orthovanadate (Na <sub>3</sub> VO <sub>4</sub> )	Sigma-Aldrich, St.Louis, USA
Trichloroacetic acid	Carl Roth GmbH & Co., Karlsruhe, Germany
Thimerosal	Carl Roth GmbH & Co., Karlsruhe, Germany
Tris-hydroxymethyl-aminomethane (Tris)	Carl Roth GmbH & Co., Karlsruhe, Germany
Triton-X-100	Carl Roth GmbH & Co., Karlsruhe, Germany
Tween-20	Carl Roth GmbH & Co., Karlsruhe, Germany

### 2.1.2 Equipment

**Table 2: List of equipment used in this thesis.**

<b>Equipment</b>	<b>Company</b>
Beckman Coulter Centrifuge Avanti J-30I (Rotor J20)	Beckman Coulter, Krefeld, Germany
Beckman Coulter Centrifuge J2-MC Centrifuge (Rotor J20)	Beckman Coulter, Krefeld, Germany
Casy (cell counter)	Roche, Basel, Switzerland
CK2 (standard light microscope)	Olympus, Hamburg, Germany
Curix 60 processor (western blot device)	Agfa, Düsseldorf, Germany
Eppendorf Centrifuge 5415D	Eppendorf, Hamburg, Germany
Eppendorf Centrifuge 5415R	Eppendorf, Hamburg, Germany
Gel Documentation Camera Felix 2000, Dark hood DH-50, transilluminator UST-20M-8R	Biostep, Jahnsdorf, Germany
LSM 710 (confocal laser scanning microscope)	Zeiss, Jena, Germany
iBlot® Gel Transfer Device	Life technologies, Carlsbad, CA, USA
NanoDrop® ND-1000 (Spectrophotometer)	peQLab, Erlangen, Germany
Nucleofector™ 2b Device	Lonza, Basel, Switzerland
Semi-dry blotting chamber	Phase, Luebeck, Germany
Sonopuls HD 200 (sonyfier)	Bandelin, Berlin, Germany
Quantitative PCR Cfx96	Biorad, Munich, Germany
Tecan Infinite 200 Reader	Tecan, Crailsheim, Germany

### 2.1.3 Consumables

**Table 3: List of consumables used in this thesis.**

<b>Consumables</b>	<b>Company</b>
8-well glass chamber slides	BD Transduction Laboratories, Heidelberg, Germany
Glass coverslips 18 mm x 18 mm	Carl Roth GmbH & Co., Karlsruhe, Germany
iBlot® Gel Transfer Stacks Nitrocellulose, Regular	Life technologies, Carlsbad, CA, USA
Multiplate™ PCR Plates (MLL9651)	Bio-Rad Laboratories, Hercules, CA, USA
NuPAGE® Novex® 4-12% Bis-Tris Midi Protein Gels	Life technologies, Carlsbad, CA, USA
Roti®-PVDF transfermembrane	Carl Roth GmbH & Co., Karlsruhe, Germany

Consumables	Company
Whatman® cellulose blotting papers, 3 mm	Schleicher & Schuell, Dassel, Germany
X-ray films	CEA, Strangnas, Sweden

### 2.1.4 Buffers and solutions

**Table 4: List of buffers and solutions used in this thesis.**

Buffers and Solutions	Composition
Agarose gel solution	1% (w/v) agarose, 0.6 µg/ml ethidium bromide (EtBr) in TAE
Blocking Solution (IF)	5% (v/v) goat serum (Invitrogen), 0.1% (v/v) Tween-20 in PBS
Blocking Solution (WB)	0.5% (v/v) blocking solution (Roche), 0.05% (v/v) Tween-20, 0.01% (v/v) thimerosal in PBS
Blotting Buffer	200 mM glycine, 25 mM Tris base, 20% (v/v) methanol in ddH <sub>2</sub> O
Detergent-free lysis buffer	50 mM HEPES, pH 7.4, 100 mM NaCl, 5 mM MgCl <sub>2</sub> , 0.5 mM EDTA, 1 mM DTT, 1 mM sodium orthovanadate, 0.5 mM PMSF plus Complete protease inhibitors in ddH <sub>2</sub> O
Elution buffer GST-fusion proteins	50 mM Tris, 10 mM reduced glutathione in ddH <sub>2</sub> O, pH 8.0
Extraction buffer	50 mM Tris (pH 7.5), 150 mM NaCl, 1 mM EDTA, 1 mM Na <sub>3</sub> VO <sub>4</sub> , 10 mM sodium fluoride, 0.5 mM PMSF, 20 mM β-glycerophosphate and Complete protease inhibitors in ddH <sub>2</sub> O
Laemmli sample buffer (5x)	400 mM Tris pH 6.8, 500 mM dithiothreitol, 50% (v/v) glycerol, 10% (w/v) SDS, 0.2% (w/v) bromophenol blue in ddH <sub>2</sub> O
LB medium (5x)	5% (w/v) peptone, 2.5% (w/v) yeast extract, 2.5% (w/v) NaCl in ddH <sub>2</sub> O for selection: LB medium + ampicillin or kanamycin for plates: LB medium + 2% (w/v) agar
1% NEB lysis buffer / 1% TEB lysis buffer	50 mM Tris (pH 7.5), 150 mM NaCl, 1% (v/v) NP-40 / 1% Triton X-100, 1 mM EDTA, 1 mM Na <sub>3</sub> VO <sub>4</sub> , 10 mM sodium fluoride, 0.5 mM PMSF, 20 mM β-glycerophosphate and Complete protease inhibitors in ddH <sub>2</sub> O
PBS	140 mM NaCl, 2.7 mM KCl, 8 mM Na <sub>2</sub> HPO <sub>4</sub> , 1.5 mM KH <sub>2</sub> PO <sub>4</sub> in ddH <sub>2</sub> O, pH 7.4
PBS-Tween	0.05% (v/v) Tween-20 in PBS

Buffers and Solutions	Composition
Permeabilization solution (IF)	0.2% (v/v) Triton X-100 in PBS
PFA	4% (v/v) PFA in PBS
RIPA lysis buffer	50 mM Tris pH 7.5, 150 mM NaCl, 10 mM NaF, 20 mM $\beta$ -glycerolphosphate, 1 mM EDTA, 1% (v/v) NP-40, 0.1% (v/v) SDS, 0.25% (v/v) NaDOC, 1 mM $\text{Na}_3\text{VO}_4$ , 0.5 mM PMSF and Complete protease inhibitors in ddH <sub>2</sub> O
S1 resuspension buffer	50 mM Tris pH 8.0, 10 mM EDTA, 0.1 mg/ml RNaseA in ddH <sub>2</sub> O
S2 lysis buffer	200 mM NaCl, 1% (w/v) SDS in ddH <sub>2</sub> O
S3 neutralization buffer	2.8 M $\text{CH}_3\text{CO}_2\text{K}$ in ddH <sub>2</sub> O, pH 5.1
Separating gel solution	8% and 10% (v/v) acrylamide, 375 mM Tris pH 8.8, 0.1% (w/v) SDS, 0.1% APS, 0.06% TEMED in ddH <sub>2</sub> O
Stacking gel solution	5% (v/v) acrylamide, 130 mM Tris pH 6.8, 0.1% (w/v) SDS, 0.1% APS, 0.1% TEMED in ddH <sub>2</sub> O
SDS-PAGE running buffer	25 mM Tris pH 8.8, 192 mM glycine, 0.1% (v/v) SDS in ddH <sub>2</sub> O
TAE buffer	40 mM Tris acetate, 1 mM EDTA in ddH <sub>2</sub> O, pH 8.0

### 2.1.5 Human cell lines

**Table 5: List of cell lines used in this thesis.**

Cell line	obtained form
Caco-2	Interlab Cell Line Collection, Genova, Italy
HEK293T	ATCC, Manassas, USA
HeLa	ATCC, Manassas, USA
MCF-7	Institute of Clinical Pharmacology, Stuttgart, Germany

### 2.1.6 Cell culture reagents and media

**Table 6: List of cell culture reagents and media used in this thesis.**

Cell culture reagents and media	Company
PureCol®-S collagen	Advanced Biomatrix, San Diego, USA
Collagen R solution	Serva, Heidelberg, Germany
Cholara toxin (CTX)	Sigma-Aldrich, St.Louis, USA

Cell culture reagents and media	Company
DharmaFECT1	Dharmacon, Lafayette, CO, USA
Doxycycline (dox)	Merck, Darmstadt, Germany
Epidermal growth factor (EGF)	R&D Systems, Minneapolis, USA
Fetal calf serum (FCS)	PAA Laboratories, Pasching, Austria
ROCK inhibitor H1152	Calbiochem, Darmstadt, Germany
Rho inhibitor CT04	Cytoskeleton, Denver, USA
Lipofectamin® RNAiMAX	Invitrogen, Karlsruhe, Germany
Lipofectamine® LTX with PLUS™	Invitrogen, Karlsruhe, Germany
Growth factor reduced matrigel	BD Bioscience, Franklin Lakes, USA
OptiMEM®	Invitrogen, Karlsruhe, Germany
RPMI 1640	Invitrogen, Karlsruhe, Germany
Trypsin-EDTA (10x)	Invitrogen, Karlsruhe, Germany
TurboFect™	Thermo Scientific, Rockford, USA

### 2.1.7 Plasmids

**Table 7: List of plasmid vectors used in this thesis.**

Plasmids	Source
pEGFP-C1 (empty vector)	Clontech laboratories, Mountain View, USA
pEGFP-C1-Anillin AHPH WT	Kindly provided by Alpha Yap, University of Queensland, Australia (Piekny and Glotzer, 2008; Priya et al., 2015)
pEGFP-C1-Anillin AHPH A70D, E758K (DM)	Kindly provided by Alpha Yap, University of Queensland, Australia (Piekny and Glotzer, 2008; Priya et al., 2015)
pEGFP-C1-DLC3 $\alpha$ WT	described in Holeiter et al., 2012
pEGFP-C1-DLC3 $\alpha$ K725E	described in Holeiter et al., 2012
pEGFP-C1- DLC3 WT $\Delta$ PDZ ligand	PCR cloning (see section 2.2.1)
pEGFP-C1-DLC3 K725E $\Delta$ PDZL	PCR cloning (see section 2.2.1)
pEGFP-C1-DLC1	described in Erlmann et al., 2009
pEGFP-C1-DLC2	described in Erlmann et al., 2009
pCR.V62-Met-Flag-DLC3 $\alpha$ WT	described in Braun et al., 2015
pCR.V62-Met-Flag DLC3 $\alpha$ K725E	described in Braun et al., 2015

Plasmids	Source
pCR.V62-Met-Flag DLC3 WT ΔPDZL	PCR cloning (see section 2.2.1)
pCR.V62-Met-Flag DLC3 K725E ΔPDZL	PCR cloning (see section 2.2.1)
pWHE636 (empty vector)	Kindly provided by Tilman Brummer, University of Freiburg, Germany
pWHE636-GFP-DLC3 WT	PCR cloning (see section 2.2.1)
pWHE636-GFP-DLC3 K725E	PCR cloning (see section 2.2.1)
pWHE636-GFP-DLC3 WT ΔPDZL	PCR cloning (see section 2.2.1)
pWHE636-GFP-DLC3 K725E ΔPDZL	PCR cloning (see section 2.2.1)
GFP-human(h)Scrib	Kindly provided by Jean-Paul Borg, Centre de Recherche en Cancérologie de Marseille, France
pEGFP-C1-Scrib LRR	PCR cloning (see section 2.2.1)
pEGFP-C1-Scrib LRR-DLC3 GAP WT	PCR cloning (see section 2.2.1)
pEGFP-C1-Scrib LRR-DLC3 GAP K725E	PCR cloning (see section 2.2.1)
pDEST15-GST-PDZ1 hScrib	Kindly provided by Jean-Paul Borg, Centre de Recherche en Cancérologie de Marseille, France
pDEST15-GST-PDZ2 hScrib	Kindly provided by Jean-Paul Borg, Centre de Recherche en Cancérologie de Marseille, France
pDEST15-GST-PDZ3 hScrib	Kindly provided by Jean-Paul Borg, Centre de Recherche en Cancérologie de Marseille, France
pDEST15-GST-PDZ4 hScrib	Kindly provided by Jean-Paul Borg, Centre de Recherche en Cancérologie de Marseille, France
pGEX-6P-3-GST-Scrib PDZ1-PDZ4	PCR cloning (see section 2.2.1)

### 2.1.8 Antibodies and fluorescent dyes

**Table 8: List of primary antibodies used for immunoblotting and immunofluorescence.**

Antibody	Species	Dilution	Company
anti-DLC3 (E-2)	mouse mAb	1:500 (WB)	Santa Cruz Biotechnology, Dallas, USA
anti-E-cadherin	mouse mAb	1:250 (IF)	BD Transduction Laboratories, Heidelberg, Germany
anti-E-cadherin	rabbit mAb	1:200 (IF)	Cell Signaling, Danvers, USA
anti-Flag M2	mouse mAb	1:2000 (WB)	Sigma-Aldrich, St.Louis, USA
anti-GAPDH	rabbit pAb	1:15000 (WB)	Sigma-Aldrich, St.Louis, USA

Material and methods

Antibody	Species	Dilution	Company
anti-GFP	mouse mAb	1:250 (IF) 1:2000(WB)	Roche Biosciences, Basel, Switzerland
anti-GST	goat pAb	1:5000 (WB)	GE Healthcare, Piscataway, USA
anti-GST IRDye 800	goat mAb	1:15000 (WB)	Licor Biotechnology, Nebraska, USA
anti-pMLC (Ser19)	rabbit pAb	1:50 (IF)	Cell Signaling, Danvers, USA
anit-RhoA (26C4)	mouse mAb	1.200 (IF)	Santa Cruz Biotechnology, Dallas, USA
anti-Scrib (C-20)	goat pAb	1:250 (WB)	Santa Cruz Biotechnology, Dallas, USA
anti-Scrib (H-300)	rabbit pAb	1:100 (IF) 1:200 (WB)	Santa Cruz Biotechnology, Dallas, USA
anti-TfnR	mouse mAb	1:1000 (WB)	Invitrogen, Karlsruhe, Germany
anti- $\alpha$ -tubulin	mouse mAb	1:2000 (WB)	Sigma-Aldrich, St.Louis, USA
anti-Cbl (A-9)	mouse mAb	(unrelated control IgG for ColP)	Santa Cruz Biotechnology, Dallas, USA

**Table 9: List of secondary antibodies used for immunoblotting and immunofluorescence.**

Antibody	Species	Dilution	Company
Alexa Fluor® 488/546/633 anti-mouse	goat	1:500 (IF)	Invitrogen, Karlsruhe, Germany
Alexa Fluor® 488/546/633 anti-rabbit	goat	1:500 (IF)	Invitrogen, Karlsruhe, Germany
Horseradish peroxidase (HRP)-anti-mouse IgG	sheep	1:1000 (WB)	GE Healthcare, Piscataway, USA
HRP-anti-rabbit IgG	donkey	1:1000 (WB)	GE Healthcare, Piscataway, USA
HRP-anti-goat IgG	donkey	1:10000 (WB)	Santa Cruz Biotechnology, Dallas, USA
IRDye 800 CW anti-mouse IgG	goat	1:15000 (WB)	Licor Biotechnology, Nebraska, USA

**Table 10: Fluorescent dyes used for immunofluorescence.**

Dye	Dilution	Company
Alexa Fluor® 633 phalloidin	1:100 (IF)	Invitrogen, Karlsruhe, Germany
DAPI	1:5000 (IF)	Sigma-Aldrich, St.Louis, USA

### 2.1.9 Kits

**Table 11: Kits used in this thesis.**

Kits	Company
Cell Line Nucleofector® Kit V	Lonza, Basel, Switzerland
DC Protein Assay	Bio-Rad, Hercules, USA
Duolink® In situ Orange Kit mouse/rabbit	Sigma-Aldrich, St.Louis, USA
HRP SuperSignal®West substrate pico	Pierce/Thermo, Rockford, USA
HRP SuperSignal®West substrate dura	Pierce/Thermo, Rockford, USA
PureLink™ HiPure Plasmid Purification Kit	Invitrogen, Karlsruhe, Germany
PureLink™ PCR Purification Kit	Invitrogen, Karlsruhe, Germany
PureLink™ Quick Gel Extraction Kit	Invitrogen, Karlsruhe, Germany
QuantiTect Primer Assays®	Qiagen, Foster City, USA
RNeasy® Plus Mini Kit	Qiagen, Foster City, USA

### 2.1.10 Enzymes

**Table 12: Enzymes used for cloning.**

Enzymes	Company
FastAP™ (Thermosensitive Alkaline Phosphatase)	Thermo Scientific, Waltham, USA
Pfu DNA Polymerase	Thermo Scientific, Waltham, USA
Restriction enzymes	Thermo Scientific, Waltham, USA
T4 DNA Ligase	Thermo Scientific, Waltham, USA

### 2.1.11 Small interfering RNA (siRNA)

All siRNAs were diluted in 1x siRNA buffer (MWG Biotech) to a concentration of 20 µM or 2 µM. As a non-targeting negative control (spNT), ON-TARGETplus® non-targeting control SMARTpool siRNA (D-001810-10, Dharmacon) was used. Three independent DLC3-specific siRNAs and three independent Scrib-specific siRNAs were used. spDLC3 refers to siGENOME SMARTpool human STARD8 (M-010254, Dharmacon), siDLC3#1 corresponds to Silencer®Select human STARD8 (s18825, Invitrogen) and siDLC3#2 is Silencer®Select human STARD8 (s18826, Invitrogen). spScrib corresponds to ON-TARGETplus® SMARTpool human Scrib (L-010500-00, Dharmacon), siScrib#1 refers to Silencer®Select human Scrib (s23970, Invitrogen) and siScrib#2 is Silencer®Select human Scrib (s23971, Invitrogen).

## 2.2 Methods

### 2.2.1 Cloning strategies

pEGFP-C1-DLC3 $\alpha$  WT and K725E, pEGFP-C1-DLC1, pEGFP-C1-DLC2, pCR.V62-Met-Flag-DLC3 $\alpha$  WT and K725E vectors were described previously (Braun et al., 2015; Erlmann et al., 2009; Holeiter et al., 2012). pEGFP-C1-Anillin AHPH WT and A70D/E758K (DM) were kindly provided by Alpha Yap (University of Queensland, Australia) (Piekny and Glotzer, 2008; Priya et al., 2015). Expression vectors encoding GFP-tagged human (h)Scribble, pDEST15-GST-PDZ1 hScribble, pDEST15-GST-PDZ2 hScribble, pDEST15-GST-PDZ3 hScribble and pDEST15-GST-PDZ4 hScribble were kindly provided by Jean-Paul Borg (Centre de Recherche en Cancérologie de Marseille, France). pCR.V62-Met-Flag DLC3 WT and K725E  $\Delta$ PDZL vectors were generated by PCR amplification using pCR.V62-Met-Flag-DLC3 $\alpha$  WT and K725E as a template, respectively, and the following forward and reverse primers: 5'-CCGGAATTCCTCTGCTGGACGTTTTCTG-3' and 5'-CCGGAATTCTCAGCCCGCTGCCTGCAGGG-3'. PCR products were cloned into the pCR.V62-Met-Flag vector by EcoRI restriction. pEGFP-C1- DLC3 WT and K725E  $\Delta$ PDZL were generated by PCR amplification using pEGFP-C1-DLC3 WT and K725E as a template, respectively, and the following forward and reverse primers: 5'-CCGGAATTCTCCTCTGCTGGACGTTTTCTG-3' and 5'-CCGGAATTCTCAGCCCGCTGCCTGCAGGG-3'. PCR products were cloned into pEGFP-C1 by EcoRI restriction. pEGFP-C1-Scribble LRR was obtained by PCR amplification of the Scribble LRR (aa1-420) using the GFP-hScribble expression vector as a template and the following forward and reverse primers: 5'-CCGGAATTCCATGCTCAAGTGCATCCCGCTG-3' and 5'-CCGGTCGACGGGCTGCTGGGGCAGCAA-3'. The PCR product was cloned into pEGFP-C1 by EcoRI/Sall restriction. pEGFP-C1-Scribble LRR-DLC3 GAP WT and K725E were generated by subcloning of the respective GAP domains from pEGFP-C1-DLC3-SAM-GAP WT and K725E (Braun et al., 2015) into pEGFP-C1-Scribble LRR lacking a stop codon by Sall restriction. pWHE636-GFP-DLC3 full-length and  $\Delta$ PDZL (GAP WT and K725E) were generated by PCR amplification using pEGFP-C1-DLC3 full-length or  $\Delta$ PDZL (GAP WT and K725E) as templates and the following forward primer 5'-CCGGCGCCGCATGGTGAGCAAGGGCGAGGAC-3' and reverse primer 5'-CCGGCGCCGCTCACAGCTTTGTCTCAGGGCCC-3' for the full-length and 5'-CCGGCGCCGCTCAGCCCGCTGCCTGCAGGG-3' for the  $\Delta$ PDZL constructs, respectively. PCR products were cloned into pWHE636 (provided by Tilman Brummer, University of Freiburg, Germany) by NotI restriction. pGEX-6P-3-GST-Scribble PDZ1-PDZ4 was obtained by PCR amplification of Scribble PDZ1-PDZ4 (aa728-1194)

using GFP-hScribble as a template and the following forward and reverse primers: 5'-CCGGAATTCCACCCTCACCATCCTGCGGC-3' and 5'-CCGGTCTGACTCAGGCCTCGAAGCCGTCACAG-3'. The PCR product was cloned into pGEX-6P-3 by EcoRI/Sall restriction. All amplified cDNAs were verified by sequencing. Oligonucleotides were from Eurofins MWG Operon (Ebersberg, Germany). All plasmid vectors used in this work are listed in Table 7.

### ***Transformation of E.coli***

Transformation of *Escherichia coli* DH5 $\alpha$  (Invitrogen) with recombinant plasmids was performed by heat shock. 100  $\mu$ l competent *E.coli* were thawed on ice and 5  $\mu$ l of ligation mixture were added. After 10 min incubation on ice, a heat shock at 42°C was applied for 1 min and the transformation mix was cooled down on ice for 2 min. Then, the sample was diluted in 1 ml LB medium and incubated at 37°C with shaking for 1 h, before the bacteria were pelleted at 5000 rpm for 1 min and resuspended in 100  $\mu$ l LB medium. The transformed bacteria were plated on LB plates containing the appropriate antibiotic (1x kanamycin or ampicillin), followed by incubation at 37°C overnight.

### ***Purification of plasmid DNA***

To isolate recombinant plasmid DNA, 2 ml of LB medium containing the appropriate antibiotic (1x kanamycin or ampicillin) were inoculated with a single *E.coli* colony and incubated overnight at 37°C with shaking. The next day, the bacteria suspension was pelleted (13,000 rpm, 2 min) and resuspended in 150  $\mu$ l buffer S1. To lyse the cells, 150  $\mu$ l buffer S2 were added and the sample was mixed by inverting. After 5 min incubation at room temperature, 150  $\mu$ l buffer S3 were added and the sample was mixed again by inverting. The precipitate was removed by centrifugation (13,000 rpm, 10 min) and the cleared supernatant was transferred into a new Eppendorf tube. The sample was mixed with 1 ml 100% ethanol, incubated on ice for 10 min and centrifuged for 5 min at 13,000 rpm. The DNA pellet was washed with 70% ethanol and spun down at 13,000 rpm for 2 min. Finally, the purified DNA was dried and dissolved in 30  $\mu$ l ddH<sub>2</sub>O. To verify the correct insertion of DNA fragments, the recombinant plasmid DNA was subjected to restriction enzyme digestion followed by agarose gel electrophoresis. To isolate larger amounts of plasmid DNA, overnight cultures of 100 ml LB medium containing kanamycin or ampicillin were inoculated with transformed *E.coli*. Plasmid DNA was purified using the PureLink™ HiPure plasmid DNA purification Kit (Invitrogen) according to the manufacturer's instructions. Cell lysates were cleared by filtration through filter papers ( $\varnothing$  125 mm, Macherey – Nagel) instead of centrifugation. The concentration of purified

DNA was measured with a spectrophotometer (NanoDrop® ND-1000, Thermo Fisher Scientific) and adjusted in ddH<sub>2</sub>O to a final concentration of 0.5 µg/µl.

### **2.2.2 Cell culture and transfection**

HEK293T, HeLa, MCF7 and Caco-2 cells were cultured in RPMI 1640 supplemented with 10% FCS and incubated in a humidified atmosphere of 5% CO<sub>2</sub> at 37 °C. Caco-2 cells were reauthenticated by SNP analysis in 2016 (Multiplexion, Immenstadt, Germany). All other cell lines were authenticated by morphology and growth characteristics and tested for mycoplasma. Cells were passaged every 3-4 days before they reached confluency using 1x Trypsin/EDTA. Every 3 months, fresh cultures were established from frozen stocks in cell culture medium and 10% DMSO stored in liquid nitrogen. Cell numbers were determined using a Casy® cell counter. For 3D cultures, Caco-2 cells were seeded on a matrix of growth factor reduced matrigel (BD) and PureCol®-S collagen (Advanced Biomatrix) (1:1) and overlaid with growth medium containing 2% matrigel. For knockdown experiments in 3D culture, 10 ng/ml EGF (R&D) was added to the medium. Three days post seeding, lumen formation was induced by 100 ng/ml cholera toxin (Sigma Aldrich). Transgene expression in Caco-2tet cells was induced with 2 µg/ml doxycycline (dox).

#### ***Transient transfection with plasmid DNA***

In HEK293T cells, plasmid transfections were performed with Turbofect® (Thermo Scientific) according to the manufacturer's instructions. 4x10<sup>5</sup> HEK293T cells were seeded in 2 ml growth medium in a 6-well format 24 h prior to transfection. For each well, a transfection mix was prepared containing 400 µl OptiMEM®, 4 µg DNA and 6 µl Turbofect® and incubated 15-20 min at room temperature. In the case of double transfections, 1 µg of each plasmid were used to obtain the same amount of total DNA. The transfection mix was added dropwise to the cells and the cells were analyzed 24 h post transfection. MCF7 cells were transiently transfected with Lipofectamine® LTX (Invitrogen) according to the manufacturer's instructions. Briefly, 3x10<sup>5</sup> MCF7 cells were seeded in 2 ml growth medium per 6-well 24 h prior to transfection. A transfection mix for each well was prepared in 500 µl OptiMEM® by adding 2.5 µg DNA and 8.5 µl Lipofectamine® LTX reagent. After 25 min incubation at room temperature, the transfection mix was added dropwise to the cells. 24 h post transfection, the cells were subjected to further analysis.

### ***Transient transfection with siRNA***

For gene silencing, MCF7 cells were reverse transfected with small interfering RNAs (siRNAs) using Lipofectamine® RNAiMAX (Invitrogen). To avoid RNA degradation, only RNase-free reaction tubes, solutions and pipette tips were used.  $3 \times 10^5$  MCF7 cells were seeded in 2 ml RPMI + 10% FCS in a 6-well format. For each well, 5 nM siRNA (6  $\mu$ l of a 2  $\mu$ M stock solution) and 5  $\mu$ l Lipofectamine® RNAiMAX were diluted in 500  $\mu$ l OptiMEM® and incubated for 10-15 min at room temperature. The transfection mix was added dropwise to the freshly seeded cells which were analyzed 72 h post transfection. For immunofluorescence experiments,  $1 \times 10^5$  MCF7 cells were seeded on collagen-coated glass coverslips in 1 ml growth medium. The transfection mix was scaled down to 5 nM siRNA and 2  $\mu$ l Lipofectamine® RNAiMAX in 200  $\mu$ l OptiMEM®. Alternatively, MCF7 cells transfected with siRNA in a 6-well format were replated onto coated glass-coverslips 48 h post transfection at high confluency and analyzed the next day. siRNA transfections in Caco-2 cells were performed using DharmaFECT1 (Dharmacon) according to the manufacturer's instructions. Briefly,  $1.5 \times 10^5$  Caco-2 cells were seeded per 12-well 24 h prior to transfection. The next day, the medium was exchanged for 800  $\mu$ l fresh RPMI + 10% FCS. 2.5  $\mu$ l siRNA (20  $\mu$ M stock) were diluted in 97.5  $\mu$ l OptiMEM®, while 2.5  $\mu$ l DharmaFECT1 were diluted in 97.5  $\mu$ l OptiMEM® in a second reaction tube and incubated for 5 min at room temperature. Subsequently, both transfection components were mixed and incubated for another 20 min at room temperature followed by dropwise addition to the cells. The next day, the Caco-2 cells were either seeded in 3D matrigel cultures or grown in 2D culture until they were further analyzed. Transient cell transfections in different cell culture formats were performed by up or down scaling of the protocols described above according to the surface areas.

### ***Generation of stable cell lines***

The generation of MCF7 cells stably expressing GFP-DLC3 WT or K725E was described previously (Holeiter et al., 2012). Stable MCF7 cells expressing GFP-DLC3 WT  $\Delta$ PDZ or K725E  $\Delta$ PDZL and GFP-Scrib LRR, LRR-GAP WT or K725E were generated by transfection of the expression vectors using Lipofectamine® LTX followed by selection with 1 mg/ml G418 (Calbiochem) and FACS sorting of GFP-positive cells. Briefly, 1.6 million cells were seeded in 10 ml RPMI + 10% FCS in a 10 cm-dish 24 h prior to transfection. A transfection mix was prepared by diluting 20  $\mu$ g plasmid DNA and 70  $\mu$ l Lipofectamine® LTX in 4 ml OptiMEM®. After 25 min incubation at room temperature, the mix was added dropwise to the cells. After 48 h, cells were subjected to selection with 1 mg/ml G480 for at least 2 weeks. Stable expression of the GFP-fusion proteins was

verified by FACS analysis and immunofluorescence microscopy. Caco-2tet cells, stably expressing the doxycycline-inducible system components rtTA and rtTS were described previously (Röring et al., 2012). Caco-2tet GFP-DLC3 WT or K725E cells and Caco-2tet GFP-DLC3 WT  $\Delta$ PDZL or K725E  $\Delta$ PDZL cells were generated by nucleofection (program B024, Kit T, Lonza) of respective pWHE-636-GFP-DLC3 vectors. Briefly, three nucleofection cuvettes were used for the generation of each cell line. For each cuvette,  $7 \times 10^5$  Caco-2tet cells stably expressing the doxycycline-inducible system components rtTA and rtTS were resuspended in 100  $\mu$ l nucleofection solution and 2  $\mu$ g linearized plasmid DNA were added. After nucleofection, the cells were recovered in 500  $\mu$ l prewarmed RPMI + 10% FCS and seeded in a 10 cm-dish containing 10 ml growth medium. 48 h post transfection, selection with 5  $\mu$ g/ml blasticidin and puromycin was started and continued for three weeks. Inducible transgene expression was verified by adding 2  $\mu$ g/ml doxycycline overnight followed by microscopic analysis.

### **2.2.3 NanoLC-MS/MS analysis and MS data processing**

Flag-tagged proteins were immunoprecipitated from cell lysates (in 1% TEB) with Flag M2 agarose (Sigma Aldrich). Beads were washed with 1% TEB and PBS followed by elution with 0.1 M glycine (pH 2.5) and neutralization with a 1/10 volume of 1 M Tris-HCl (pH8.0). Protein expression and immunopurification were verified by parallel immunoblotting. Eluates were loaded on a NuPAGE Bis-Tris 4-12% gradient gel (Invitrogen) for a short gel run and proteins were in-gel digested with trypsin (Borchert et al., 2010). Peptide mixtures were separated on the EasyLC nano-HPLC (Thermo Scientific) coupled to an LTQ Orbitrap Elite (Thermo Scientific). Binding and chromatographic separation of peptides was performed on a 15 cm fused silica emitter of 75  $\mu$ m inner diameter (Proxeon Biosystems), in-house packed with reversed-phase ReproSil-Pur C18-AQ 3  $\mu$ m resin (Dr. Maisch GmbH). Peptide mixtures were injected in HPLC solvent A (0.5% acetic acid) at a flow rate of 500 nl/min and subsequently eluted with an 87 minute segmented gradient of 10–50% HPLC solvent B (80% acetonitrile in 0.5% acetic acid) at a flow rate of 200 nl/min. The mass spectrometer was operated in the data-dependent mode to automatically switch between MS and MS/MS acquisition. Precursor ions were acquired in the mass range from m/z 300-2000 in the Orbitrap mass analyzer at a resolution of 120,000. The accumulation target value was set to 106 charges. The 20 most intense ions were sequentially isolated and fragmented in the linear ion trap using collision-induced dissociation (CID) at the ion accumulation target value of 5000 and default CID settings. Ions already selected for MS/MS were dynamically excluded for 60 s. Acquired MS spectra were processed with MaxQuant software package version 1.5.2.8 (Cox and Mann,

2008) with integrated Andromeda search engine (Cox et al., 2011). Database search was performed against a target-decoy *Homo sapiens* database obtained from Uniprot, containing 91,675 protein entries and against databases containing sequences of different Flag-tagged DLC3 variants and 245 commonly observed contaminants. Endoprotease trypsin was defined as the protease with a maximum missed cleavage of two. Oxidation of methionines and N-terminal acetylation were specified as variable modifications, whereas carbamidomethylation on cysteines was defined as a fixed modification. Initial maximum allowed mass tolerance was set to 4.5 ppm (for the survey scan) and 0.5 Da for CID fragment ions. A false discovery rate of 1% was applied at the peptide and protein level. The iBAQ method as implemented in MaxQuant was used for intensity-based absolute quantification (Schwanhausser et al., 2011). Bioinformatic downstream annotation (GOCC and Pfam) analysis was performed using the Perseus Software package version 1.5.0.15.

#### **2.2.4 Cell lysis, cellular fractionation and immunoprecipitation**

Cells were lysed on ice for 10 min in cold RIPA buffer or for immunoprecipitation in NEB buffer containing 0.5% NP-40. Whole cell lysates were clarified by centrifugation for 10 min at 13,000 rpm and 4°C. The supernatant was transferred into a new reaction tube and the protein concentration was determined with the DC Protein Assay (BioRad) according to the manufacturer's protocol. For separation of the soluble, cytoplasmic fraction (=supernatant) and the detergent-soluble fraction (=pellet), cells were lysed in detergent-free lysis buffer. After three freeze/thaw cycles in liquid nitrogen, samples were cleared by centrifugation (20 min, 13,000 rpm) and the supernatant was collected. The pellet was solubilized in 1% NEB buffer, followed by centrifugation (10 min, 13,000 rpm). Equal amounts of the fractions were diluted in 0.5% NEB buffer (1:1) and enriched by anti-GFP immunoprecipitation. The purity of the fractions was controlled by immunoblotting of GAPDH and TfR as cytoplasmic and membrane markers. For all other immunoprecipitations, equal amounts of protein were diluted with extraction buffer to a final concentration of 0.25% NP-40 and incubated with specific antibodies (1-2 µg) for 5 h at 4°C with shaking. Immune complexes were collected using protein G agarose (KPL) (1h, 4°C), washed three times with 1ml 0.25% NEB and centrifuged at 5,000 rpm for 1 min at 4°C. Precipitated proteins were released by boiling in Laemmli sample buffer for 5 min at 95°C.

### **2.2.5 SDS-PAGE and immunoblotting**

After protein extraction, samples were denatured in Laemmli buffer for 10 min at 95°C. Equal amounts of protein were separated by SDS-PAGE using 8% or 10% polyacrylamide gels and were transferred to polyvinylidene difluoride membranes (Roth) by semi-dry blotting. Alternatively, lysates were loaded on 4-12% NuPAGE® Novex Bis-Tris gels (Invitrogen) and transferred to nitrocellulose membranes (iBlot®Gel Transfer Stacks; Invitrogen). Membranes were blocked with 0.5% blocking reagent (Roche) in PBS containing 0.05% Tween-20 and 0.01% thimerosal for 30 min, stained with primary antibodies at 4°C overnight and incubated with HRP-conjugated secondary antibodies for 1 h at room temperature. Proteins were visualized using an ECL detection system (Pierce) and X-ray films (CEA RP New, AGFA) which were developed with an automatic Curix 60 processor (AGFA). Alternatively, protein detection was performed with the IR-labeled antibodies IRDye 800 goat anti-GST and IRDye 800 CW goat anti-mouse IgG (Licor Biotechnology) using an Odyssey device (Licor Biotechnology). Quantification of immunoblots was performed by densitometric analysis using ImageJ (NIMH; Bethesda, Maryland, USA).

### **2.2.6 Bacterial expression of GST proteins**

*E.coli* were transformed with bacterial expression vectors and protein expression was induced with 0.5 mM IPTG for 3 h at 30°C. The bacterial cultures were harvested and pellets were resuspended in PBS containing Complete protease inhibitors. The suspension was sonicated 3x for 10 s on ice, incubated on ice for 15 min and Triton-X-100 was added to a final concentration of 1% before the lysate was centrifuged for 10 min at 10,000 g. Purification of GST-tagged proteins was performed with glutathione resin (GE Healthcare). The resin was washed with PBS and the purity of bound GST proteins was determined by SDS-PAGE and Coomassie staining.

### **2.2.7 Far-Western blotting and pulldowns**

For Far-Western blotting, GST-Scrib PDZ1-PDZ4 proteins or GST alone were eluted from the resin using 10 mM reduced glutathione in 50 mM Tris-HCl (pH8.0). Western blot membranes were incubated with 400 nM recombinant GST-fusion proteins in 0.5% blocking reagent (Roche) in PBS containing 0.05% Tween-20 and 0.01% thimerosal at 4°C overnight. Membranes were washed with PBS containing 0.05% Tween-20, incubated with primary and HRP-labeled secondary antibodies for 1 h at room temperature, followed by protein detection using an ECL detection system (Pierce).

Pulldowns were performed by incubation of HEK293T cell lysates (in 0.25% NEB) with immobilized GST-tagged proteins on a glutathione resin for 2 h. The beads were washed 3x with 0.25% NEB, proteins were released by boiling in Laemmli buffer (5 min, 95°C) and subjected to SDS-PAGE and immunoblotting.

### **2.2.8 Immunofluorescence microscopy**

For immunofluorescence analysis, cells were grown on coverslips coated with 10 µg/ml collagen R (Serva) and fixed with 4% PFA in PBS for 15 min at room temperature. For staining of membrane-associated RhoA, samples were processed by trichloroacetic acid fixation (TCA) instead of PFA fixation using a freshly prepared TCA solution (10% (w/v) in ddH<sub>2</sub>O) in which the samples were incubated for 15 min on ice. All samples were then washed with PBS and incubated in 150 mM glycine in PBS for 15 min. For experiments in 3D matrigel cultures, cells were grown on matrigel and collagen (1:1) coated 8-well glass chamber slides (BD) and fixed with 4% PFA in PBS for 15 min at 37°C. All samples were permeabilized with 0.2% Triton X-100 in PBS for 10 min and blocked with 5% goat serum in PBS containing 0.1% Tween-20 for 30 min. Cells were stained with primary antibodies diluted in blocking buffer for 2 h at room temperature, washed 3x with PBS containing 0.1% Tween-20 and incubated with Alexa Fluor® (488,546 or 633)-labeled secondary antibodies for 1 h (2D culture) or 2 h (3D culture) at room temperature. F-actin and nuclei were counterstained with Alexa Fluor-labeled phalloidin and DAPI, before the coverslips were mounted in Fluoromount-G ® (Southern Biotech). Samples were analyzed on a confocal laser scanning microscope (LSM 710, Zeiss) equipped with an oil immersion objective Plan-Apochromat 63x/1.40 DIC M27 lens using 488, 561 and 633 nm excitation. Maximum intensity projections, linear adjustments of brightness and contrast, and acquisition of line scans were done with ZEN software (Zeiss). For quantification of fluorescence intensities, images were acquired with the same confocal settings and junctional and cytoplasmic signals were measured with ImageJ. The Mander's coefficient was determined using the JACoP plugin (Bolte and Cordelières, 2006). For quantification of polarized Caco-2 cysts, Caco-2 spheroids with a round morphology, a cell-free lumen and distinct F-actin staining of the apical surface were scored as normal, whereas flat cysts with no or multiple lumens were scored as abnormal.

### **2.2.9 RNA isolation and quantitative PCR**

Isolation of total RNA from cells was carried out with the RNeasy® Plus Mini Kit (Qiagen, Foster City, CA, USA) according to the manufacturer's instructions. RNA concentrations

were determined using a Nanophotometer at OD 260/280 nm. Q-PCR was performed with QuantiTect Primer Assays® for SYBR® Green-based expression analysis (Qiagen) using a Cfx96 device (Biorad) according to the manufacture's protocol for one-step RT-PCR. Primers used were 5'-CATGGAGCGCAGGGACC-3' and 5'-GGGAAGCACTTCACCTTCCT-3' for DLC3 (Biomers.net; Ulm, Germany) and Hs\_PPIA\_4\_SG QuantiTect Primer Assay (Qiagen). Changes in the relative expression level were determined using the  $2^{-\Delta\Delta C_t}$  method (Biorad CFX manager software 3.1.). PPIA was used as an endogenous control gene for normalization.

#### **2.2.10 *In situ* proximity ligation assay (PLA)**

The PLA assay was performed using the Duolink® In situ Orange Kit (Sigma-Aldrich). Cells were fixed, permeabilized and stained with primary antibodies (mouse GFP-specific and rabbit Scribble-specific antibody) as described for immunofluorescence analysis. For blocking, the buffer provided by the Duolink system was used. Incubation with PLA probes, ligation and amplification were performed according to the manufacturer's instructions using the detection reagents "orange". Cells were stained with Alexa Fluor-labeled phalloidin and mounted in DAPI-containing Duolink mounting medium. PLA signals were imaged with a confocal LSM 710 microscope.

#### **2.2.11 Cell disaggregation assay**

Cells were seeded in 25  $\mu$ l drops ( $1 \times 10^6$  cells/ml) onto the lid of a culture dish and incubated in an inverted manner overnight to allow the formation of cell aggregates. ROCK inhibitor (H1152) was added 6 h post seeding. The next day, aggregates were pipetted up and down (15x with a 20  $\mu$ l pipette) and photographed at 2x magnification using an Evos FL cell imaging system (Advanced microscopy group (AMG)). The area covered by the remaining cell clusters larger than 40,000  $\mu\text{m}^2$  was quantified using ImageJ.

#### **2.2.12 Scratch assay**

To image protein localization at the leading edge of cells during directed cell migration, polarization of cells towards a wound scratch was investigated. To this end, cells were seeded at high confluency ( $8 \times 10^5$  cells/coverlip) and the next day, the cell monolayer was scratched with a yellow pipette tip. Cells were allowed to polarize and migrate into the wound for 6 h, before samples were subjected to PFA fixation and immunostaining. Representative images of cells at the leading edge were acquired.

### **2.2.13 Statistical analysis**

Data are shown as mean  $\pm$  S.E.M.; 'n' refers to the number of analyzed cells, cysts or cell aggregates/experiment and 'N' to the number of independent experiments. Statistical significance was analyzed by t-test and one-way ANOVA followed by Tukey's post-test (GraphPad Prism version 4.03; GraphPad Software Inc., La Jolla, CA). p-values below 0.05 were considered as significant (\*p < 0.05; \*\* p < 0.01; \*\*\* p < 0.001; ns, not significant, p > 0.05).

### 3. Results

#### 3.1 Identification of DLC3 protein interaction partners

To identify molecular factors that specify DLC3 localization, a mass spectrometry analysis of DLC3-interacting proteins was performed. Flag-tagged wildtype (WT) DLC3 and a DLC3 point mutant (K725E) previously shown to be GAP inactive (Holeiter et al., 2012) were transiently expressed in HEK293T cells and immunopurified from cell lysates using immobilized anti-Flag agarose. Upon elution of immunopurified protein complexes, followed by SDS-PAGE and tryptic in-gel digestion, samples were analyzed by nano-liquid chromatography-tandem mass spectrometry (nanoLC-MS/MS) (Fig. 7). For each detected co-immunoprecipitating protein, semi-quantitative iBAQ (intensity based absolute quantification) values were calculated to take into account the number of theoretically observable peptides of a protein (see methods for details). To exclude the bulk of non-specific binders we set an arbitrary iBAQ threshold of  $\geq 100\,000$  and considered only the highest scoring proteins that associated with DLC3 WT and K725E but were not present in the empty vector control. This analysis yielded 228 proteins (Table S1).

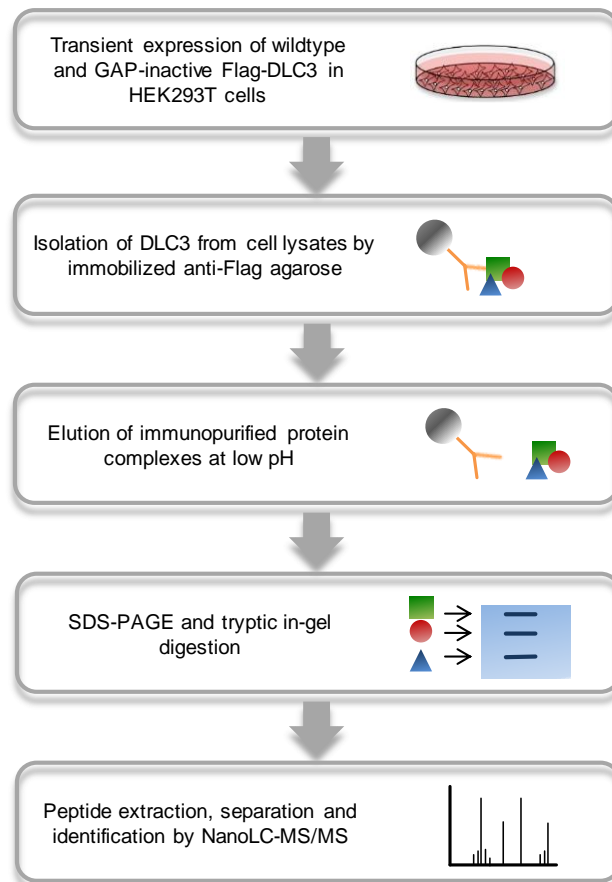


**Figure 7: Workflow of affinity purification and mass spectrometry analysis to identify DLC3 protein binding partners.**

In accordance with the role of DLC3 in the control of endocytic membrane trafficking and transferrin receptor recycling (Braun et al., 2015), several proteins involved in vesicular transport, including the early endosome marker Rab5, transferrin receptor (TfnR) and SNX27, a regulator of endocytic recycling, were contained in the list of DLC3 interactors (Table 13 and Table S1).

**Table 13: DLC3 binding partners involved in endocytic trafficking, cell signaling and with an adaptor or scaffold function.** Mass spectrometry hits associated with specific cellular functions were extracted from Table S1 and are listed.

Protein names	Gene names
<b>Endocytic trafficking</b>	
ADP-ribosylation factor 4	ARF4
ADP-ribosylation factor-like protein 1	ARL1
AP-2 complex subunit sigma	AP2S1
Ras-related protein Rab-5C;Ras-related protein Rab-5B	RAB5C;RAB5A;RAB5B
Sorting nexin-27	SNX27
Transferrin receptor protein 1;Transferrin receptor protein 1	TFRC
Vesicle transport through interaction with t-SNAREs homolog 1B	VTI1B
<b>Cell signaling</b>	
Diacylglycerol kinase;Diacylglycerol kinase epsilon	DGKE
Phosphatidylinositol 3-kinase regulatory subunit alpha	PIK3R1
Phosphatidylinositol 3-kinase regulatory subunit beta	PIK3R2
Ras-related C3 botulinum toxin substrate 1	RAC1
TBC1 domain family member 4	TBC1D4
Type 1 phosphatidylinositol 4,5-bisphosphate 4-phosphatase	TMEM55B
<b>Adaptor / Scaffold proteins</b>	
Alpha-catulin	CTNNAL1
Growth factor receptor-bound protein 2	GRB2
Ras GTPase-activating-like protein IQGAP1	IQGAP1
KN motif and ankyrin repeat domain-containing protein 2	KANK2

Considering that DLC3 localizes to Rab8-positive tubular structures (Braun et al., 2015), it is also striking that the Rab8-GAP protein TBC1D4 (also known as AS160) was detected as a DLC3 binding partner. Furthermore, several scaffold proteins including the focal adhesion-associated adaptor Kank2 and IQGAP1, a large scaffold involved in actin cytoskeleton organization and different signaling pathways, were among the mass

spectrometry results (Table 13 and Table S1). The interaction of DLC3 with IQGAP1, TBC1D4 and SNX27<sup>1</sup> were validated by co-immunoprecipitation of the tagged proteins from HEK293T cell lysates. Additionally, it was shown that IQGAP1 and TBC1D4 interact not only with DLC3, but also bind to the structurally related family members DLC1 and DLC2 (data not shown). Since the major goal of this work was to reveal how DLC3 is recruited to cell-cell adhesions, the list of DLC3 binding partners was systematically analyzed for cell junction-associated candidates. According to GOCC data base annotation, 17 proteins were associated with the category 'cell junction' (Table 14).

**Table 14: Cell junction-associated DLC3 binding partners according to GOCC database annotation.**

Cell junction		
Protein names	Gene names	PDZ
Protein scribble homolog	SCRIB	+
Disks large homolog 1	DLG1	+
Golgi-associated PDZ and coiled-coil motif-containing protein	GOPC	+
Protein lin-7 homolog C;Protein lin-7 homolog B; Protein lin-7 homolog A	LIN7C;LIN7A;LIN7B	+
Alpha-1-syntrophin	SNTA1	+
Beta-1-syntrophin	SNTB1	+
Beta-2-syntrophin	SNTB2	+
Angiomotin-like protein 2	AMOTL2	-
Cyclin-dependent kinase 4	CDK4	-
Cytochrome c1, heme protein, mitochondrial	CYC1	-
DnaJ homolog subfamily A member 3, mitochondrial	DNAJA3	-
Dystrobrevin alpha	DTNA	-
Dystrobrevin;Dystrobrevin beta	DTNB	-
BTB/POZ domain-containing protein KCTD12	KCTD12	-
Obscurin-like protein 1	OBSL1	-
Plakophilin-2	PKP2	-
Utrophin	UTRN	-

Interestingly, seven of these proteins contain PDZ domains, which are prominent protein interaction platforms. These PDZ domain proteins included Scribble, Dlg1, GOPC, Lin-7 and  $\alpha$ 1-/ $\beta$ 1-/ $\beta$ 2-syntrophin (Table 14). Our biological follow-up was focused on the polarity protein Scribble because it localizes to adherens junctions and the basolateral membrane

<sup>1</sup> Master Thesis Yannick Frey. CRISPR-Cas9 mediated genome engineering of DLC3 to disrupt the novel interaction with SNX27. Institute of Cell Biology and Immunology, University of Stuttgart. 2015.

of polarized epithelial cells, and functions as a potential tumor suppressor (Dow et al., 2003; Navarro et al., 2005; Qin et al., 2005).

### 3.2 DLC3 interacts with the basolateral polarity protein Scribble

To first validate the interaction of DLC3 and Scribble biochemically, GFP-Scribble was transiently expressed in HEK293T cells, immunoprecipitated from cell lysates by an anti-GFP antibody and binding of co-expressed Flag-tagged DLC3 was analyzed by immunoblotting (Fig. 8A). In agreement with the mass spectrometry analysis, Scribble immunoprecipitation revealed that wildtype (WT) and GAP-inactive (K725E) DLC3 were bound by the polarity protein with comparable affinity, indicating that the interaction occurs independently of the GAP activity of DLC3 (Fig. 8B). In addition, the interaction of endogenous DLC3 and Scribble was confirmed by co-immunoprecipitation of the proteins from HeLa cell lysates using a DLC3-specific antibody (Fig. 8C).

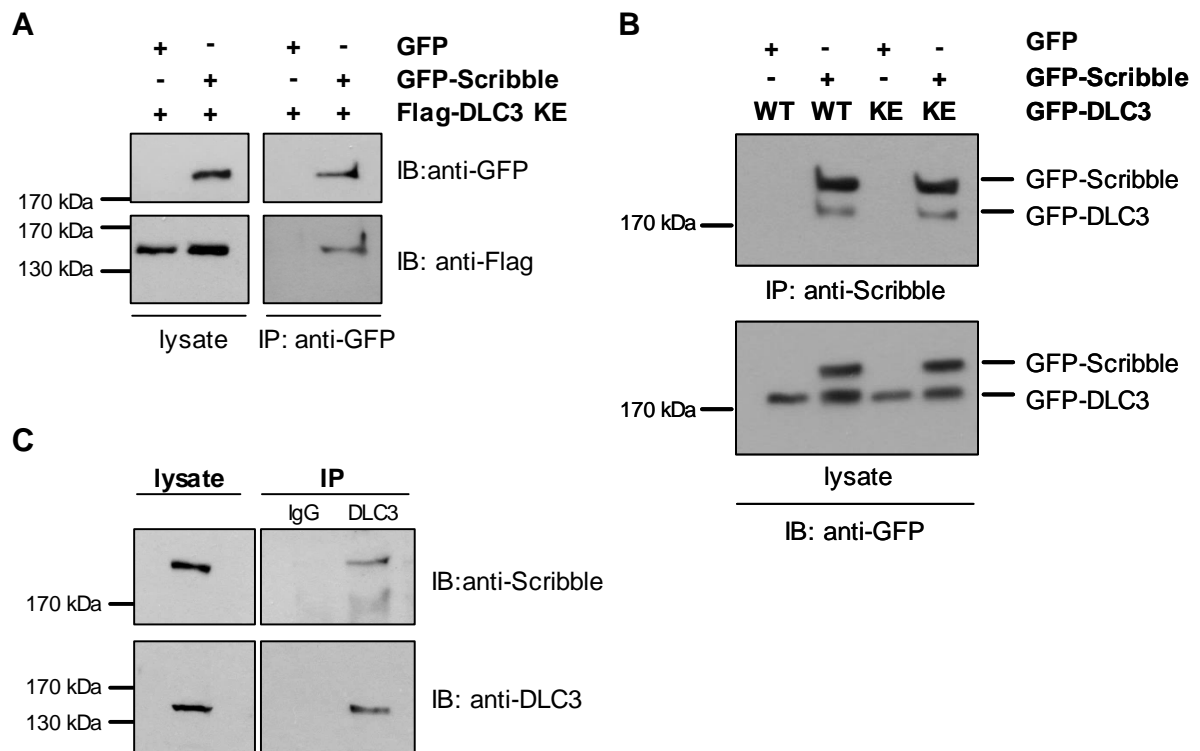


**Figure 8: DLC3 interacts with the polarity protein Scribble.** (A) HEK293T cells were transfected with expression vectors encoding GFP-Scribble or GFP alone along with Flag-DLC3 K725E, respectively. The next day, lysates were immunoprecipitated (IP) with an anti-GFP antibody. Samples were analyzed by immunoblotting (IB) using anti-GFP and anti-Flag antibodies. (B) GFP-Scribble or GFP alone and GFP-DLC3 WT or K725E, respectively, were co-expressed in HEK293T cells. The next day, lysates were immunoprecipitated with an anti-Scribble antibody. Samples were analyzed by immunoblotting using an anti-GFP antibody. (C) Endogenous DLC3 was immunoprecipitated from HeLa cell lysates and co-immunoprecipitation of endogenous Scribble was analyzed by immunoblotting. An unrelated IgG was used as a control.

## Results

Considering the structural similarity of the three DLC family proteins, the question arose whether Scribble also interacts with DLC1 and DLC2. However, in Scribble immunoprecipitates, co-expressed DLC1 and DLC2 were not detectable even in long exposures (Fig. 9 and data not shown), indicating predominant interaction with the DLC3 isoform.

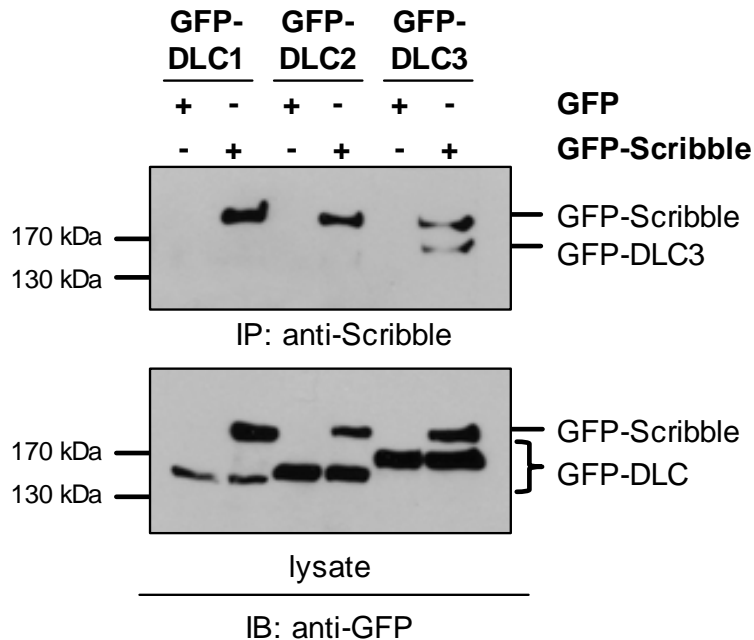


**Figure 9: Scribble is an isoform-specific binding partner of DLC3.** HEK293T cells were transfected with expression vectors encoding GFP-Scribble or GFP alone and GFP-DLC1, GFP-DLC2 or GFP-DLC3, respectively. 24 h post transfection, cell lysates were immunoprecipitated with a Scribble-specific antibody and analyzed by immunoblotting using an anti-GFP antibody.

To map the binding regions which mediate the DLC3-Scribble interaction, functional protein domains were considered more precisely. Scribble contains four PDZ domains (Humbert et al., 2008) that often mediate protein interactions with C-terminal PDZ ligand (PDZL) motifs (x-S/T-x-L/V) (Nourry et al., 2003). Intriguingly, DLC3 contains such a C-terminal class I PDZL motif (ETKL) that is absent in DLC1 and DLC2 (Fig. 10A). To prove a direct PDZ domain-mediated interaction of Scribble with DLC3, we generated DLC3  $\Delta$ PDZL, a deletion mutant lacking the five C-terminal amino acids, and analyzed binding to Scribble by Far-Western blotting. To this end, Flag-tagged full-length (FL) DLC3 and DLC3  $\Delta$ PDZL were expressed in HEK293T cells, enriched by immunoprecipitation and transferred to membrane. Membranes were then incubated with a recombinant Scribble protein fragment encompassing the PDZ domains (GST-Scribble PDZ1-PDZ4) or GST alone as a control. Immunostaining revealed that the PDZ domains of Scribble bound to the full-length DLC3 protein, whereas deletion of the PDZL motif abrogated Scribble binding (Fig. 10A). Thus, it can be concluded that the interaction of DLC3 and Scribble is direct and mediated by the PDZ domains of Scribble and the C-terminal PDZL

motif of DLC3. Finally, to determine which of the four Scribble PDZ domains was involved in DLC3 binding, pulldown experiments of DLC3 with immobilized GST-tagged Scribble PDZ1, PDZ2, PDZ3 or PDZ4 were performed. Immunoblotting showed that DLC3 was primarily bound by Scribble PDZ3 and to a lesser extent by Scribble PDZ4 (Fig. 10B).

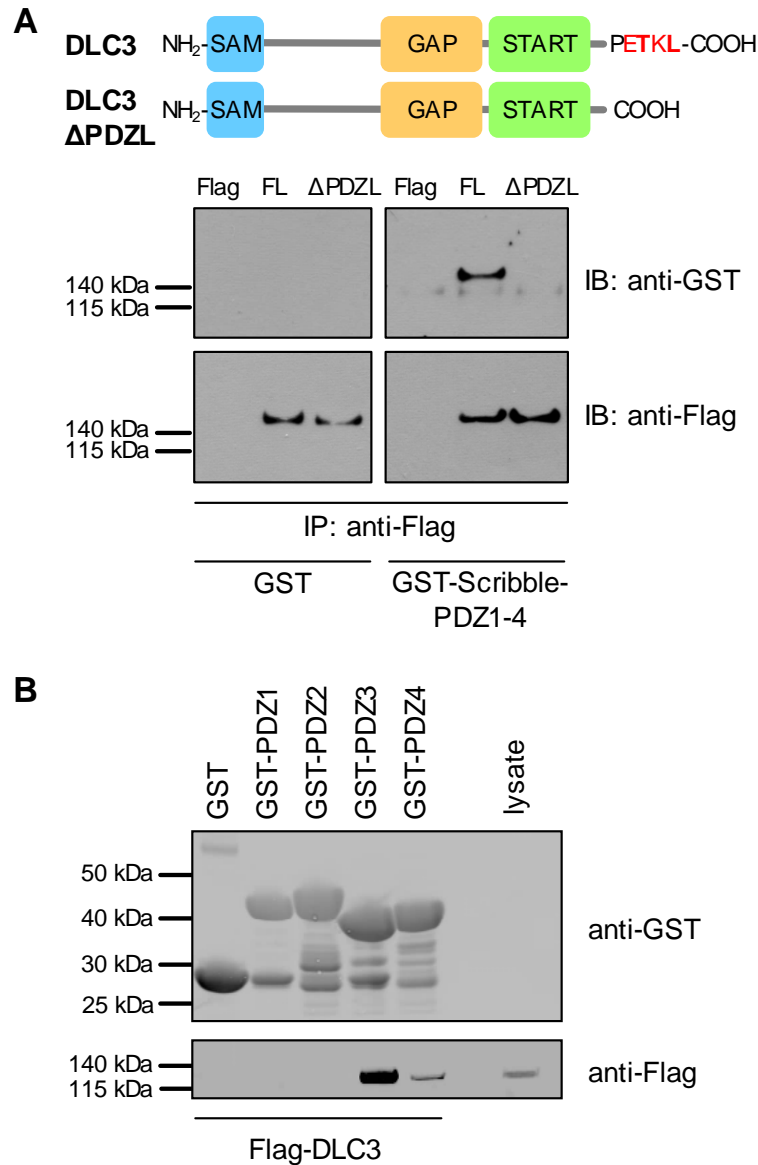


**Figure 10: DLC3 directly interacts with Scribble via a C-terminal PDZ ligand motif.** (A) Domain organization of human DLC3 and DLC3  $\Delta$ PDZL lacking the last five amino acids (PETKL). SAM = sterile alpha motif, START = steroidogenic acute regulatory protein-related lipid transfer domain, PDZL = PSD-95, Dlg and ZO-1 ligand. HEK293T cells were transfected with plasmids encoding Flag-DLC3 full-length (FL), Flag-DLC3  $\Delta$ PDZL or empty Flag vector. 24 h post transfection, Flag-DLC3 proteins were immunoprecipitated from cell lysates and subjected to immunoblotting. For Far-Western blot analysis, membranes were incubated with recombinant GST-Scribble PDZ1-PDZ4 protein or GST as a control and stained with GST- and Flag-specific antibodies. (B) Pulldown of Flag-DLC3 transiently expressed in HEK293T cells with glutathione beads coupled to GST-Scribble PDZ1, PDZ2, PDZ3 or PDZ4 or GST alone. Bound proteins were analyzed by immunoblotting with anti-GST and anti-Flag antibodies.

To verify the interaction of DLC3 and Scribble at the cellular level, we made use of an *in situ* proximity ligation assay (PLA) (Fig.11). These studies were done in MCF7 cells stably expressing GFP-DLC3 because DLC3-specific antibodies were not suited for the detection of the endogenous protein by immunofluorescence. Because cell morphology is not perturbed by GAP-inactive DLC3, in contrast to the wildtype form, cells expressing DLC3 K725E were preferably used for the co-localization studies with endogenous Scribble.

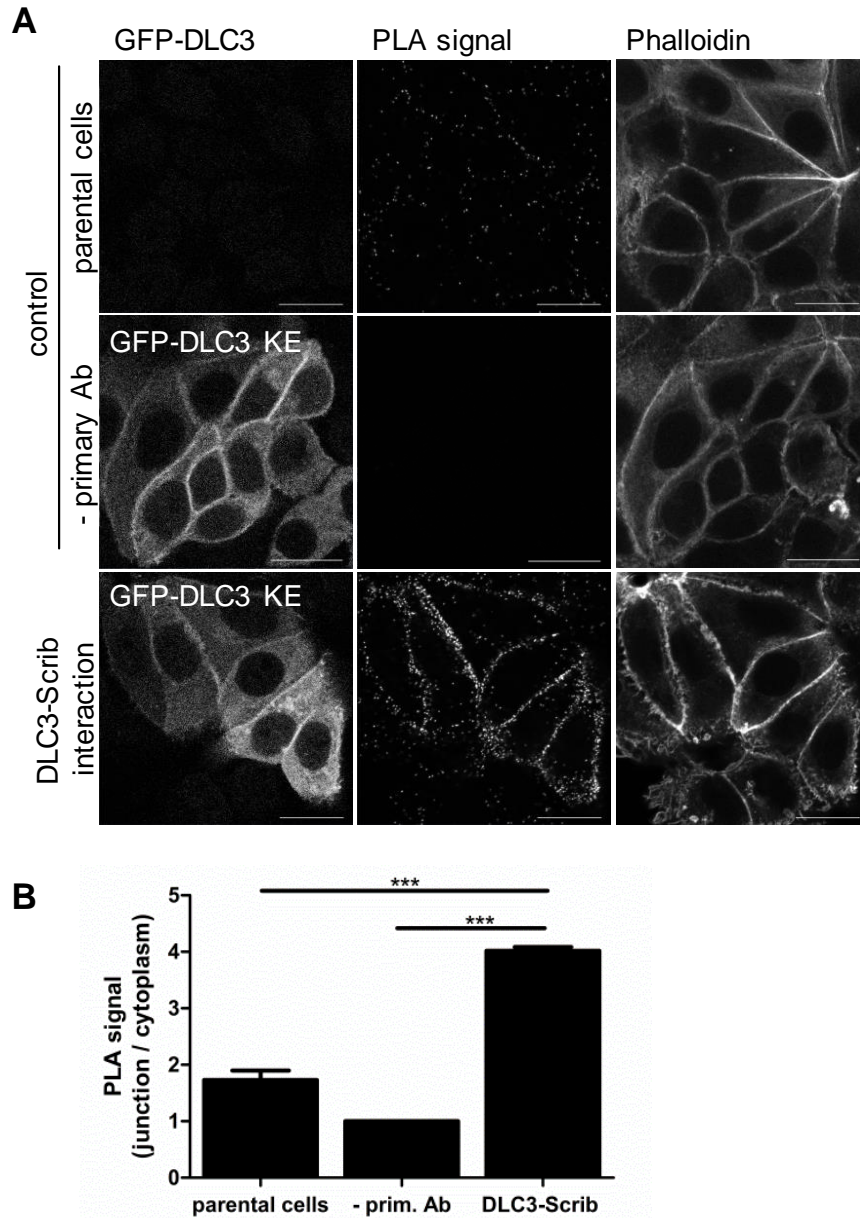


**Figure 11: DLC3 interacts with Scribble *in situ* at cell-cell adhesions.** (A) MCF7 cells stably expressing GFP-DLC3 K725E and parental cells as a control were analyzed by *in situ* proximity ligation assay (PLA) using anti-GFP and anti-Scribble antibodies. As an additional control, the reaction was performed without primary antibodies. Protein-protein interactions are visualized as distinct fluorescent spots (PLA signal). F-actin was stained with Alexa Fluor 633-labeled phalloidin. (B) Quantification of the junctional to cytoplasmic fluorescence intensity ratio of the PLA signal (n=20 cells; N=3; one-way ANOVA).

Indeed, the proximity ligation reaction led to the accumulation of discrete fluorescent spots at cell-cell adhesions, whereas almost no PLA signal was observed in the control without primary antibodies and only weak background signals were seen in cells lacking GFP-DLC3 expression (Fig. 11A). The significant increase of the junctional PLA signal compared to the controls confirms its specificity and proves the *in situ* interaction of DLC3 and Scribble at cell-cell contacts (Fig. 11B).

### 3.3 DLC3 localization is specified by its PDZL motif and Scribble

To next investigate whether DLC3 localization depends on Scribble, MCF7 cells stably expressing GAP-inactive DLC3 were transfected with non-targeting (spNT) or Scribble-specific (spScrib) small interfering RNAs (siRNAs) and immunostained three days post transfection. In control cells, DLC3 strongly colocalized with E-cadherin at cell-cell adhesions (Fig.12A).

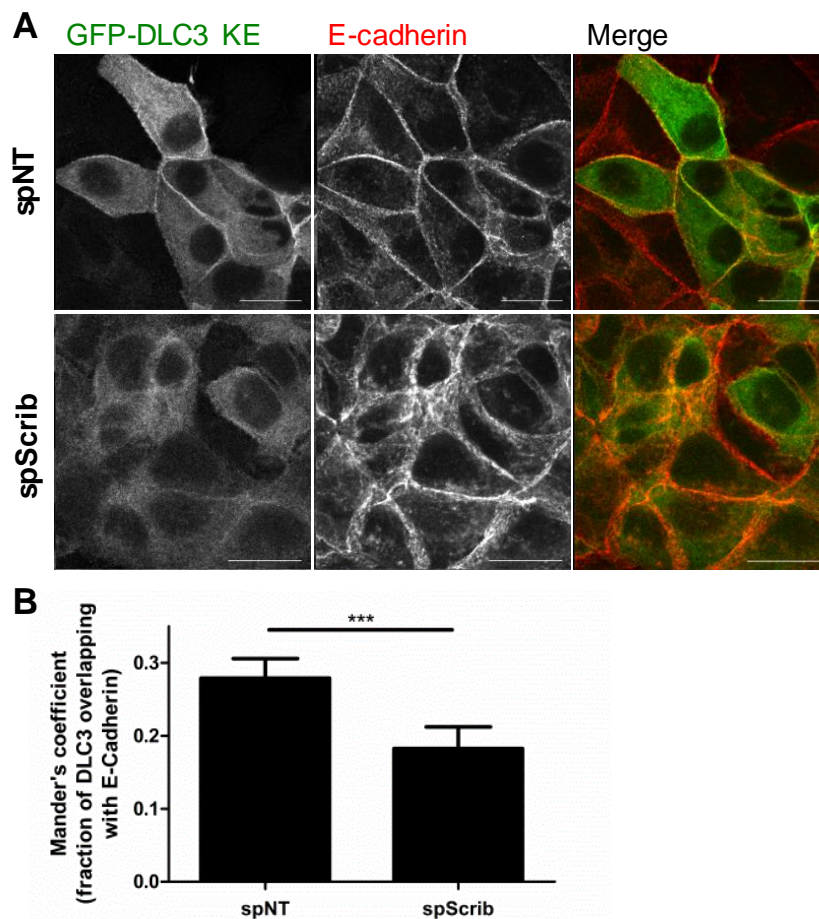


**Figure 12: DLC3 accumulation at cell-cell contacts depends on Scribble.** (A) MCF7 cells stably expressing GFP-DLC3 K725E were transfected with non-targeting (spNT) and Scribble-specific (spScrib) siRNAs, respectively. 72 h post transfection, cells were fixed and stained with GFP- and E-cadherin-specific antibodies. The images shown are maximum intensity projections of several confocal sections. Scale bars, 20  $\mu$ m. (B) Quantification of the fraction of DLC3 (K725E) overlapping with E-cadherin by Mander's colocalization coefficient (n=12; N=3; paired t-test).

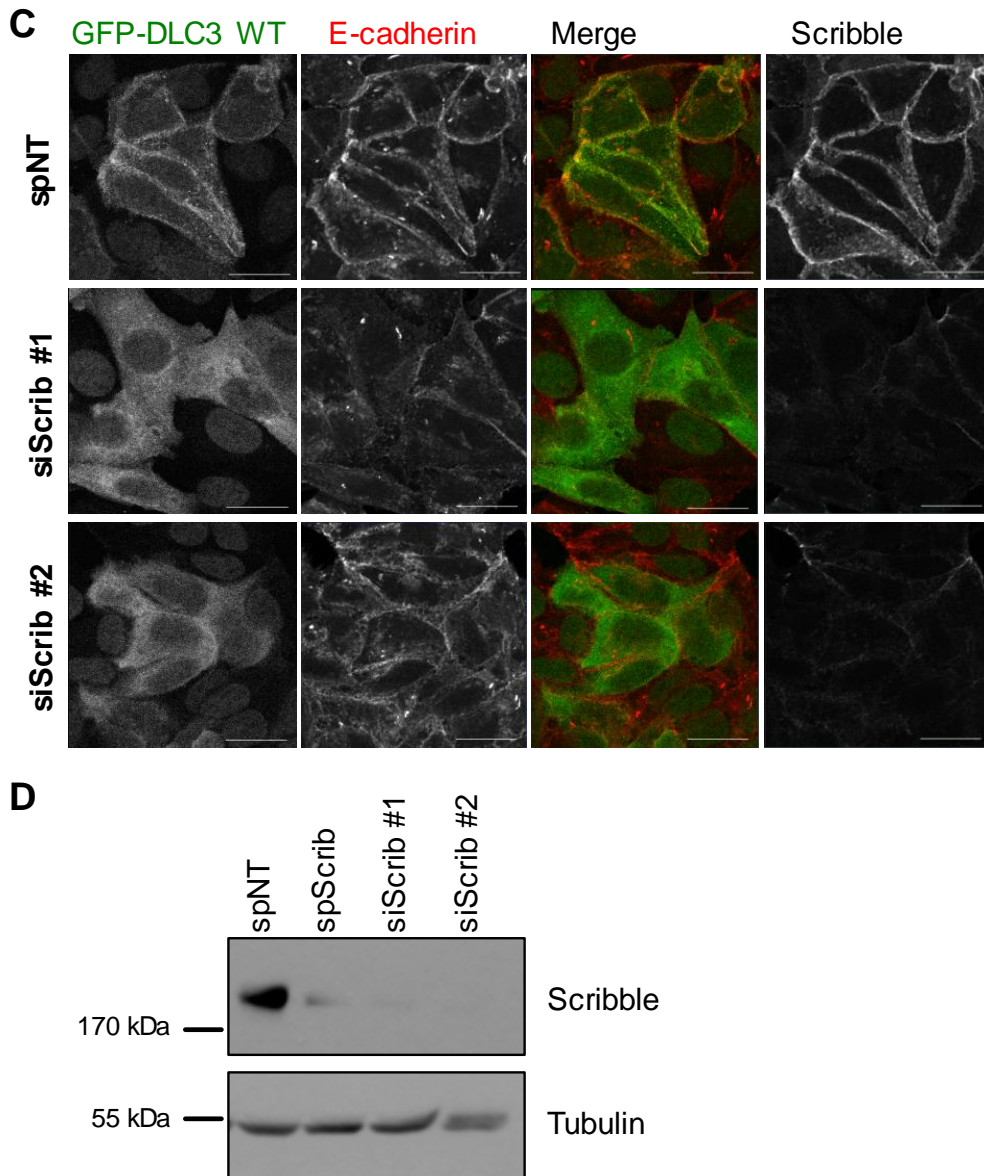


**Figure 12:** (C) Validation of DLC3 localization in MCF7 cells stably expressing GAP-active (WT) GFP-DLC3 upon transfection with non-targeting (spNT) and independent Scribble-specific (siScrib#1 and siScrib#2) siRNAs, respectively. 72 h post transfection, cells were fixed and stained with E-cadherin- and Scribble-specific antibodies. (D) Whole cell lysates of MCF7 cells were analyzed by immunoblotting with anti-Scribble and anti-tubulin antibodies.

In addition, we verified that junctional DLC3 localization is independent of its GAP activity, as seen by the comparable cellular distribution of DLC3 WT and the GAP-inactive form (Fig. 12A,C). Interestingly, upon Scribble depletion, DLC3 no longer accumulated at cell-cell contacts and was homogeneously distributed within the cell, which was observed for the wildtype and GAP-inactive protein (Fig. 12A,C). Although adherens junctions were less ordered in cells lacking Scribble, junctional E-cadherin localization was partially retained, whereas DLC3 was completely mislocalized from cell-cell contacts as confirmed by a significantly reduced Mander's colocalization coefficient in the knockdown

cells (Fig. 12B). Efficient downregulation of Scribble was verified by immunoblotting (Fig. 12D) and independent siRNAs targeting Scribble yielded similar results, ruling out off-target effects (DLC3 WT: Fig.12C,D; DLC3 K725E: data not shown). These findings strongly suggest that DLC3 localization is not only altered due to cell-cell contact destabilization, but depends directly on the presence of Scribble. To address the question whether the PDZL motif is important for DLC3 localization, MCF7 cells stably expressing GFP-DLC3 full-length and  $\Delta$ PDZL variants were generated and analyzed by immunostaining. Interestingly, PDZL motif deletion impaired the clustering of both wildtype and GAP-inactive DLC3 at cell-cell contacts (Fig. 13A,C). Quantification of the junctional GFP-DLC3 signal further confirmed the loss of DLC3 accumulation at cell adhesions upon PDZL deletion (Fig. 13B). Taken together, these results provide evidence that the PDZL motif controls the localization of DLC3 at cell-cell contacts.

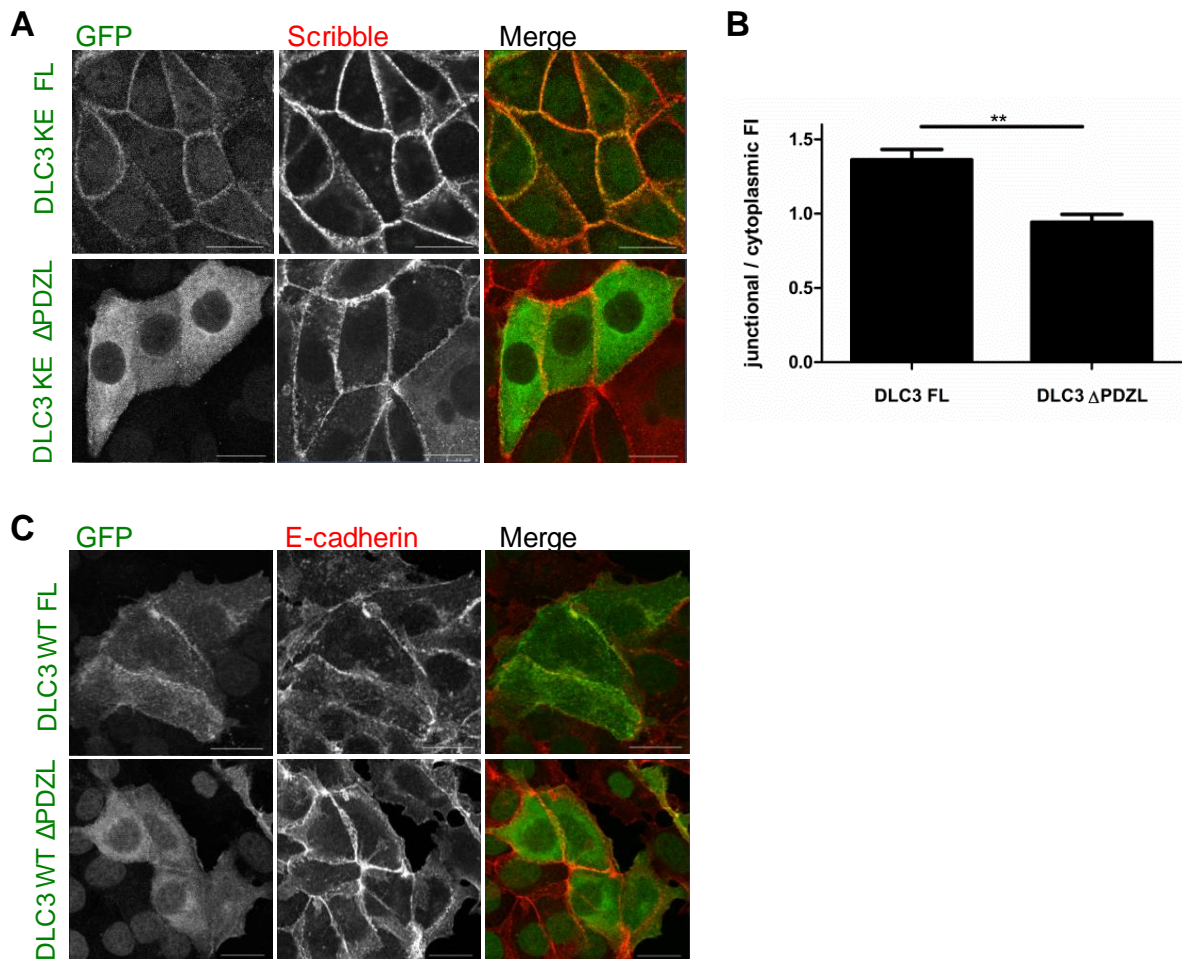


**Figure 13: The PDZL motif controls DLC3 localization at cell junctions.** (A) Stable MCF7 cells expressing GFP-DLC3 K725E FL or  $\Delta$ PDZL were stained with anti-GFP and anti-Scribble antibodies. The images shown are maximum intensity projections of several confocal sections. Scale bars, 20  $\mu$ m. (B) Quantification of the junctional to cytoplasmic fluorescence intensity (FI) ratio of GFP-DLC3 K725E FL and  $\Delta$ PDZL (n=20 cells; N=3; paired t-test). (C) Validation of DLC3 localization in MCF7 cells stably expressing GAP-active (WT) GFP-DLC3 full-length and  $\Delta$ PDZL, respectively, stained with an E-cadherin-specific antibody.

### 3.4 DLC3 regulates RhoA-ROCK signaling to maintain cell-cell contacts and Scribble localization

To directly assess RhoA activity at cell-cell adhesions in dependence of DLC3 expression, a GFP-Anillin AHPH location biosensor for active RhoA was employed. This biosensor encodes the C-terminal part of the scaffold protein anillin, which specifically binds GTP-RhoA (Piekny and Glotzer, 2008; Priya et al., 2015). MCF7 cells transiently transfected with non-targeting (spNT) or DLC3-specific (spDLC3) siRNAs were co-transfected with plasmids encoding the wildtype biosensor and, as a control, a mutant deficient in RhoA binding (GFP-Anillin AHPH DM), respectively (Fig. 14A). Efficient downregulation of DLC3 was verified by quantitative PCR (Fig. 14C). In control cells, the wildtype biosensor was distributed evenly in the cells, with no obvious signs of locally elevated RhoA activation. However, in DLC3-depleted cells, GFP-Anillin AHPH WT was enriched in many small aggregates all along the destabilized cell-cell contacts, whereas the control sensor exhibited uniform cytoplasmic and nuclear localization (Fig. 14A).

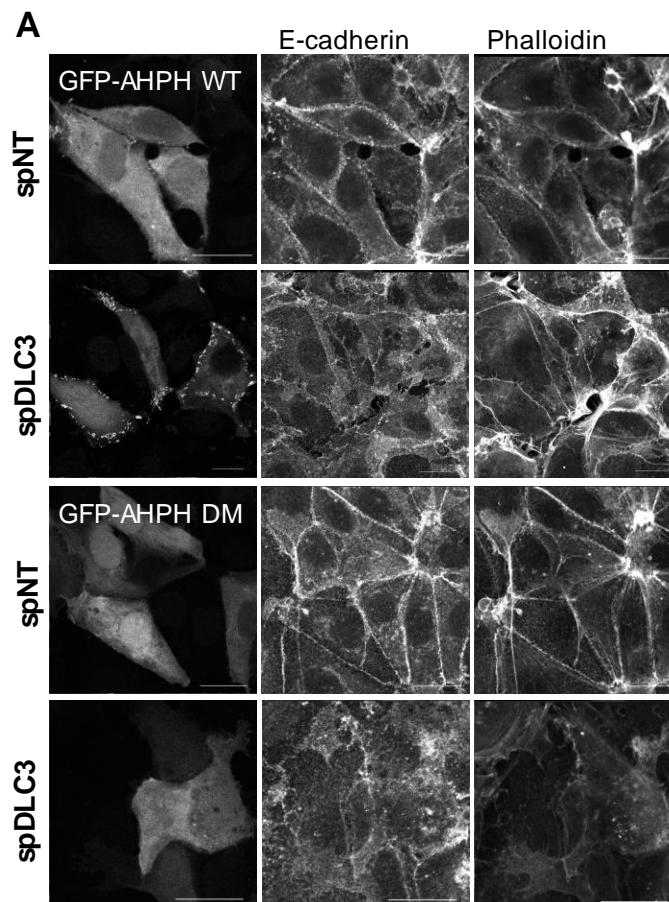


**Figure 14: DLC3 depletion enhances RhoA activity at cell-cell adhesions.** (A) MCF7 cells were transfected with non-targeting (spNT) or DLC3-specific (spDLC3) siRNAs. Two days later, cells were transfected with plasmids encoding the RhoA location biosensor GFP-Anillin AHPH and A70D/E758K (DM) as control sensor, respectively. The next day, cells were fixed and stained for E-cadherin and F-actin (Phalloidin). Representative maximum intensity projections are shown.

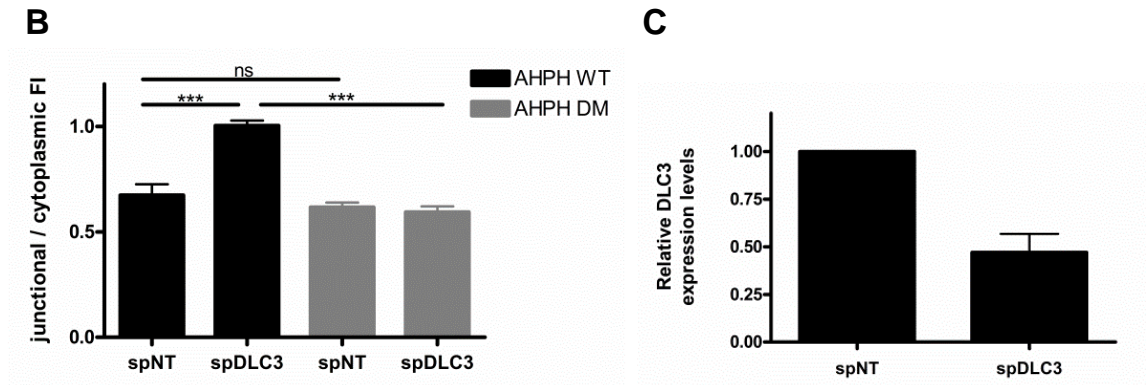


**Figure 14:** (B) Quantification of the junctional to cytoplasmic fluorescence intensity (FI) ratio of the GFP-AHPH reporter (n=20 cells; N=3; one-way ANOVA). (C) RNA was extracted 72 h post transfection and relative DLC3 expression levels normalized to PPIA as a control gene were determined by quantitative PCR (N=2).

Quantification of the junctional biosensor signal revealed a significant increase in the DLC3 knockdown cells in comparison to the control samples, supporting a role for DLC3 as a RhoGAP at cell adhesions (Fig. 14B). To further prove that DLC3 controls Rho-ROCK signaling at cell-cell contacts, phosphorylation of the ROCK substrate myosin light chain (MLC) was investigated by immunostaining (Fig. 15).

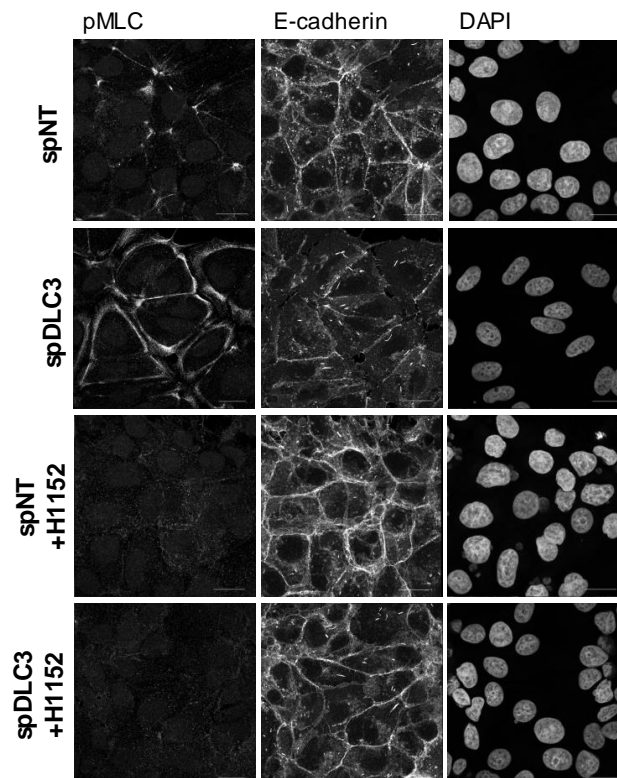


**Figure 15: Increased junctional pMLC levels in DLC3-knockdown cells.** MCF7 cells were transfected with non-targeting (spNT) and DLC3-specific (spDLC3) siRNAs, respectively. Two days later, cells were treated with ROCK inhibitor overnight (H1152; 10  $\mu$ M) where indicated. The next day, cells were fixed and stained for pMLC and E-cadherin. Nuclei were counterstained with DAPI. The images shown are maximum intensity projections of several confocal sections. Scale bars, 20  $\mu$ m.

The specificity of the pMLC signal was controlled by ROCK inhibitor (H1152) treatment. The low junctional pMLC levels detected in the control cells are in line with the low basal RhoA activity visualized by the biosensor at these sites. However, DLC3 depletion substantially increased the pMLC signals at cell-cell adhesions, confirming that DLC3 restricts junctional Rho-ROCK signaling (Fig. 15). Next, we performed a cell disaggregation assay to investigate whether the cell adhesion defect in DLC3-depleted cells can be restored by pharmacological ROCK inhibition (Fig. 16).

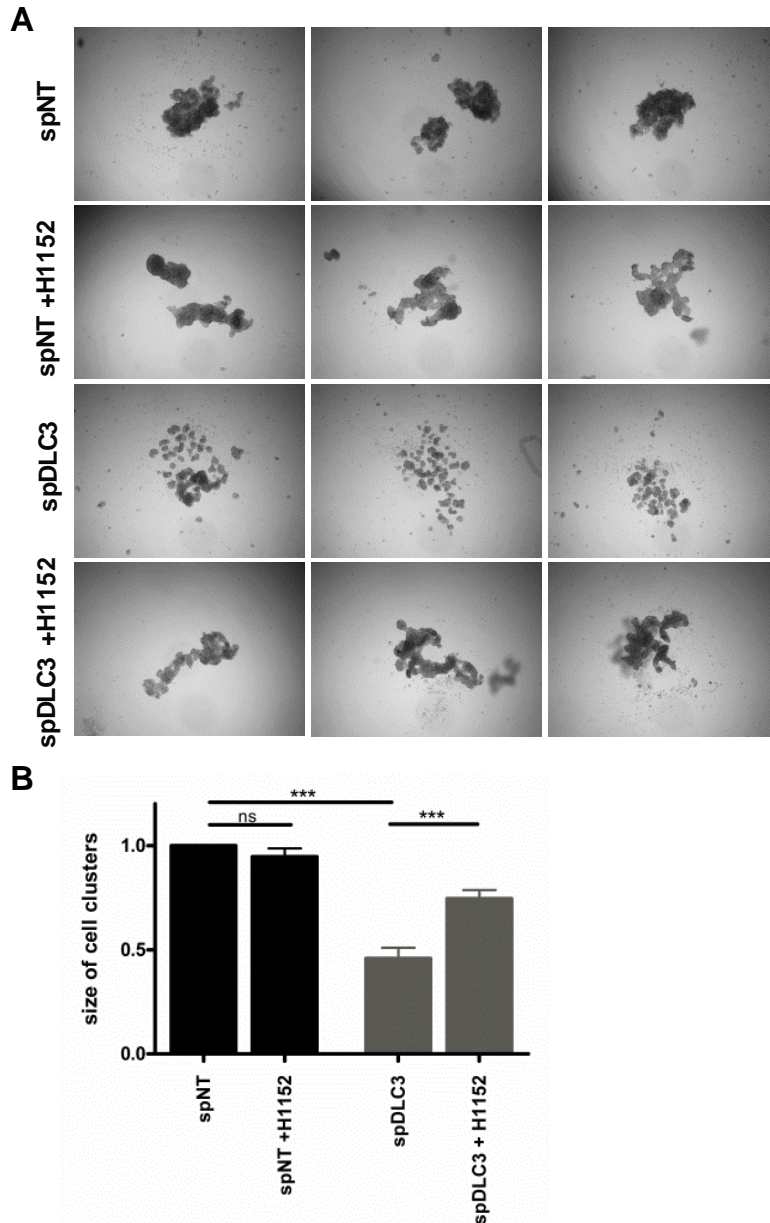


**Figure 16: ROCK inhibition rescues the cell adhesion defect caused by DLC3 depletion.** (A) MCF7 cells were transfected with non-targeting (spNT) and DLC3-specific (spDLC3) siRNAs, respectively. Two days later, cells were seeded in hanging drops. After 6 h, ROCK inhibitor (H1152; 10  $\mu$ M) was added to the drops and incubated overnight. The next day, cell aggregates were dissociated by pipetting and photographed. Scale bars, 1 mm. (B) Quantification of the cell disaggregation shown in A. The area covered by cell clusters larger than 40,000  $\mu$ m<sup>2</sup> was determined (mean  $\pm$ S.E.M. of 40 cell clusters derived from two independent experiments; one-way ANOVA).

To this end, DLC3-depleted MCF7 cells were seeded in hanging drops to allow the formation of cell aggregates. After treatment with ROCK inhibitor overnight, cell aggregates were dissociated by pipetting and disaggregation was determined by quantification of cell cluster sizes above a set threshold (see methods for details) (Fig. 16A,B). Indeed, ROCK inhibition partially rescued the cell junction destabilization caused by DLC3 knockdown and preserved intact cell clusters. Taken together, these findings prove that DLC3 functions as a junction-associated regulator of RhoA-ROCK signaling and provide an explanation for the requirement of DLC3 for adherens junction integrity (Holeiter et al., 2012). To investigate the impact of DLC3 depletion on Scribble localization, MCF7 cells transfected with non-targeting (spNT) and DLC3-specific (spDLC3) siRNAs were stained for Scribble and E-cadherin (Fig. 17A,B).

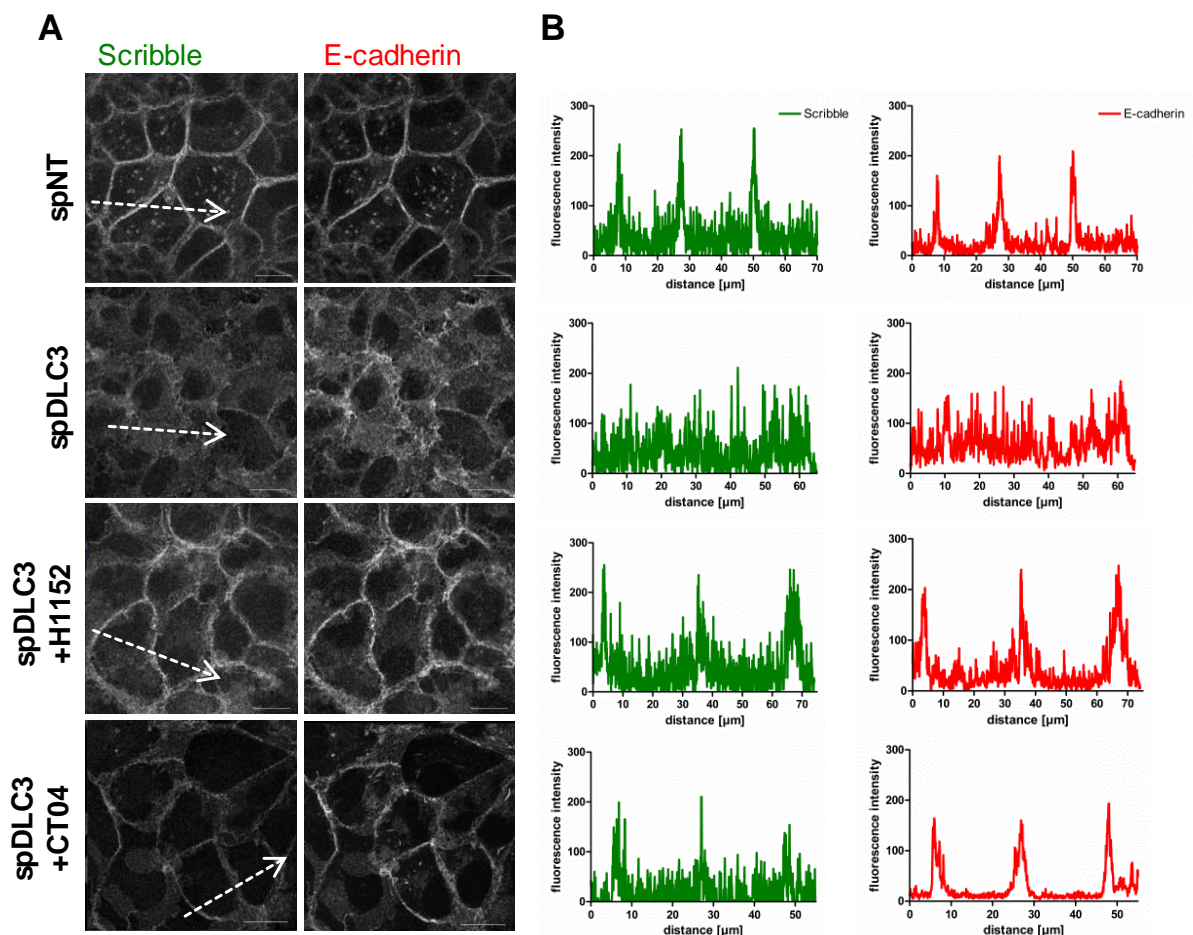
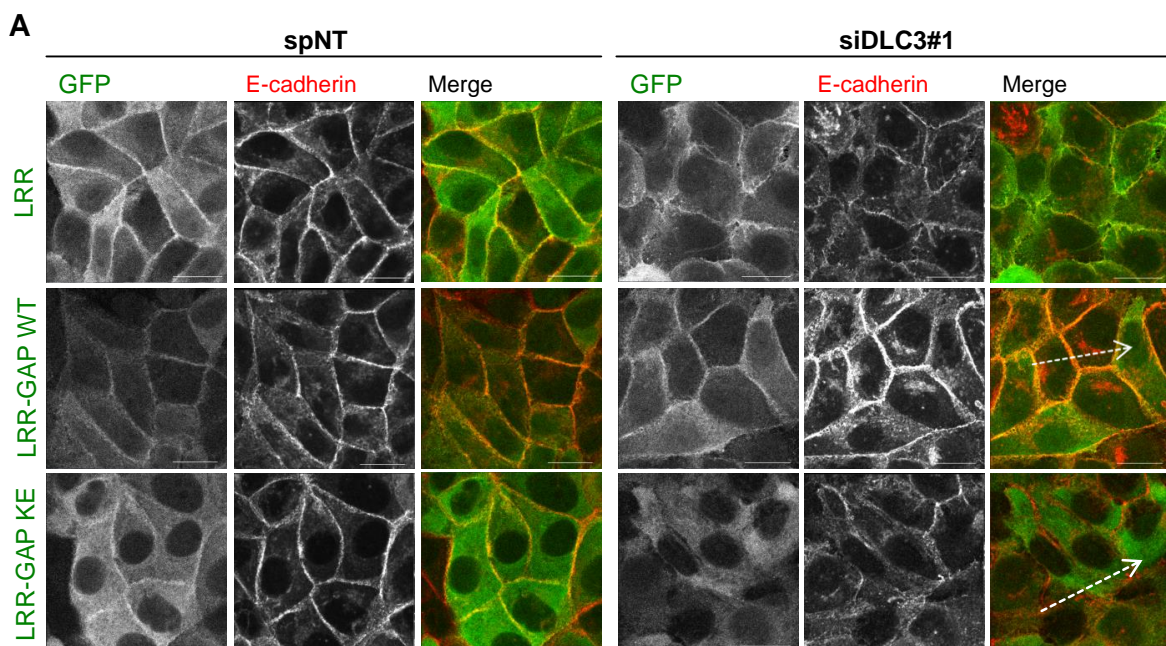


**Figure 17: Scribble localization and cell junction integrity depend on DLC3 as a regulator of Rho-ROCK activity.** (A) MCF7 cells were transfected with non-targeting (spNT) or DLC3-specific (spDLC3) siRNAs. Two days later, cells were treated with ROCK inhibitor overnight (H1152; 10  $\mu$ M) or on day 3 with Rho inhibitor (CT04; 50 ng/ml) for 5 h where indicated. Cells were fixed and stained for Scribble and E-cadherin. Representative maximum intensity projections are shown. Scale bars, 20  $\mu$ m. (B) The fluorescence intensities of Scribble and E-cadherin along the white arrows in A are depicted.

The junctional association of Scribble, as seen in the control cells, was abrogated by DLC3 knockdown, which was also characterized by impaired cell-cell adhesions. Interestingly, treatment of DLC3-depleted cells with ROCK (H1152) or Rho (CT04) inhibitor not only rescued the disruption of cell-cell contacts, but also restored Scribble localization (Fig. 17A,B). These data imply a mutual dependence of DLC3 and Scribble: On the one hand, Scribble localization depends on properly balanced RhoA-ROCK signaling at cell junctions controlled by the RhoGAP function of DLC3; on the other hand, DLC3 targeting to cell-cell contacts relies on the scaffolding function of Scribble.

### 3.5 A targeted GAP domain rescues adherens junction destabilization upon DLC3 knockdown

The N-terminal leucine rich-repeat (LRR) domains target the Scribble protein to the basolateral membrane and are important for its role in the establishment and maintenance of cell polarity (Navarro et al., 2005; Zeitler et al., 2004). To interrogate whether the GAP domain of DLC3 is sufficient for local Scribble-mediated regulation of Rho signaling, we artificially recruited the DLC3 GAP domain to cell-cell adhesions by fusing it to the LRR domains of Scribble. MCF7 cells stably expressing the GFP-tagged targeted wildtype GAP domain were generated and, as controls, cell lines stably expressing the targeted inactive GAP domain and LRR only. Then, gene silencing was performed using a DLC3-specific siRNA (siDLC3#1) that does not target the DLC3 GAP domain and knockdown efficiency was controlled by quantitative PCR (Fig. 18A,C).



## Results

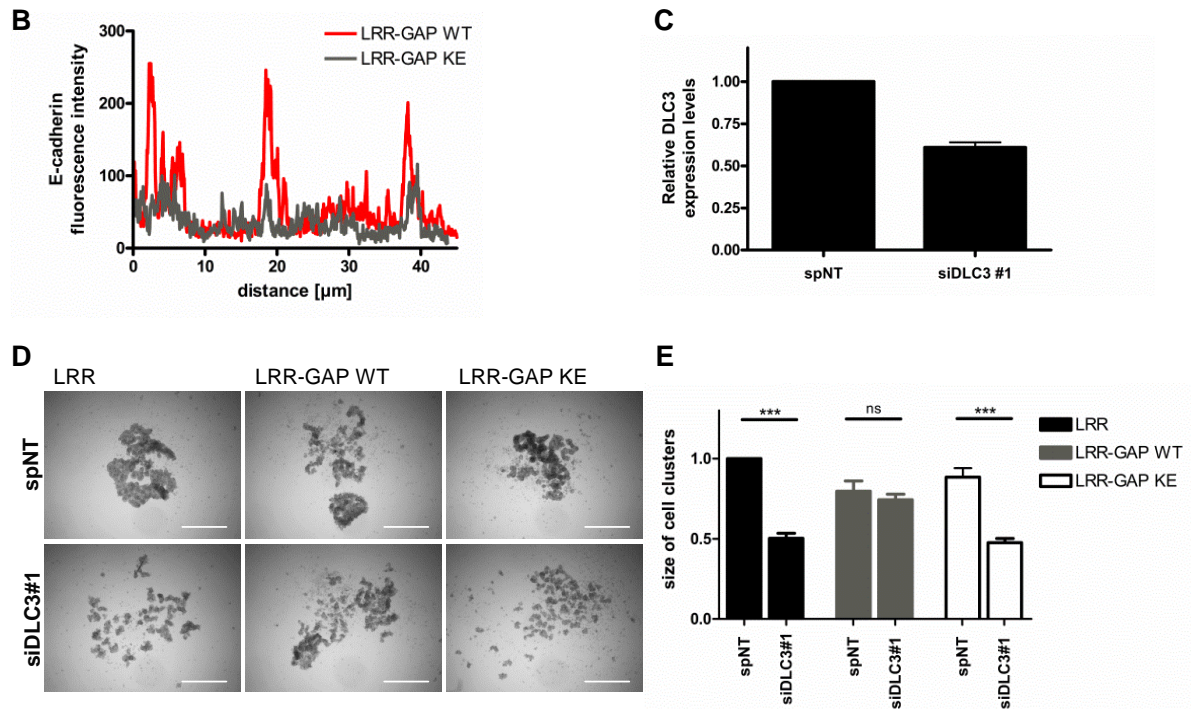


**Figure 18: Targeting of the DLC3 GAP domain to cell-cell contacts by Scribble-LRR domains rescues adherens junction destabilization upon DLC3 knockdown.** Stable MCF7 cells expressing GFP-Scribble LRR, LRR-DLC3 GAP WT or K725E, respectively, were transfected with non-targeting (spNT) or DLC3-specific (siDLC3#1) siRNAs. (A) 72 h post transfection, cells were fixed and stained with GFP- and E-cadherin-specific antibodies. The images shown are maximum intensity projections of several confocal sections. Scale bars, 20  $\mu\text{m}$ . (B) The fluorescence intensities of the E-cadherin signal along the white arrows in A are depicted. (C) RNA was extracted 72 h post transfection and relative DLC3 expression levels normalized to PPIA as a control gene were determined by quantitative PCR (N=2). (D) 72 h post transfection, cells were seeded in hanging drops. The next day, cell aggregates were dissociated by pipetting and photographed. Scale bars, 1 mm. (E) Quantification of the cell disaggregation shown in D. The area covered by cell clusters larger than 40,000  $\mu\text{m}^2$  was determined (mean  $\pm$  S.E.M. of 40 cell clusters derived from two independent experiments; one-way ANOVA).

LRR-mediated targeting was successful, as seen by the colocalization of LRR, LRR-GAP WT and LRR-GAP K725E with E cadherin in the stable control cells (Fig. 18A, left panel). Upon DLC3 depletion, cell-cell adhesions were disrupted in MCF7 cells expressing LRR alone or the inactive targeted GAP domain, which was accompanied by the redistribution of the LRR fusion proteins. Remarkably, LRR-mediated targeting of the wildtype DLC3 GAP domain rescued the disorganized E-cadherin staining and preserved the localization of the fusion protein to cell-cell adhesions (Fig. 18A, right panel; Fig. 18B). To quantify cell junction stability in dependence of targeted GAP activity, we next performed cell disaggregation assays in stable MCF7 cells expressing the LRR-GAP fusion proteins (Fig. 18D). In LRR- and LRR-GAP K725E-expressing control cells, DLC3 knockdown enhanced cell disaggregation by 50% (Fig. 18E). However, in accordance with our immunofluorescence data, LRR-mediated targeting of a functional DLC3 GAP domain completely rescued the cell disaggregation induced by DLC3 depletion (Fig. 18E).

Consequently, correct positioning of the DLC3 GAP activity at cell-cell adhesions by Scribble appears to be crucial for maintaining junctional integrity.

### 3.6 DLC3 localization at the leading edge depends on Scribble and is required for local Rho-ROCK regulation

In addition to its association with adherens junctions, Scribble localization at the leading edge of migrating cells has been reported. There, Scribble controls cell polarity and migration, for example by regulating Rac and Cdc42 activation via its interaction with the GEF protein  $\beta$ -Pix (Dow et al., 2006; Nola et al., 2008; Osmani et al., 2006). To address whether DLC3 might be recruited to the cellular front during directed cell migration in dependence of Scribble, we scratched confluent MCF7 monolayers stably expressing GFP-DLC3 and allowed the cells to polarize and migrate into the wound for 6 h (Fig. 19).

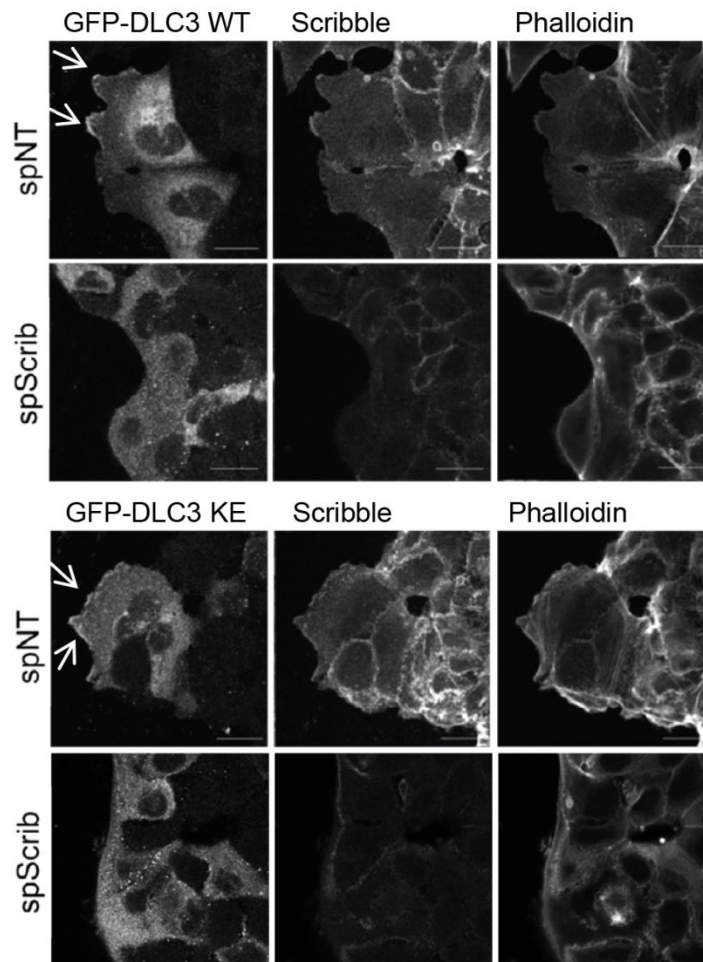


**Figure 19: DLC3 localization at the leading edge of migrating cells depends on Scribble.** Confluent layers of MCF7 cells stably expressing GFP-DLC3 WT and K725E, respectively, were scratched with a pipette tip. After 6 h migration, cells were fixed and stained with GFP- and Scribble-specific antibodies and Phalloidin (F-actin). Representative maximum intensity projections of the leading edge are shown. Scale bar, 20  $\mu$ m.

Immunostaining revealed an accumulation of wildtype and GAP-inactive DLC3 at membrane protrusions at the leading edge where it partially colocalized with endogenous Scribble. However, upon Scribble knockdown DLC3 enrichment at the cellular front was impaired and less or smaller membrane protrusions were formed (Fig. 19). Thus, the presence of Scribble seems to be required for DLC3 accumulation at the leading edge during directed cell migration and for polarization of the cells towards the wound scratch. To further examine the role of DLC3 and Scribble in regulating Rho signaling at the wound edge, we stained endogenous RhoA in DLC3- and Scribble-depleted MCF7 cells after sample preparation by trichloroacetic acid (TCA) fixation (Fig. 20A).

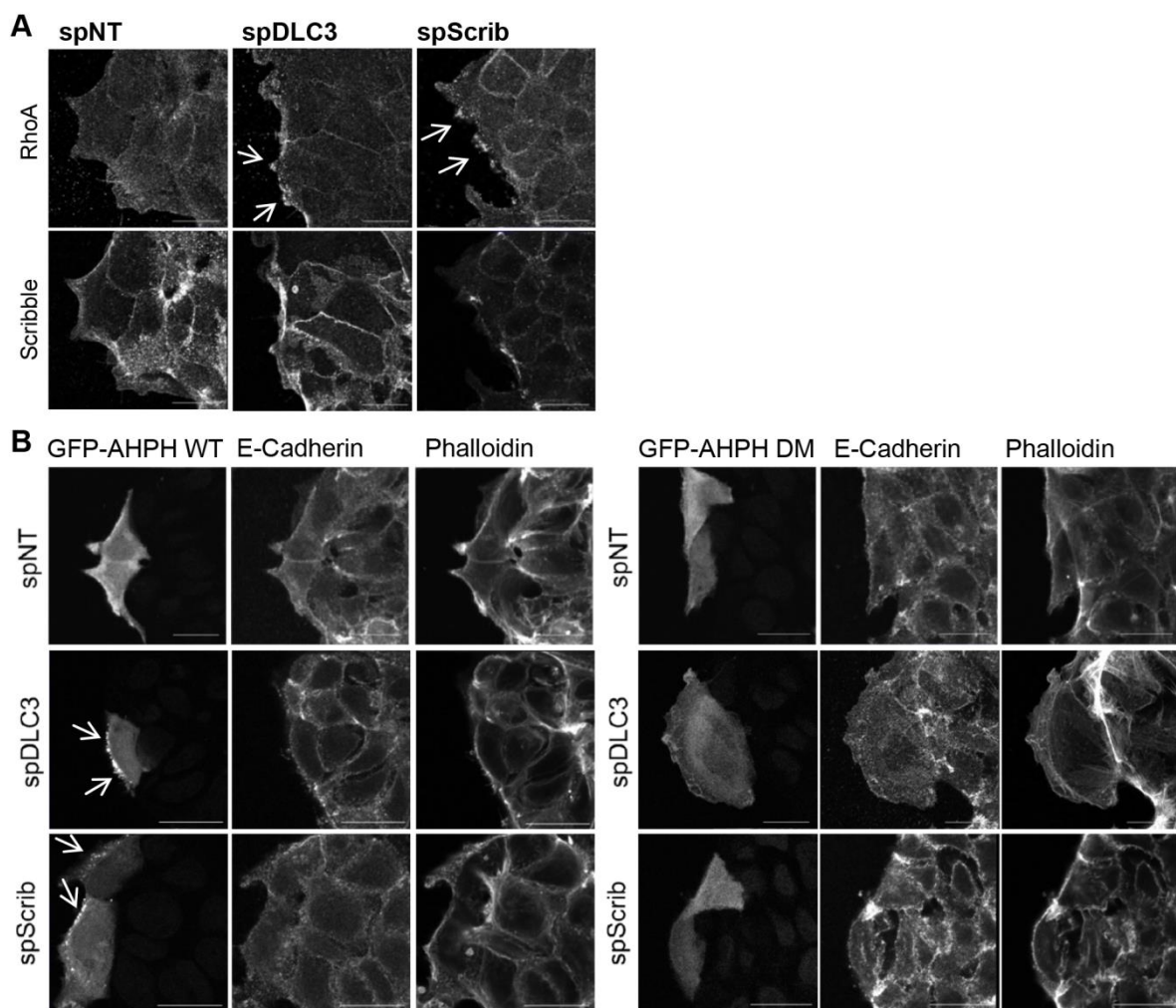


**Figure 20: DLC3 and Scribble knockdown cause RhoA accumulation and activation at the wound edge.** MCF7 cells were transfected with non-targeting (spNT), DLC3-specific (spDLC3) and Scribble-specific (spScrib) siRNAs, respectively. (A) After 72 h, confluent cell layers were scratched with a pipette tip and after 6 h migration, cells were fixed with trichloroacetic acid (TCA) and stained for RhoA and Scribble. (B) After two days, cells were transfected with plasmids encoding GFP-Anillin AHPH and A70D/E758K (DM), respectively, and were plated at high confluence onto collagen-coated glass coverslips. The next day, monolayers were wounded, fixed after 6 h migration and stained for E-cadherin and F-actin (Phalloidin). The images shown are maximum intensity projections of several confocal sections. Scale bars, 20  $\mu$ m.

Interestingly, upon DLC3 and Scribble knockdown, RhoA accumulation at distinct spots along the leading edge was detected reflecting elevated RhoA membrane association, and thus activation. In line with these findings, a scratch assay with knockdown cells transfected with the location biosensor for active RhoA (GFP-AHPH) yielded similar results (Fig. 20B). In contrast to the control samples, DLC3- and Scribble-depleted cells facing the wound scratch exhibited distinct biosensor accumulations along the leading edge. Finally, immunostaining of the ROCK substrate pMLC under these conditions revealed increased fluorescence intensities all along the cellular front of DLC3- and Scribble-knockdown cells compared to control cells or ROCK inhibitor treated cells (Fig. 21). Taken together, these data suggest that DLC3 and Scribble are important for restricting Rho-ROCK signaling at the leading edge of cells that polarize during directed migration.

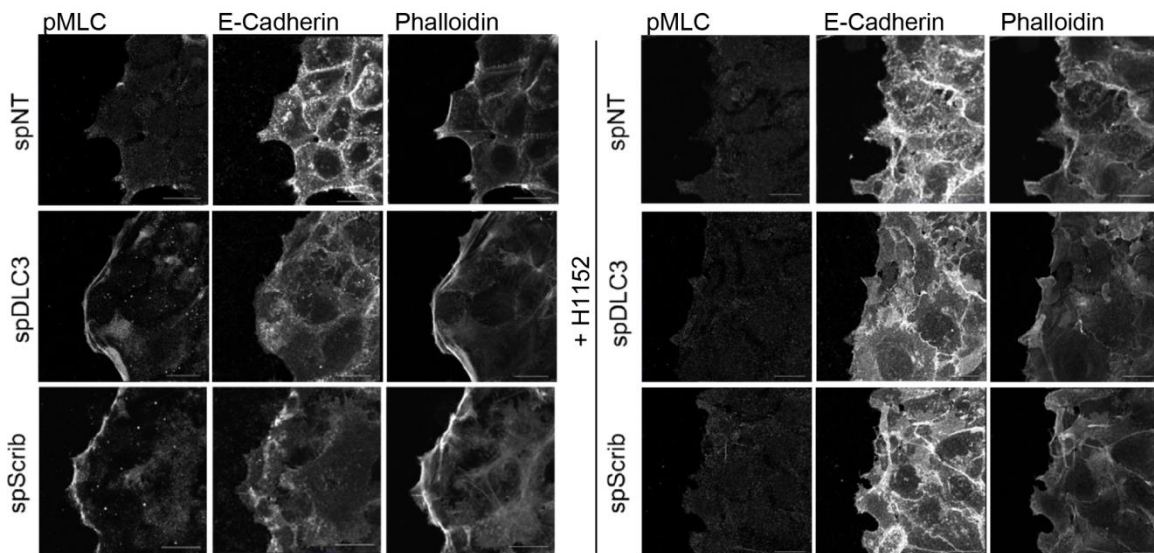
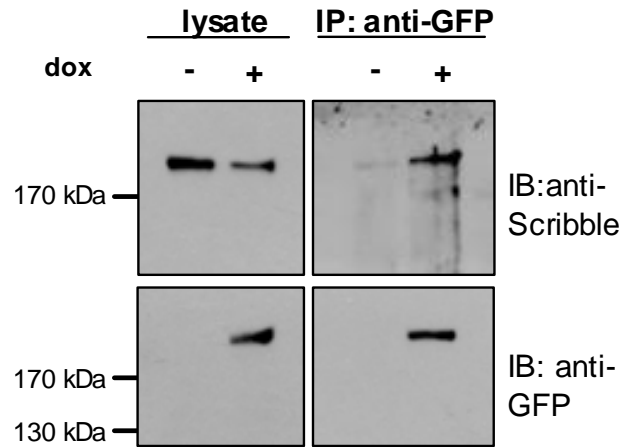


**Figure 21: Increased pMLC levels at the cellular front of DLC3- and Scribble-depleted cells.** MCF7 cells were transfected with the indicated siRNAs and migration into a wound scratch was performed as described in Fig. 20 in the presence of ROCK inhibitor (H1152, 10 $\mu$ M, 6 h) where indicated. Cells were stained for pMLC, E-cadherin and F-actin (Phalloidin). Representative maximum intensity projections of the leading edge are shown. Scale bar, 20  $\mu$ m.

### 3.7 The PDZL motif determines DLC3 localization at cell junctions and basolateral membranes in polarized Caco-2 cells

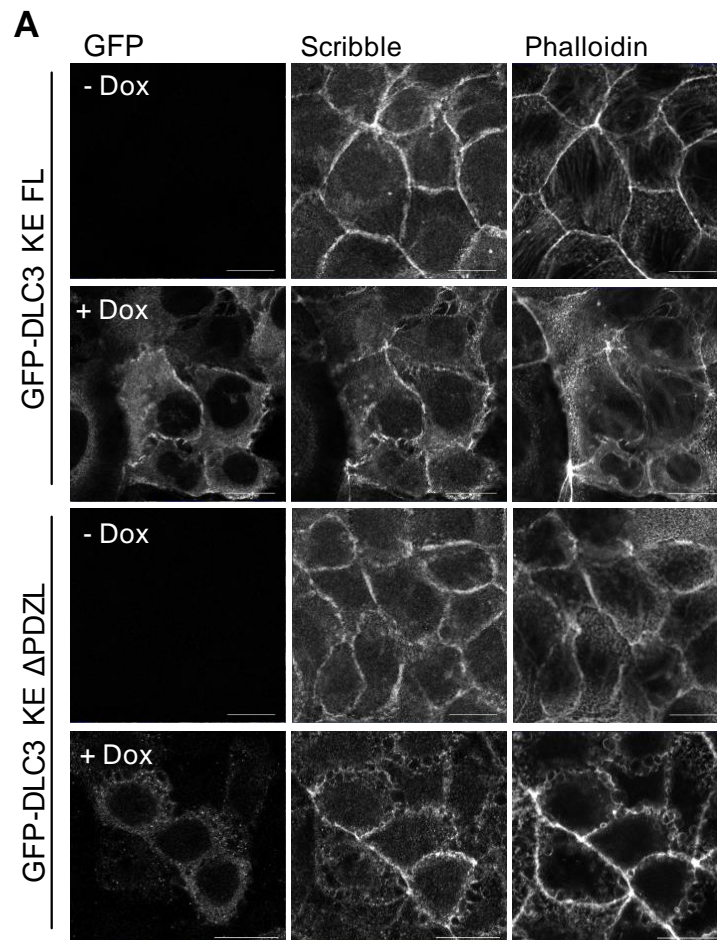
To analyze whether the PDZL-mediated interaction of DLC3 and Scribble is also relevant in other cellular systems, we generated Caco-2 colorectal carcinoma cells inducibly expressing the different DLC3 variants. We then switched on the expression of GAP-inactive, full-length DLC3 and the DLC3 PDZL deletion mutant by doxycycline treatment in established 2D monolayers (Fig. 23A). Full-length DLC3 accumulated at cell junctions

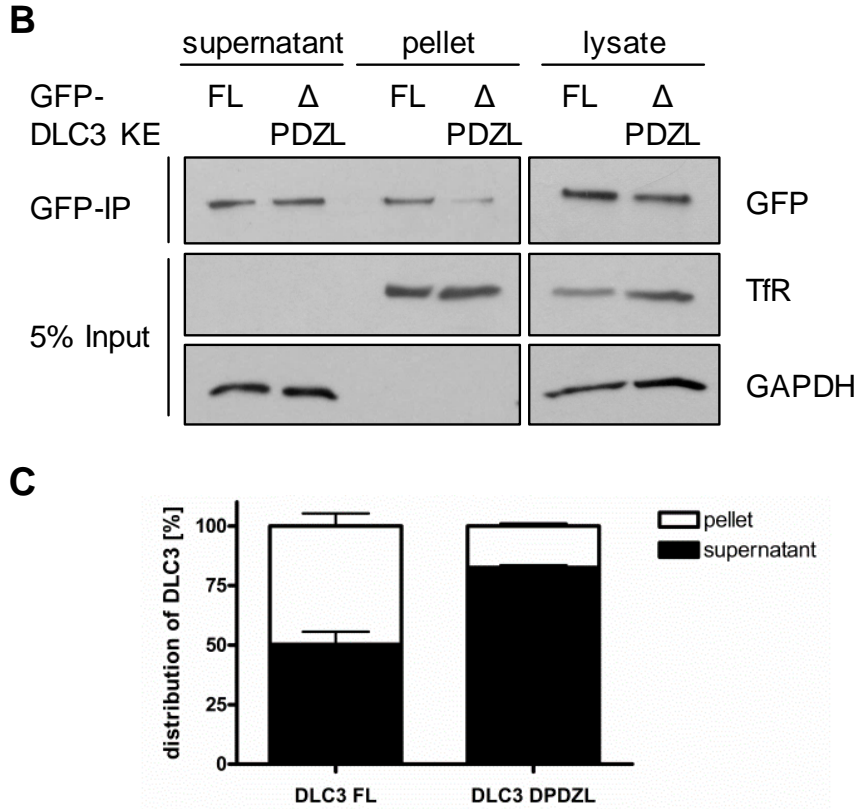
where it colocalized with endogenous Scribble (Fig. 23A) and the interaction of full-length GFP-DLC3 with endogenous Scribble was also confirmed biochemically (Fig. 22).



**Figure 22: DLC3 and Scribble interact in Caco-2 cells.** Caco-2 cells inducibly expressing GFP-DLC3 K725E were seeded and the next day, protein expression was induced by 2  $\mu$ g/ml dox for 24 h where indicated. Cell lysates were immunoprecipitated with an anti-GFP antibody. Samples were analyzed by immunoblotting using anti-GFP and anti-Scribble antibodies.

In full accordance with the results obtained in stable MCF7 cells, opposed to full-length DLC3, DLC3  $\Delta$ PDZL was distributed uniformly in the cells (Fig. 23A).

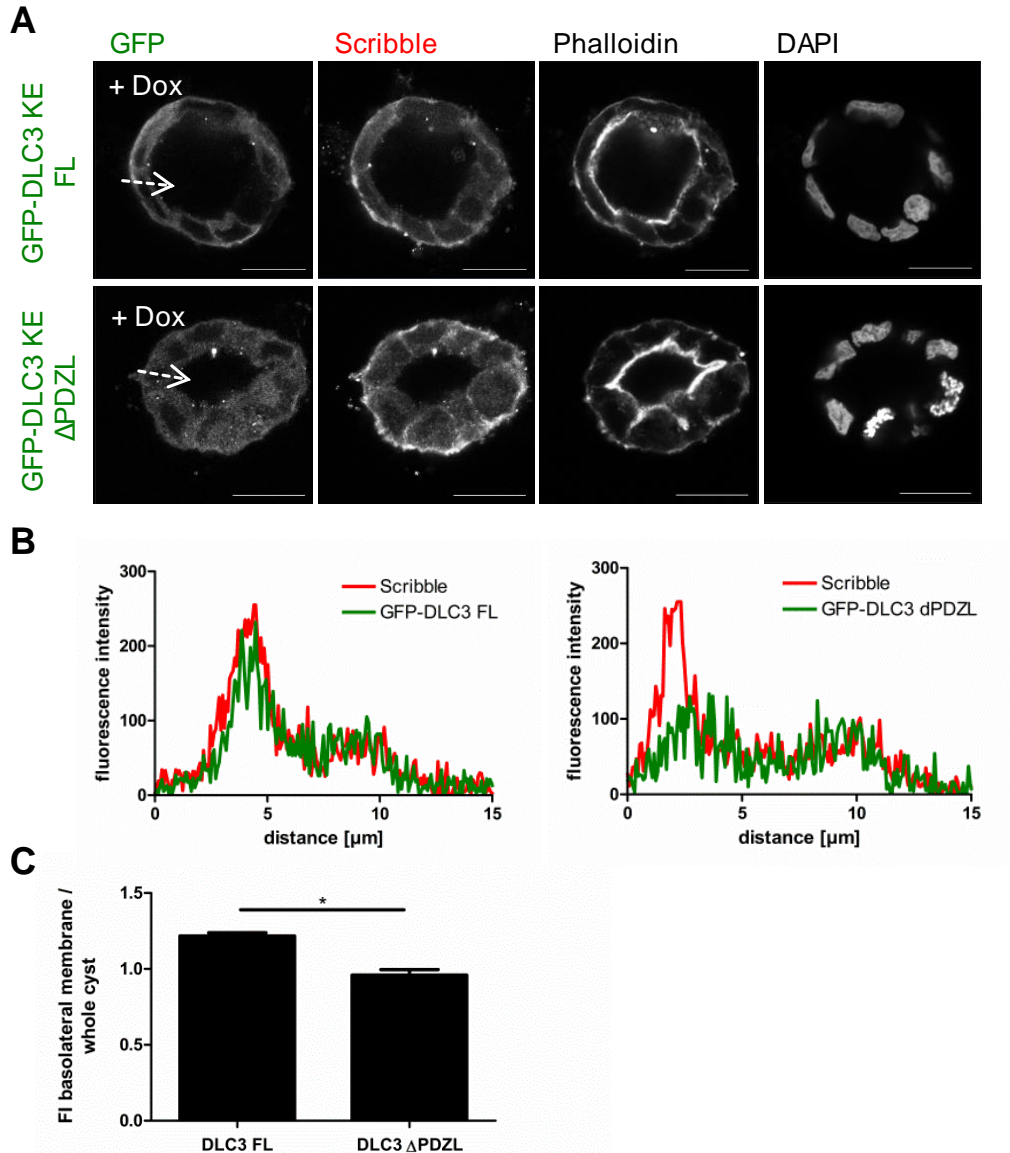




**Figure 23: The PDZ ligand motif determines junctional accumulation and membrane association of DLC3 in Caco-2 cells.** (A) Caco-2tet GFP-DLC3 K725E full-length (FL) and  $\Delta$ PDZL cells were grown on glass coverslips for seven days. Where indicated, DLC3 expression was induced by addition of 2  $\mu$ g/ml dox for 10 h. Cells were fixed and stained for GFP, Scribble and F-actin (Phalloidin). The images shown are confocal sections of representative cells. Scale bars, 20  $\mu$ m. (B) Caco-2tet GFP-DLC3 K725E FL and  $\Delta$ PDZL cells were seeded and the next day, DLC3 expression was induced with doxycycline for 10 h. Cellular fractions were generated and GFP-DLC3 was enriched by anti-GFP immunoprecipitation. Fractions and immunopurified proteins were analyzed by immunoblotting with anti-GFP, anti-transferrin receptor (TfR) and anti-GAPDH antibodies. (C) Quantification of the distribution of DLC3 FL and  $\Delta$ PDZL in the soluble cytosolic fraction (supernatant) and the detergent-soluble pellet fraction (N=2).

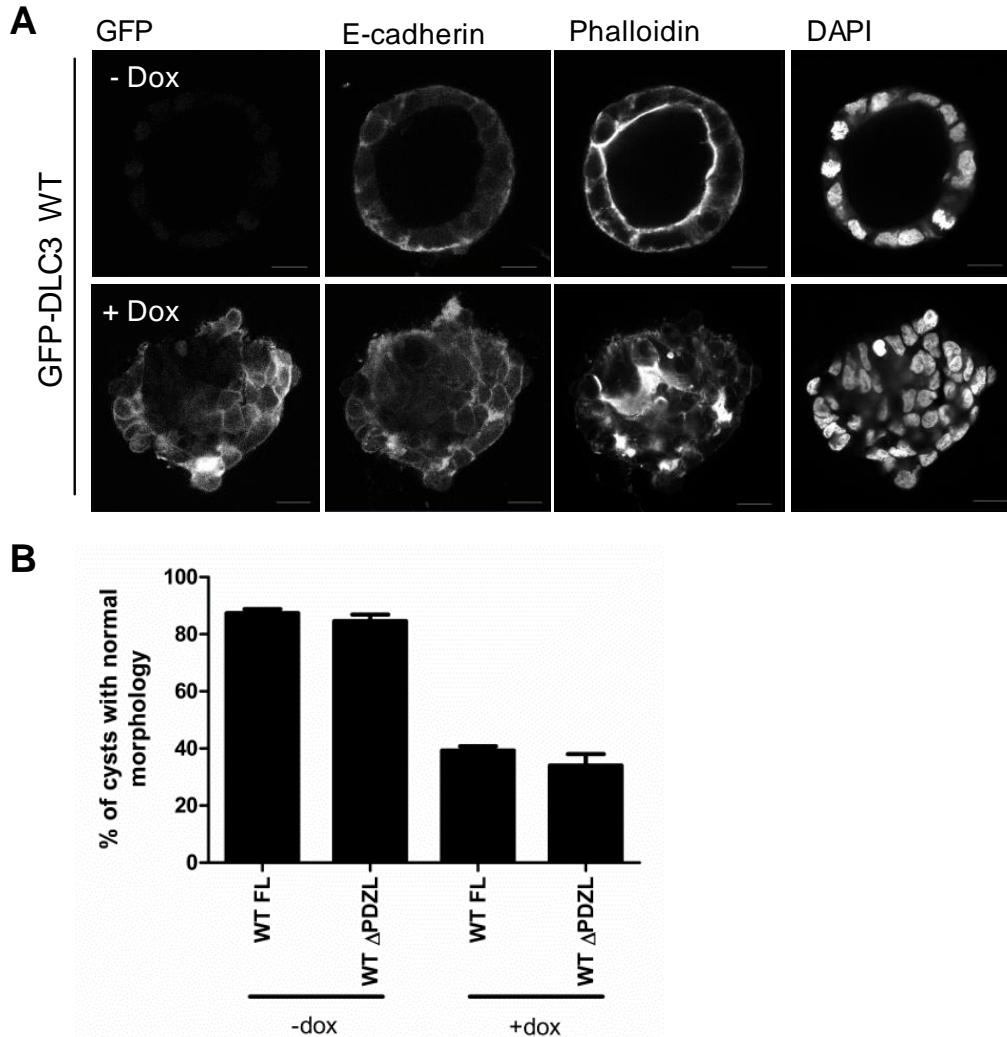
To quantify PDZL-motif-dependent subcellular distribution of DLC3, we performed fractionations of cells treated with doxycycline for 10 h only to avoid saturation with excessive protein. Prior to immunoblotting, the GFP-DLC3 proteins were enriched by immunoprecipitation from the supernatant fraction containing soluble cytosolic proteins and the pellet fraction containing detergent-soluble proteins. Compared to the full-length protein, the amount of DLC3  $\Delta$ PDZL in the detergent-soluble fraction was clearly reduced (Fig. 23B,C), supporting the idea that the PDZL motif is required for membrane recruitment of DLC3. We then analyzed DLC3 localization and function in 3D matrigel cultures, in which Caco-2 cells form polarized cysts consisting of a single epithelial cell layer with apical-basolateral polarity surrounding a hollow lumen. Expression of DLC3 WT in fully established cysts led to the collapse of lumens (Fig. 25A), whereas Caco-2 cysts

expressing GAP-inactive DLC3 K725E retained their polarized morphology associated with basolateral Scribble and apical F-actin accumulation (Fig. 24A). Consistent with the results in 2D monolayers, full-length DLC3 colocalized with Scribble at the basolateral membrane, which was significantly reduced by PDZL deletion (Fig. 24A,B,C). Taken together, our findings show that the PDZL motif is essential for the basolateral membrane localization of DLC3 in polarized Caco-2 cells and highlight the importance of properly balanced DLC3 GAP activity for the maintenance of the polarized morphology.



**Figure 24: Basolateral DLC3 localization in polarized Caco-2 cysts is controlled by its PDZL motif.** (A) Caco-2tet GFP-DLC3 K725E full-length (FL) and  $\Delta$ PDZL cells were grown in 3D matrigel culture. Three days post seeding, cholera toxin was added to induce lumen formation. The next day, DLC3 expression was induced by doxycycline addition for 10 h. Cultures were fixed and stained for GFP, Scribble and F-actin (Phalloidin). Nuclei were counterstained with DAPI. Shown are maximum intensity projections of confocal sections of the midplane of representative cysts. Scale bars, 20  $\mu\text{m}$ . (B) The fluorescence intensities of GFP-DLC3 and Scribble along the white arrows in A are depicted. (C) Quantification of the fluorescence intensity (FI) ratio of the basolateral signal to that of the whole cyst of GFP-DLC3 K725E FL and  $\Delta$ PDZL, respectively ( $n \geq 12$ ;  $N = 3$ ; paired t-test).

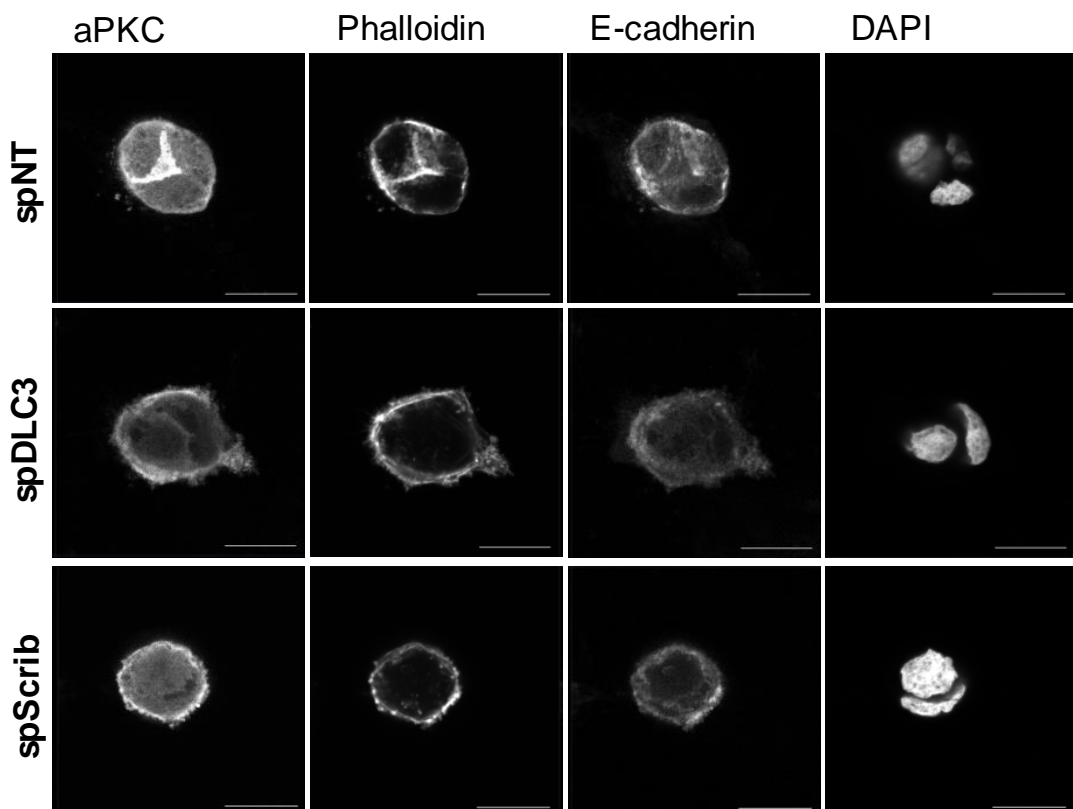
Unfortunately, based on the quantification of the number of cysts with a normal polarized morphology, we could not demonstrate any altered biological function for GAP-competent DLC3  $\Delta$ PDZL (Fig. 25B), which is most likely due to the saturation of cells with overexpressed protein. To assess such functional differences, DLC3 expression should be driven by a weaker promoter.



**Figure 25: Expression of GAP-active DLC3 disrupts the polarized morphology of established *Caco-2* cysts.** (A) *Caco-2*tet GFP-DLC3 WT cells were grown in 3D matrigel culture. Three days post seeding, cholera toxin was added to induce lumen formation. The next day, GFP-DLC3 WT expression was induced by doxycycline overnight. The next day, cultures were fixed and stained for GFP, E-cadherin and F-actin. Nuclei were counterstained with DAPI. Shown are maximum intensity projections of confocal sections of the midplane of representative cysts. Scale bars, 20  $\mu$ m. (B) The percentage of *Caco-2* cysts with normal morphology after overnight induction of GAP-active GFP-DLC3 FL and  $\Delta$ PDZL, respectively, was determined. (n=100; N=3).

### 3.8 DLC3 and Scribble are required for polarization and lumen formation of Caco-2 cysts in 3D culture

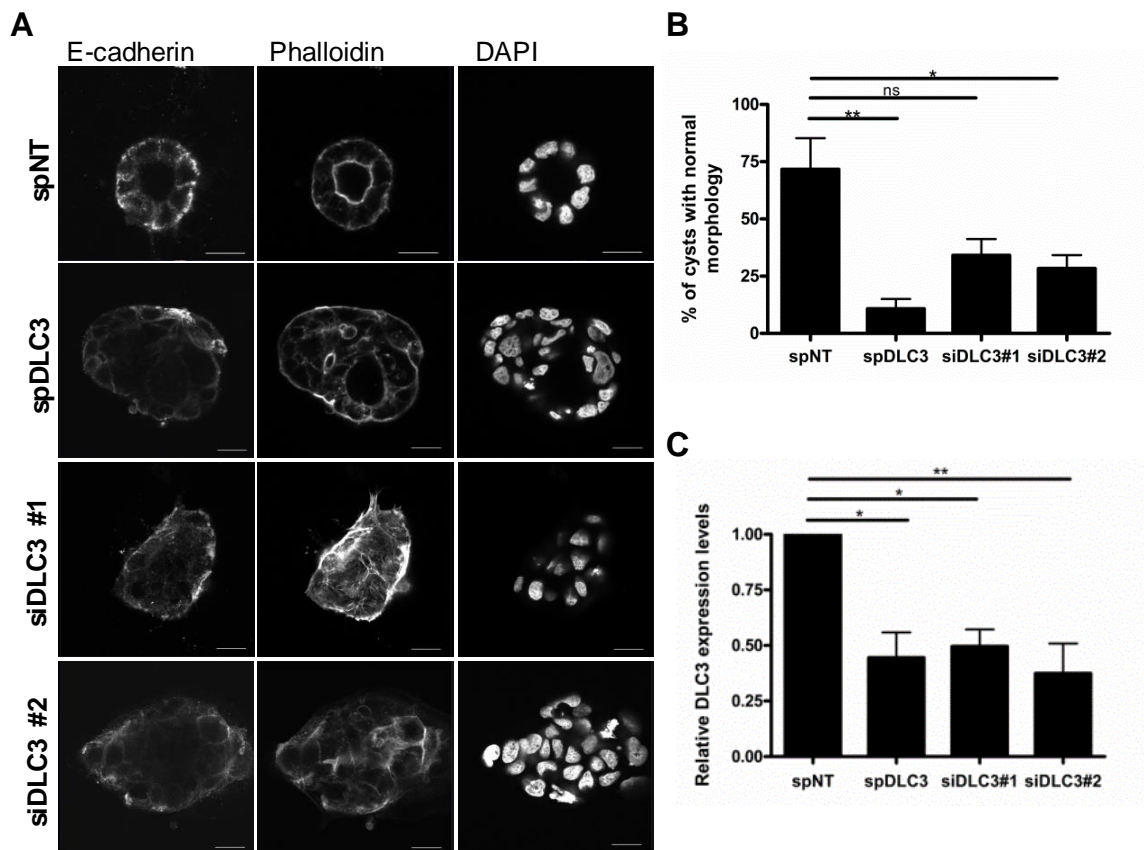
Finally, to study their role in polarized epithelial morphogenesis, we knocked down DLC3 and Scribble before seeding of cells into 3D matrigel cultures containing EGF. Previous studies have shown that EGF stimulates proliferation of Caco-2 cells, leading to a larger size of cysts, but it does not interfere with polarized cyst development (Möller et al., 2014). After two days, cultures were fixed and stained for aPKC, E-cadherin and F-actin (Phalloidin). Already at the two-cell stage of Caco-2 cyst differentiation, apical-basolateral polarization can be assessed by enrichment of the apical markers aPKC and F-actin at the cell-cell interface. This apical surface is preserved during cyst development and specifies the initiation site for lumen formation. Upon DLC3 and Scribble depletion, however, cells failed to form the apical polarity axis seen in the control samples and diffuse aPKC and Phalloidin staining patterns were observed instead (Fig. 26).



**Figure 26: DLC3 and Scribble depletion impair apical-basolateral polarization at the two-cell stage during Caco-2 cyst development.** Caco-2 cells were transfected with non-targeting (spNT), DLC3-specific (spDLC3) or Scribble-specific (spScrib) siRNAs, respectively. The next day, cells were seeded in 3D cultures containing 10 ng/ml EGF. After 48 h, cultures were fixed and stained with anti-aPKC and anti-E-cadherin antibodies and Phalloidin (F-actin). Nuclei were counterstained with DAPI. The images shown are maximum intensity projections of several confocal sections. Scale bars, 20  $\mu$ m.

## Results

To further monitor the morphogenesis of DLC3- and Scribble-depleted cysts, cells were maintained in 3D culture for four days. On day 3, lumen formation was induced with cholera toxin and, the next day, the cysts were fixed and stained for E-cadherin and F-actin as basolateral and apical markers, respectively (Fig. 27A,D). Efficient downregulation of DLC3 and Scribble were confirmed by quantitative PCR and immunoblotting, respectively (Fig. 27C,F). We found that upon DLC3 and Scribble knockdown, Caco-2 cells failed to form cysts with a single lumen, distinct apical F-actin staining, and E-cadherin distribution was no longer restricted to basolateral membranes. DLC3 and Scribble depletion resulted in similar phenotypes characterized by the formation of flat and spread multicellular structures with multiple or no lumens (Fig. 27A,D). Quantification revealed that more than 70% of the Caco-2 control cysts developed normally, as assessed by their round morphology, well-defined apical F-actin staining and the presence of a single apical lumen. By contrast, DLC3 and Scribble knockdown caused a significant reduction of cysts with normal morphology (spDLC3: 11% and spScrib: 28%; Fig. 27B,E), which was confirmed by independent siRNAs targeting DLC3 and Scribble (Fig. 27A-F). Taken together, these data provide evidence that DLC3 and Scribble are both required for polarized epithelial morphogenesis and lumen formation of Caco-2 cells.



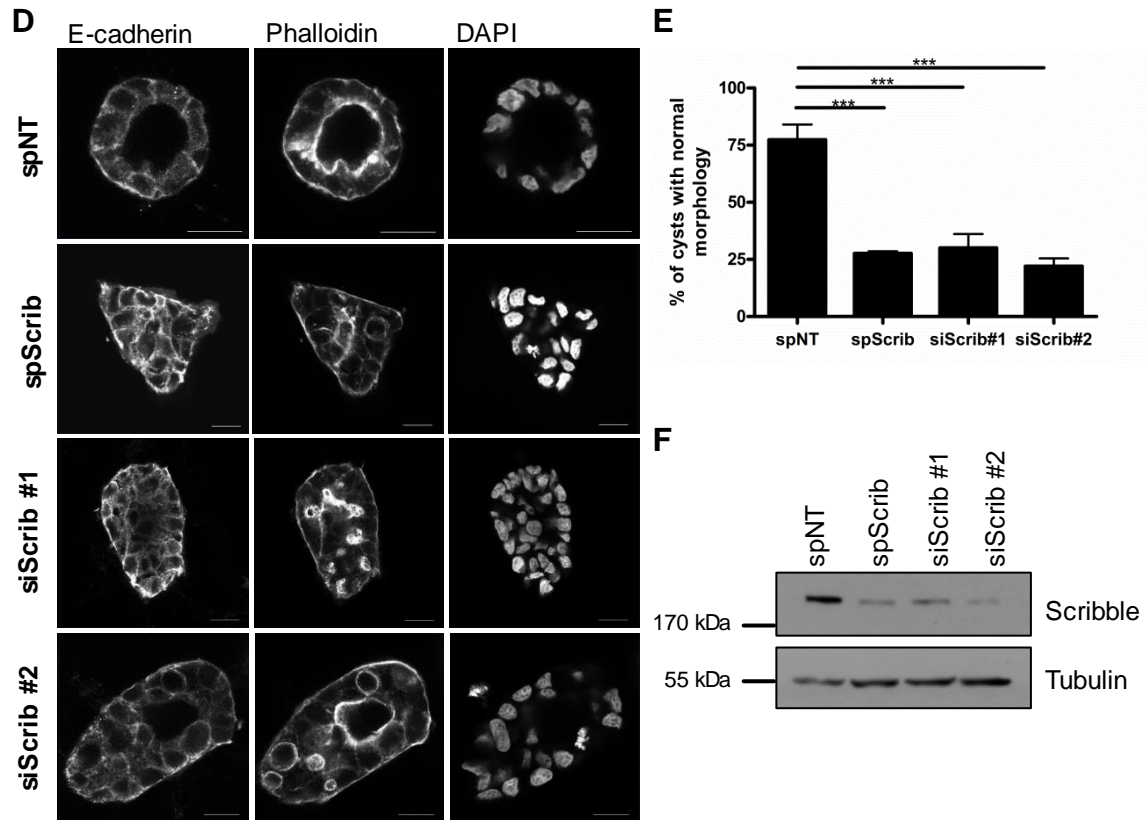


**Figure 27: DLC3 and Scribble knockdown cause aberrant morphogenesis of Caco-2 cysts.** (A+D) Caco-2 cells were transfected with non-targeting (spNT), DLC3-specific (spDLC3, siDLC3#1 and siDLC3#2) or Scribble-specific (spScrib, siScrib#1 and siScrib#2) siRNAs, respectively. The next day, cells were seeded in 3D cultures containing 10 ng/ml EGF. After three days, lumen formation was induced with cholera toxin. The next day, cultures were fixed and stained with an anti-E-cadherin antibody and Phalloidin (F-actin). Nuclei were counterstained with DAPI. Shown are confocal sections of the midplane of representative cysts. Scale bars, 20  $\mu$ m. (B+E) The percentage of Caco-2 cysts with normal morphology was determined (n=100; N=3; paired t-test). (C) Verification of DLC3 depletion in Caco-2 cells by quantitative PCR. RNA was extracted 72 h after transfection of the indicated siRNAs. Relative DLC3 expression levels normalized to PPIA as an endogenous control gene were determined (N=3; one-way ANOVA). (F) Whole cell lysates of Caco-2 cells were analyzed by Western blotting with anti-Scribble and anti-tubulin antibodies.

## 4. Discussion

### 4.1 The DLC3-Scribble complex regulates Rho signaling at adherens junctions

The formation and maintenance of cell-cell adhesions and epithelial polarity requires spatiotemporally restricted activation of different Rho GTPases. How this is achieved by GEF and GAP proteins and how these Rho regulators themselves are controlled, is still poorly understood. Protein interactions are important control mechanisms that specify the subcellular localization of GEFs and GAPs and modulate their activities. Since the RhoGAPs of the DLC family seem to differ in their functions, it is of special interest to elucidate how the least studied DLC3 isoform is targeted to specific subcellular sites to act on distinct GTPase pools. Thus, the major aim of this thesis was to determine DLC3 binding partners and especially to reveal by which mechanism DLC3 is recruited to cell-cell adhesions to maintain their integrity (Holeiter et al., 2012). First, DLC3 interactors were identified using a proteomic approach and junction-associated candidates were considered more closely. As a result, the basolateral polarity protein and tumor suppressor Scribble was discovered as the first isoform-specific scaffold for DLC3 at cell-cell contacts. Biochemical characterization revealed that the interaction is mediated by the PDZ domains of Scribble and a unique C-terminal PDZ ligand (PDZL) motif contained in DLC3. Moreover, using a location biosensor for active RhoA and a LRR-targeted GAP domain, convincing evidence was provided showing that DLC3 is required for local RhoA regulation at cell-cell adhesions to control E-cadherin function. Furthermore, a mutual dependence of DLC3 and Scribble concerning their localization was elucidated: On the one hand, Scribble functions as a scaffold to recruit DLC3, thereby ensuring locally restricted Rho activity at cell-cell contacts and basolateral membranes. On the other hand, as a negative regulator of Rho-ROCK signaling, DLC3 is required for adherens junction maintenance and, consequently, for junctional Scribble localization.

Scribble modulates Rac activity in epithelial cells by recruiting the RacGEF  $\beta$ -Pix to adherens junctions through a PDZ domain-interaction (Frank et al., 2012; Zhan et al., 2008). In addition, in this work a new role of Scribble in the control of junctional Rho signaling was revealed by targeting DLC3, as a RhoGAP, to basolateral membranes to locally restrict RhoA activity. Thus, Scribble contributes in a dual manner to the establishment of antagonistic Rho and Rac activity gradients along the apical-basal axis of epithelial cells. Interestingly, loss of DLC3 and Scribble result in similar phenotypes with regard to E-cadherin localization and epithelial integrity. Scribble depletion is associated

with altered adherens junction structure, cell aggregation defects and increased sheet migration, which are consequences of attenuated E-cadherin-p120-catenin binding and E-cadherin internalization, among others (Lohia et al., 2012; Qin et al., 2005). Similarly, loss of DLC3 mislocalizes E-cadherin and  $\beta$ -catenin from adherens junctions, reduces cell-cell adhesion and enhances cell migration (Holeiter et al., 2012). Hence, the physical binding of DLC3 and Scribble seems to translate into a biological interaction. In further studies, it would be interesting to investigate whether loss of DLC3, as a candidate tumor suppressor, also cooperates with oncogenes like Ras in cell transformation and invasion, as it was described for the tumor suppressor Scribble (Dow et al., 2008; Pagliarini and Xu, 2003).

Constitutively active RhoA leads to aberrant ROCK signaling and increased cell contractility, which in turn disrupts cell-cell adhesions and impairs polarized epithelial morphogenesis (Paszek et al., 2005; Sahai and Marshall, 2002b). Consequently, tight regulation of local Rho-ROCK activity is required to organize epithelial architecture. In this thesis, experimental proof for the role of DLC3 as a junctional regulator of Rho-ROCK signaling was obtained by various assays: On the one hand, using a biosensor for active RhoA, DLC3-mediated regulation of junctional RhoA activity was verified. On the other hand, rescue of junction destabilization by Rho and ROCK inhibitors in DLC3-depleted cells confirmed the requirement for DLC3 in spatially restricting Rho-ROCK signaling. Moreover, it was proven that targeting of the DLC3 GAP domain to basolateral membranes by Scribble is sufficient to maintain adherens junction integrity. Interestingly, while junctional E-cadherin localization was restored in DLC3-depleted cells expressing the targeted GAP domain, additional perinuclear E-cadherin accumulation was observed under these conditions (see Fig. 18A, right panel). This indicates that positioning of DLC3's GAP activity by Scribble specifically restores the DLC3-knockdown phenotype at cell junctions, but apparently fails to compensate for other functions of the RhoGAP in protein transport and turn-over.

The Scribble complex component discs large (Dlg) was also identified as a DLC3 binding partner by our mass spectrometry analysis, further supporting the relevance of the Scribble complex for DLC3 recruitment (Table 14). Since the Dlg-intensity values were much lower than those of Scribble, we assume that the interaction might be indirect and probably mediated by Scribble. However, it is possible that there are alternative protein interactions supporting Scribble in the recruitment of DLC3 to cell-cell contacts. Furthermore, we detected in our proteomic approach several components of the syntrophin-utrophin-dystrobrevin complex, which constitutes a scaffold for mechanical

stabilization during contraction of muscle cells (Albrecht and Froehner, 2002). Considering that  $\beta$ 2-syntrophin was recently reported to be crucial for junction assembly and apical-basal polarity in epithelial cells (Mack et al., 2012), DLC3 targeting to cell junctions might also be mediated by this alternative scaffold in addition to Scribble. Taking into account that the syntrophin complex is particularly important in muscle cells, it is conceivable that DLC3 might have yet unknown functions in such cells.

## **4.2 DLC3 and Scribble in the establishment of epithelial polarity**

In addition to maintaining adherens junction stability, DLC3 and Scribble were identified to play a role in epithelial morphogenesis. Gene silencing experiments in Caco-2 three-dimensional cultures revealed that upon DLC3 or Scribble knockdown, cyst polarization and lumen formation were impaired. In previous studies, no prominent phenotype was observed upon DLC3 or Scribble depletion in MCF10A acini (Dow et al., 2006; Holeiter et al., 2012), which contrasts with our findings in the Caco-2 system. However, it is important to note that only in the presence of EGF did we detect severe polarity defects in DLC3- and Scribble-depleted cells. This is in accordance with the observation that specific oncogene activation or cytokine exposure cooperates with the loss of Scribble in disrupting epithelial differentiation and inducing invasive phenotypes (Chatterjee et al., 2012; Waghmare and Kango-Singh, 2016). Moreover, Scribble depletion was shown to impair HGF-mediated epithelial morphogenesis of MDCK cells in three-dimensional cultures, supporting the idea that loss of Scribble cooperates with growth factor signaling to induce polarity defects (Eastburn et al., 2012).

It is striking that already at the two-cell stage of cyst development, polarity defects were observed in DLC3- and Scribble-depleted cells. The apical membrane initiation site (AMIS), which is generated by polarized transport of apical components after the first cell division and later specifies the initiation site for lumen formation (Overeem et al., 2015), was not established in the knockdown cysts. Instead, diffuse staining patterns of the apical markers aPKC and phalloidin were detected. These findings indicate that aberrant cyst morphology in the absence of DLC3 and Scribble is not only a result of junction destabilization, but also due to a failure in asymmetric protein distribution and establishment of polarity. Considering that DLC3 and Scribble are both involved in coordinating endocytic membrane trafficking, and EGF increases E-cadherin turnover (Bryant et al., 2007), the impaired polarization of DLC3- and Scribble-depleted cysts might be caused by altered vesicular trafficking. DLC3 was shown to regulate Rab8-dependent trafficking and to be involved in transferrin and EGFR recycling (Braun et al., 2015).

Rab8/Rab11-driven endocytic recycling is important for junctional maintenance of E-cadherin and for the enrichment of apical components at the cell-cell interface during cyst development, identifying these Rab proteins as important regulators of lumenogenesis (Bryant et al., 2010; Desclozeaux et al., 2008; Sakamori et al., 2012). Furthermore, a more global role of DLC3 in coordinating the transport of different cargos is conceivable, which might also include trafficking of junctional components like E-cadherin. In this context, it would be interesting to examine in more detail the impact of DLC3 depletion on the abundance of junctional and transmembrane proteins in general on the cell surface using a quantitative proteomic approach. Similar to DLC3, Scribble is implicated in endocytic trafficking processes. Particularly, Scribble was described to control trafficking of retromer-dependent cargos like E-cadherin (de Vreede et al., 2014; Lohia et al., 2012), suggesting an important role for Scribble in vesicular transport. Thus, in addition to their local role at adherens junctions, by regulating protein trafficking, Scribble and DLC3 might both be relevant for asymmetric protein distribution during the establishment of cell polarity. In future studies, analysis of DLC3 localization in combination with Rho activity patterns should shed light onto the precise site of DLC3 action at the two-cell stage of cyst morphogenesis.

Spatiotemporally controlled Rho-ROCK activity is important for polarized epithelial morphogenesis, since it contributes to apical-basolateral membrane specification and correct lumen formation (Overeem et al., 2015). In particular, this includes high Rho-ROCK activity at the cell surface facing the extracellular matrix (ECM) during the initial phase of polarization, followed by integrin-mediated p190RhoGAP recruitment to reduce Rho activation at the basolateral membrane in the two-cell stage of cyst differentiation (Bryant et al., 2014; Yu et al., 2008). Further examples for the involvement of Rho regulators during three-dimensional morphogenesis are p114RhoGEF and the RhoGAP ArhGAP29, which are both required for lumen formation by controlling the Rho-ROCK-myosin II pathway (Kim et al., 2015; Xu et al., 2011). Considering that Caco-2 morphology and lumen integrity are perturbed by expression of GAP-active, wildtype DLC3, and loss of DLC3 also interferes with polarized cyst development, it would be interesting to uncover the exact consequences of deregulated Rho signaling on the polarity defect in DLC3-knockdown cysts. Since immunostaining of active RhoA and pMLC were not successful, and also transient transfection of the RhoA biosensor was not compatible with the Caco-2 3D-cultures, the generation of inducible Caco-2 cells expressing the biosensor upon doxycycline induction might help to answer this question. In such cells, the effects of DLC3 and Scribble depletion on Rho regulation during the different steps of cyst morphogenesis could be precisely monitored.

Moreover, it is possible that other Rho GTPases in addition to RhoA are deregulated and contribute to the aberrant morphogenesis of the knockdown cysts. In the context of DLC3-coordinated endocytic trafficking, the RhoB isoform is discussed as a new potential substrate of DLC3 (Braun et al., 2015). RhoB is typically localized on endosomes, was reported to delay EGFR trafficking (Fernandez-Borja et al., 2005; Gampel et al., 1999), a phenotype also observed upon DLC3 depletion, and only simultaneous knockdown of RhoA and RhoB restored transferrin recycling upon loss of DLC3 (Braun et al., 2015). Interestingly, a novel function of RhoB at cell-cell contacts was recently discovered. In particular, it was shown that RhoB colocalized with E-cadherin at cell junctions in prostate cancer cells where it controlled E-cadherin expression and the strength of cell-cell adhesions (Vega et al., 2015). In addition, RhoB was reported to traffic to cell borders during junction formation to regulate endothelial barrier integrity and Rac trafficking to and its activity at membrane protrusions (Marcos-Ramiro et al., 2016). Hence, DLC3 might be involved in the regulation of RhoB activity at cell-cell contacts, in addition to its role as a junctional RhoA regulator as found in this work. A difficulty for further investigations, however, is the compensatory RhoB upregulation often observed upon RhoA depletion, which impedes the analysis of isoform-specific effects. Consequently, the use of RhoB-specific FRET biosensors would help to elucidate spatiotemporal RhoB activation patterns. Furthermore, DLC3 was shown to exhibit weak GAP activity towards Cdc42, at least *in vitro* (Kawai et al., 2007), while Scribble is able to indirectly modulate Cdc42 activation through the interaction with the Cdc42GEF  $\beta$ -Pix (Audebert et al., 2004). Considering that Cdc42 is relevant for apical-basal polarization, polarized protein trafficking and spindle positioning during lumen formation (Bray et al., 2011; Jaffe et al., 2008; Mack and Georgiou, 2014; Ngok et al., 2014), further investigations might address a potential direct or indirect role of Cdc42 in the development of the DLC3- and Scribble-knockdown phenotypes. Generally, it remains to be determined how the substrate specificity of GAPs like DLC3 for Rho proteins and the selection of certain downstream signaling pathways are controlled. Probably, besides structural requirements, this might depend on the cellular context, specific interaction partners and posttranslational modifications of the Rho regulators.

### **4.3 A novel function of DLC3 at the leading edge**

Previously unknown roles of DLC3 and Scribble in the restriction of RhoA signaling at the leading edge during directed cell migration were revealed by this thesis. Particularly, it was shown that Scribble is required for DLC3 accumulation at membrane protrusions at the leading edge. Moreover, DLC3 and Scribble both turned out to be essential for

inhibiting RhoA-ROCK activation at wound edges, which was confirmed by RhoA and pMLC stainings, and also by RhoA biosensor analysis. In the past, Scribble has already been identified to regulate Rac and Cdc42 activation at the leading edge of breast cancer cells and astrocytes via  $\beta$ -Pix recruitment (Dow et al., 2006; Nola et al., 2008; Osmani et al., 2006). However, to the best of our knowledge, it is a novel finding that Scribble also controls RhoA signaling at the cellular front. Front-rear polarization is typically characterized by elevated Rac/Cdc42 and restricted RhoA activation at the leading edge and an opposite scenario at the rear of the cell promoting cell migration. In the light of the potential tumor suppressive properties of Scribble and DLC3 associated with their roles in adherens junction maintenance, it seems surprising at the first sight that they are involved in the establishment of leading edge polarity. However, taking into account that Scribble and the DLC family member DLC1 are both crucial for embryonic development and tissue morphogenesis in *Drosophila* and mice (Bilder and Perrimon, 2000; Durkin et al., 2005; Durkin et al., 2007b; Pearson et al., 2011), it is tempting to speculate that also DLC3 might possess such context-specific functions as a polarity regulator during development.

The establishment of leading edge polarity is a complex process and so far we cannot distinguish whether impaired DLC3 accumulation is directly attributed to the loss of Scribble or an indirect effect of polarity disruption. To ensure correct levels of GTPase activation at the leading edge, various regulatory mechanisms seem to be necessary. For example, RhoA is kept in check at the cellular front by PKA-mediated phosphorylation on Ser188 inducing its cytosolic translocation and sequestration by GDIs (Lang et al., 1996; Tkachenko et al., 2011). In parallel, this mechanism promotes Rac-driven protrusion formation and migration by sequestering GDIs away from Rac (Rolli-Derkinderen et al., 2010). Deregulated Rho signaling at the leading edge has extensive consequences on cell polarity and increased ROCK activation disrupts the Par3 polarity complex at the cellular front and interferes with Rac/Cdc42-driven migration (Iden and Collard, 2008; Nakayama et al., 2008). Such observations emphasize the need for tight spatiotemporal Rho regulation by GEFs and GAPs at the leading edge, to which DLC3 and Scribble seem to make a contribution. A role of DLC1 in Rho regulation at cellular protrusions has already been described, as revealed by cortical Dia accumulation and enhanced wound closure properties of MCF7 breast cancer cells upon DLC1 depletion (Holeiter et al., 2008). This is in accordance with the revised concept of Rho activation during directed cell migration which includes high Rho-Dia activity during the initial phase of protrusion formation to promote actin filament assembly. By contrast, loss of DLC3 and Scribble led to increased pMLC signals at the leading edge, which is an indication of enhanced cell contractility. Thus, it remains to be determined how cell migration might be affected in the

knockdown cells. In general, cell motility depends on the exact level of Rho activation. This becomes clear, for example, in view of the contrasting consequences of DLC2 depletion on cell migration (Khalil et al., 2014; Lin et al., 2010). A certain degree of Rho activity is required for Dia-mediated actin polymerization, protrusion formation and thus for migration, but excessively high Rho levels inhibit cell motility due to actomyosin contraction. Consequently, the precise involvement of DLC3 in front-rear polarization and its control mechanisms during directed cell migration still have to be investigated, whereas a regulatory function for the DLC1 isoform has already been established in this process. In particular, in response to EGF stimulation, tensin3-DLC1 and PTEN-PI3K complexes reassemble to form PTEN-DLC1 and tensin3-PI3K complexes. This reformation of protein complexes increases Rho activity at the rear of the cell due to stabilization of DLC1's auto-inhibited conformation by PTEN, while leading to PI3K-mediated GEF recruitment and Rac activation at the cellular front (Campa et al., 2015; Cao et al., 2015). Taken together, DLC3 and Scribble seem to be important for the control of local Rho signaling and the establishment of cell polarity in different cellular processes, including epithelial morphogenesis, lumen formation and also transition to front-rear polarity, suggesting a more global physiological role for the DLC3-Scribble interaction.

Considering that Scribble engages in many different protein interactions, one might speculate that DLC3 competes with other proteins for Scribble binding. Biochemical characterization revealed that the DLC3-Scribble interaction is mediated mainly by the PDZ3 domain of Scribble which binds to the C-terminal PDZ ligand motif contained in DLC3. Interestingly, it was shown that the planar cell polarity protein Vangl also interacts with Scribble PDZ3 (Courbard et al., 2009). Under certain conditions and in striking contrast to its role as a tumor suppressor, binding of Scribble to a NOS1AP-Vangl complex at lamellipodia of breast cancer cells was correlated with enhanced cell migration and tumor progression (Anastas et al., 2012). Considering that DLC3 possesses potential tumor suppressive functions, DLC3 might compete with Vangl for Scribble binding, thereby regulating the tumor-suppressive versus oncogenic functions of Scribble. In addition, loss of the membrane localization of Scribble also leads to a gain of tumor-promoting properties (Elsam and Humbert, 2013). Thus, cytoplasmic sequestration of DLC3 by mislocalized Scribble, similar to a mechanism described for the tumor suppressor PTEN (Feigin et al., 2014), might interfere with the function of DLC3 in cell adhesion and promote cell motility. Consequently, it can be assumed that the precise cellular context determines the role of the DLC3-Scribble interaction and the way both proteins modulate each other's function.

#### **4.4 PDZ ligand binding – a mechanism for DLC3 recruitment in different contexts?**

In this work, I could show that the PDZ ligand motif is crucial for DLC3 recruitment to cell junctions and basolateral membranes. Thus, it is interesting to note that in different types of cancer mutations in the DLC3 coding sequence are reported (<https://www.cbioportal.org>), some of which generate a premature stop codon (DLC3 E686\*; DLC3 A874S fs\*16), yielding proteins that contain an intact GAP domain, but lack the PDZ ligand motif. According to our data, these DLC3 mutants are expected to be mislocalized from cell adhesions and thus devoid of biological functions in terms of junctional RhoA regulation. Consequently, it would be interesting to examine the functional consequences of PDZL deletion in more detail. In my experiments, expression of wildtype, GAP-active DLC3 interfered with the polarized structure of established Caco-2 cysts causing a collapse of lumens. However, I could not quantify clear differences in the disruptive effect upon PDZL deletion, probably due to saturation of the cell with excessive amounts of protein even after short-time induction. Driving protein expression by a weaker promoter, one would expect to assess different impacts of DLC3 full-length and  $\Delta$ PDZL expression on cyst integrity based on altered cellular distribution of DLC3's GAP activity.

Given that PDZ domain-PDZL binding is a common protein targeting mechanism, it might be instructive to address whether DLC3 is regulated by other PDZ-interactions besides its junctional recruitment by Scribble. In our proteomic analysis, sorting nexin 27 (SNX27) was identified as a potential DLC3 binding partner (Table 13). Within the sorting nexin family, SNX27 is the only PDZ protein and it localizes to endosomes to regulate endocytic recycling of many receptors and ion channels (Steinberg et al., 2013). A striking parallel is the finding that SNX27 interacts with the C-terminal PDZL motif of the RacGEF  $\beta$ -Pix to recruit it to endosomes controlling protein trafficking and cell motility (Valdes et al., 2011). Considering that DLC3 is also involved in coordinating endocytic trafficking (Braun et al., 2015), SNX27 is a binding partner of special interest which might help to understand DLC3 targeting to and regulation at endosomes and the recycling compartment. In this context, the question arises how the dynamics of different DLC3 protein interactions are regulated. It remains to be investigated whether Scribble competes with other proteins, like SNX27, for DLC3 binding and whether there are distinct DLC3 pools that are involved in different protein interactions. DLC3 seems to traffic through the cell and function at various subcellular sites. However, besides its junctional recruitment by Scribble and targeting via focal adhesion adaptors, it is still unclear which molecular factors specify its endosomal localization and function. In addition to studying the list of DLC3 interactors

identified in this work, more sophisticated proteomic approaches might be required to further elucidate the complex network of DLC3 interactions in time and space. For example, expression of DLC3 proteins coupled to a biotin ligase that labels proximal proteins *in situ* in combination with streptavidin affinity purification might be a promising strategy to enrich physiologically relevant DLC3 binding partners under selected experimental conditions prior to mass spectrometry analysis.

Junctional recruitment of DLC3 by its PDZ ligand motif is an isoform-specific regulatory mechanism because the DLC family members DLC1 and DLC2 lack a C-terminal class I PDZL motif and, as a consequence, they do not interact with Scribble. DLC1 was shown to be targeted to cell-cell adhesions by binding to  $\alpha$ -catenin in a GAP-dependent manner (Tripathi et al., 2012), whereas DLC2 was reported to control junction integrity by regulating microtubule growth and spindle positioning via Cdc42-mDia signaling (Vitiello et al., 2014). Thus, the presence of a unique PDZ ligand motif in DLC3 strongly supports the idea that the different DLC family members possess isoform-specific functions due to distinct regulatory mechanisms and interaction partners. The PDZ ligand motif of DLC3 might also be of biological relevance to its localization at focal adhesions. So far, it is unknown whether DLC3 lacking the PDZL motif still localizes to focal adhesions. Considering that until today all DLC family members were reported at focal adhesions through binding to tensin and talin adaptors (Kawai et al., 2009; Li et al., 2011; Liao et al., 2007; Qian et al., 2007), it would be worthwhile to investigate whether PDZL-mediated recruitment might also represent a DLC3-specific regulatory mechanism at this subcellular site. One could imagine that similar to DLC1 (Cao et al., 2012; Tripathi et al., 2014a), conformational changes in the DLC3 protein structure might alter its activity or the accessibility of the PDZ ligand motif and thus DLC3's biological activity at focal adhesions. In addition to the cellular fractionation performed in this work, which revealed reduced amounts of DLC3  $\Delta$ PDZL in the detergent-soluble membrane fraction compared to the full-length protein, separation of the cytoskeletal fraction would be of interest to determine further roles of the PDZ ligand motif. It should be noted that the focal adhesion adaptor Kank2 was also among our mass spectrometry results. Kank2 was found to bind to talin controlling the association of microtubule-stabilizing complexes with focal adhesions (Bouchet et al., 2016). Considering that DLC3 interacts with the same region of talin as Kank2, the R7/R8-domain (Li et al., 2011), one might speculate that both proteins compete for talin binding to regulate focal adhesion structure and dynamics. However, it remains to be investigated whether Kank2 binds DLC3 directly or may rather be recruited indirectly within a focal adhesion-associated multi-protein complex.

Since DLC3 is a multi-domain protein, it is not surprising that besides the PDZ ligand motif, other domains contribute to its subcellular localization and membrane association. For example, the SAM domain was shown to target DLC3 to Golgi membranes (Braun et al., 2015), whereas a polybasic region conserved in all three DLC isoforms mediates the association with phosphatidylinositol-4,5-bisphosphate-enriched membranes (Erlmann et al., 2009). Thus, in addition to protein interactions, lipid binding might add another layer of complexity to the regulatory network of DLC3. In this context, a second polybasic region was identified in the N-terminal region of DLC3 which is essential for DLC3 localization to Rab8-positive membrane tubules and able to bind several phospholipids, especially phosphatidic acid and phosphatidylinositol-4-phosphate (PI4P), at least under *in vitro* conditions.<sup>2</sup> Moreover, the precise role of the DLC3 START domain and the identity of its lipid ligand remain to be determined.

#### **4.5 Molecular mechanisms to spatiotemporally control DLC3 and its protein interactions**

DLC3 functions at distinct subcellular sites, which points out the need for a variety of molecular mechanisms to modulate its localized activity. The formation of specific protein complexes involving scaffold proteins represents one strategy to coordinate the modes of action of Rho regulators like DLC3. As a multi-domain protein, DLC3 has the ability to interact with scaffold proteins through different domains. It can be assumed that in addition to Scribble-mediated recruitment to cell-cell adhesions and focal adhesion targeting via tensin and talin adaptors, DLC3 localization and function are regulated through further scaffolds. Until today, the complex network of scaffold interactions involved in spatiotemporal Rho regulation is only rudimentarily understood. For example at adherens junctions, Ajuba acts as a scaffold to stabilize Rac (Nola et al., 2011), while Elmo2 targets the RacGEF DOCK1 to developing adhesions to coordinate Rac activity and strengthen E-cadherin-mediated cell-cell contacts (Toret et al., 2014). To better understand how DLC3 is targeted to destinations of the trafficking machinery for local Rho regulation, further DLC3 adaptor proteins have to be characterized. Scaffolds specify not only protein localization, but they also determine the specificity of GEFs and GAPs for certain GTPases and effectors and provide the ability for crosstalk between different pathways (Buchsbaum, 2007; Marinissen and Gutkind, 2005; Pan et al., 2012). In line with this, JIP2 and spinophilin function as platforms for the RacGEF Tiam and its effectors p38

---

<sup>2</sup> PhD Thesis Anja Braun. Regulation of endocytic membrane trafficking by the GTPase-activating protein Deleted in Liver Cancer 3 (DLC3). Institute of Cell Biology and Immunology, University of Stuttgart. 2015.

and p70 S6 kinase, respectively, to coordinate differential downstream responses (Buchsbaum et al., 2002; Buchsbaum et al., 2003). Moreover, with regard to RhoA signaling, the scaffold protein CNK1, for example, links RhoA and its GEFs Net1 and p115RhoGEF to the JNK signaling pathway (Jaffe et al., 2005). Thus, it remains to be examined which scaffolds might control DLC3 signaling specificity and organize its protein interactions in different biological contexts. Interestingly, IQGAP1, a large scaffold protein and master regulator of several GTPases, was detected in our proteomic approach (Table 13) and validated biochemically as a DLC3 binding partner (data not shown). IQGAP1 has been reported to recruit Rho regulators, like Tiam and RacGAP1, and Rho effector proteins, like N-WASP, Arp2/3 and Dia, to modulate spatial Rho signaling (Jacquemet and Humphries, 2013). Moreover, IQGAP1 represents a platform for simultaneous binding of p190RhoGAP and RhoA to suppress RhoA activity and restrict airway smooth muscle contractility (Bhattacharya et al., 2014). Consequently, a potential role for IQGAP1 in controlling DLC3-dependent localized Rho activity and the role of further adaptor proteins identified as DLC3 interactors in our analysis, such as  $\alpha$ -catulin, Kank2 and Grb2 (Table 13), still have to be investigated.

For the local regulation of different GTPase pools, specific combinations of GEF and GAP proteins are necessary, which both have to be positioned by scaffolds to ensure adequate downstream signaling. GEF and GAP proteins can coexist in the same regulatory complex to fine-tune Rho signaling. By recruiting DLC3 and  $\beta$ -Pix (Frank et al., 2012; Zhan et al., 2008), Scribble represents a scaffold for regulators of different Rho GTPases to antagonize their activities. By contrast, the coexistence of GEFs and GAPs in the same regulatory complex controlling the same GTPase is also possible and might be required for an appropriate balance of Rho activation. For example, the RacGEF Tiam and the RacGAP Bcr form a complex and act in concert to control optimal Rac activation levels during excitatory synapse development (Um et al., 2014). Thus, the question arises which GEF protein might function as an antagonist of DLC3 function at distinct subcellular destinations or in specific pathways. Scaffold proteins could position DLC3 and its counteracting GEF for spatial Rho regulation by simultaneous binding forming a multi-protein complex. Alternatively, the antagonizing Rho regulators might also compete for recruitment by the same scaffold. Considering that PDZL motifs are enriched among RhoGEF and RhoGAP proteins in comparison to other protein families (Giallourakis et al., 2006), and that ~40% of RhoGEFs contain such a motif at their C-terminus (García-Mata and Burrige, 2006), PDZ-interactions seem to be a common targeting mechanism among Rho regulators. Many PDZ proteins contain multiple, adjacent PDZ domains and their targets often display affinities for several of these domains, as shown for example for

some Scribble interaction partners (Nagasaka et al., 2010). This suggests that DLC3 and its potential antagonizing GEF might be recruited simultaneously by PDZ domain scaffolds like Scribble. To understand how such regulatory complexes help to coordinate Rho signaling, it will also be important to analyze by which means complex formation is controlled. There is growing evidence for the regulation of Rho GTPases and their regulators by different types of post-translational modifications (Hodge and Ridley, 2016). Thus, DLC3-specific modifications have to be examined to elucidate how its biological functions and the dynamics of its protein interactions are specified. Considering that the tumor suppressor PTEN is acetylated on a lysine residue within its PDZ ligand motif (Ikenoue et al., 2008), it is possible that DLC3 is controlled in a similar manner to modulate its interaction with PDZ domain proteins. Moreover, it has been shown that PDZ-interactions are regulated by phosphorylation of serine or threonine residues within the PDZL motif or at positions in its vicinity (Kim and Sheng, 2004; Sheng and Sala, 2001), which might also apply to DLC3.

Furthermore, the isolation of several proteins involved in the ubiquitin-proteasome pathway, including the ubiquitin ligases HUWE-1 and CHIP (Table S1), provides a hint that DLC3 might be regulated by ubiquitylation. Ubiquitylation is a common mechanism to control Rho GTPase signaling and RhoA levels are confined at the leading edge of migrating cells by recruitment of the ubiquitin ligase SMURF1 (Hodge and Ridley, 2016; Wang et al., 2003). In addition, DLC1 is regulated by a CRL4A-ubiquitin ligase complex and degraded by the proteasome (Kim et al., 2013). Considering that DLC3 has a very potent biological activity even at low expression levels, one might speculate that it is present in an active conformation in the cell and might be regulated by a high turn-over through the ubiquitin-proteasome pathway. Interestingly, we detected a confluence-dependent increase of DLC3 protein levels (data not shown), suggesting that the PDZ-interaction might stabilize DLC3 at cell junctions. This is reminiscent of the PDZ-mediated complex assembly of the RhoGEF Net1 and the Scribble complex component Dlg, which protects Net1 from degradation at cell adhesions (Carr et al., 2009; García-Mata et al., 2007). In addition, the junction-associated RacGEF Tiam was reported to be degraded by HGF-induced ubiquitylation, which was associated with the disruption of cell-cell contacts in MDCK cells (Vaughan et al., 2015). In further experiments, the potential impact of Scribble or growth factor treatment on DLC3 protein levels should be investigated to identify cellular conditions that influence DLC3 protein stability. In summary, a diverse range of molecular mechanisms is likely to exist which might be responsible for the regulation of DLC3 function in different cellular contexts.

## 4.6 Conclusions and outlook

Despite their structural similarity, the three DLC proteins are proposed to execute also non-redundant functions associated with their different subcellular localizations. In this work, I revealed a new isoform-specific regulatory mechanism for DLC3 by identifying Scribble as a scaffold for the RhoGAP at adherens junctions. My findings provide evidence that the DLC3-Scribble complex is responsible for the spatial balance of Rho-ROCK signaling to preserve cell junctions. Furthermore, a novel role of DLC3 and Scribble in the establishment of epithelial cell polarity and lumen integrity was uncovered. To better understand the molecular regulation of DLC3 also at other subcellular sites, further protein and lipid interactions and the impact of post-translational modifications have to be addressed. Moreover, the development of highly specific antibodies to investigate endogenous DLC3 by immunofluorescence represents a future goal. High resolution microscopy and live cell imaging might help to resolve the dynamics of fluorescently-tagged DLC3 and its binding partners, while genetically encoded FRET biosensors are powerful tools to study the spatiotemporal aspects of DLC3-controlled Rho regulation. Taking into account that DLC proteins are also able to carry out GAP-independent functions, which seem to support their potential tumor suppressive properties, the picture gets even more complex (Barras and Widmann, 2013). Thus, future investigations might shed more light on the changes of DLC3 localization and function during transition of epithelial cells displaying apical-basolateral polarity to front-rear polarized migratory cells. Finally, elucidating in more depth the control mechanisms underlying the different subcellular DLC3 pools and how they impact downstream signaling, will improve our understanding of DLC3's biological functions and its potential role in tumor suppression.

## Supplements

**Table S1: DLC3 protein interaction partners identified by mass spectrometry analysis.** Co-immunoprecipitating proteins with iBAQ values  $\geq 100\ 000$  (DLC3 WT and K725E), iBAQ(control)=0 and Q=0 are shown and are ranked according to iBAQ(DLC3 WT).

Protein names	Protein IDs	Gene names	iBAQ (control)	iBAQ (DLC3 $\alpha$ wt)	iBAQ (DLC3 $\alpha$ K725E)	Q-value
40S ribosomal protein S27	P42677;Q5T4L4	RPS27	0	119950000	77710000	0
Mitochondrial import receptor subunit TOM40 homolog	O96008;O96008-2;K7EKG4	TOMM40	0	16214000	49760000	0
Up-regulated during skeletal muscle growth protein 5	Q961X5	USMG5	0	13257000	14714000	0
Phosphate carrier protein, mitochondrial	F8VVM2;Q00325-2;Q00325;F8VWQ0;F8VZL5;F8VWR4	SLC25A3	0	11332000	22773000	0
BAG family molecular chaperone regulator 2	O95816;O95816-2	BAG2	0	10483000	33602000	0
Very-long-chain enoyl-CoA	Q9NZ01;MOQXM3	TECR	0	8163000	15496000	0
F-box/WD repeat-containing protein 11	Q9UKB1-2;Q9UKB1-3;Q9UKB1	FBXW11	0	5852100	6702500	0
Voltage-dependent anion-selective channel protein 3	Q9Y277;Q9Y277-2;E5RFP6;E5RJN6;E5	VDAC3	0	5408600	13216000	0
ADP-ribosylation factor-like protein 1	F8VP99;F8VP63;F8VYN9;P40616-	ARL1	0	5382400	9459700	0
60S ribosomal protein L27a	P46776;E9PJD9;E9PL6;E9PLX7	RPL27A	0	4418200	5035400	0
Protein transport protein Sec61 subunit beta	P60468	SEC61B	0	4039100	3992600	0
Mitochondrial dicarboxylate carrier	Q9UBX3;Q9UBX3-2;F6RGN5	SLC25A10	0	3992300	8976900	0
Microsomal glutathione S-transferase 3	Q5VV89;O14880;Q5VV87	MGST3	0	3923300	9118100	0
Tricarboxylate transport protein, mitochondrial	P53007;B4DP62	SLC25A1	0	3874200	5159200	0
Protein cornichon homolog 4	A6NLH6;Q9P003	CNIH4	0	3729900	9539400	0
DnaJ homolog subfamily B member 6	O75190;O75190-3;E9PH18;C9J2C4;O75190-2;O75190-4;C9JDX6;F8WCZ4;C9	DNAJB6	0	3649300	5307500	0
Cytoskeleton-associated protein 4	Q07065	CKAP4	0	3401900	4858100	0
Voltage-dependent anion-selective channel protein 2	P45880;A0A0A0MR02;P45880-2;P45880-1;Q5JSD2;Q5JSD1	VDAC2	0	3227500	8160500	0
HIG1 domain family member 1A, mitochondrial	Q9Y241;C9JAW5;C9JNU6;Q9Y241-2	HIGD1A	0	2960800	3611800	0
Mitochondrial import receptor subunit TOM20 homolog	Q15388	TOMM20	0	2943300	7000400	0
ATP synthase subunit g,	E9PN17;O75964	ATP5L	0	2917400	6214700	0
Small nuclear ribonucleoprotein E	P62304;A6NHK2	SNRPE	0	2826600	5967800	0
Signal recognition particle 14 kDa protein	P37108;H0YLA2	SRP14	0	2731500	3249100	0
Cytochrome c oxidase subunit NDUFA4	O00483	NDUFA4	0	2642200	5251700	0

Supplements

Protein names	Protein IDs	Gene names	iBAQ (control)	iBAQ (DLC3α wt)	iBAQ (DLC3α K725E)	Q-value
ER lumen protein-retaining receptor 1;ER lumen protein-retaining receptor;ER lumen protein-retaining receptor 2	P24390-2;P24390;M0R1Y2;P33947-2	KDEL1;KDEL R2	0	2452000	4410100	0
Membrane-associated progesterone receptor component 1	O00264	PGRMC1	0	2423600	8341800	0
Probable hydrolase PNKD	Q8N490-2	PNKD	0	2370200	4057600	0
Type 1 phosphatidylinositol 4,5-bisphosphate 4-phosphatase	Q86T03;Q86T03-2;G3V5T5	TMEM55B	0	2337800	1594800	0
Transmembrane protein 33	P57088;D6RAA6;H0Y8N0	TMEM33	0	2232400	4928300	0
DnaJ homolog subfamily A member 2	O60884	DNAJA2	0	1999000	5145000	0
Trifunctional enzyme subunit beta, mitochondrial;3-ketoacyl-CoA thiolase	P55084-2;P55084;B5MD38;F5GZQ3	HADHB	0	1903000	1138700	0
DnaJ homolog subfamily C member 11	Q9NVH1-3;Q9NVH1;Q9NVH1-2	DNAJC11	0	1895900	3190900	0
ADP-ribosylation factor 4	P18085;C9JPM4;C9JAK5	ARF4	0	1888700	3198000	0
Programmed cell death protein 2	Q16342-3;Q16342;F5H4V9	PDCD2	0	1873000	2490800	0
E3 ubiquitin-protein ligase CHIP	Q9UNE7;Q9UNE7-2;H3BS86	STUB1	0	1856300	8106300	0
ER lumen protein-retaining receptor 2	P33947	KDEL2	0	1854400	1526900	0
Small integral membrane protein 4	Q8WV10	SMIM4	0	1846200	1942700	0
40S ribosomal protein S10	P46783;F6U211;S4R435	RPS10;RPS10-NUDT3	0	1669500	2429200	0
Proteasome subunit beta type-2	P49721	PSMB2	0	1644200	4363800	0
NADH dehydrogenase [ubiquinone] 1 beta subcomplex subunit 4	O95168-2;O95168;F2Z3P9;C9JXQ9	NDUFB4	0	1575900	194640	0
Programmed cell death protein 2-like	Q9BRP1	PDCD2L	0	1545000	1051100	0
Calcium-binding mitochondrial carrier protein Aralar2	Q9UJS0;Q9UJS0-2	SLC25A13	0	1525700	3046300	0
Trifunctional enzyme subunit alpha, mitochondrial;Long-chain enoyl-CoA hydratase;Long chain 3-hydroxyacyl-CoA dehydrogenase	P40939	HADHA	0	1512800	494890	0
E3 ubiquitin-protein ligase HUWE1	Q7Z6Z7-2;Q7Z6Z7-3;Q7Z6Z7	HUWE1	0	1509500	2193600	0
Proteasome subunit alpha type;Proteasome subunit alpha type-2	AOA024RA52;P25787	PSMA2	0	1500100	2154000	0
Cytochrome b-c1 complex subunit 9	Q9UDW1;Q9NZY4;Q9UDW1-2	UQCR10	0	1467700	2684900	0
60S ribosomal protein L10a	P62906	RPL10A	0	1463800	2496600	0
Glutaminyl-peptide cyclotransferase-like protein	Q9NXS2-3;Q9NXS2	QPCTL	0	1433400	2985100	0

Supplements

Protein names	Protein IDs	Gene names	iBAQ (control)	iBAQ (DLC3 $\alpha$ wt)	iBAQ (DLC3 $\alpha$ K725E)	Q-value
40S ribosomal protein S3a	P61247;D6RAT0;H0Y9Y4;D6RG13;D6R9B6;H0Y8L7;D6RB09;E9PFI5;D6RAS7	RPS3A	0	1430700	3487200	0
Long-chain fatty acid transport protein 4	Q6P1M0	SLC27A4	0	1397700	2453500	0
Mitochondrial import receptor subunit TOM22 homolog	Q9NS69	TOMM22	0	1376000	2640500	0
Serine/threonine-protein phosphatase 2B catalytic subunit alpha isoform;Serine/threonine-protein phosphatase	Q08209-2;Q08209;E7ETC2;Q08209-5;Q08209-3;E9PPC8;E9PK68;Q08209-4	PPP3CA	0	1371400	2047300	0
Serine/threonine-protein phosphatase;Serine/threonine-protein phosphatase 5	H0YDU8;P53041;A8MU39	PPP5C	0	1362800	3217500	0
Casein kinase I isoform epsilon	P49674;H0Y645;B0QY35;B0QY34	CSNK1E	0	1357800	634110	0
DnaJ homolog subfamily A member 3, mitochondrial	Q96EY1-2;Q96EY1;Q96EY1-3	DNAJA3	0	1347200	1676600	0
CDP-diacylglycerol--inositol 3-phosphatidyltransferase	B3KY94;O14735-3;O14735	CDIPT	0	1346300	2330000	0
Suppressor of G2 allele of SKP1 homolog	Q9Y2Z0;Q9Y2Z0-2	SUGT1	0	1321200	4427500	0
Protein transport protein Sec61 subunit alpha isoform 1	B4DR61;P61619;P61619-3	SEC61A1	0	1310400	736810	0
DnaJ homolog subfamily C member 7	Q99615;Q99615-2;K7ESP1;K7EIH8;K7EPP7	DNAJC7	0	1284600	4511900	0
Transmembrane protein 70, mitochondrial	Q9BUB7;Q9BUB7-2	TMEM70	0	1221700	1104600	0
Cullin-1	Q13616;A0A0C4DGX4	CUL1	0	1148400	800540	0
Histone acetyltransferase type B catalytic subunit	O14929;O14929-2	HAT1	0	1135600	3007400	0
Dolichol-phosphate mannosyltransferase subunit 1	Q5QPK2;H0Y368;O60762;Q5QPJ9	DPM1	0	1118300	2038900	0
Acylglycerol kinase, mitochondrial	E9PC15;Q53H12;A0A0G2JLG5;E9PG39	AGK	0	1068500	2270400	0
Fatty acyl-CoA reductase 1	Q8WVX9;E9PNW8	FAR1	0	1006000	1262300	0
Mitochondrial import inner membrane translocase subunit Tim23;Putative mitochondrial import inner membrane translocase subunit Tim23B	O14925;Q5SRD1;B4DK6	TIMM23;TIMM23B	0	980760	608350	0
40S ribosomal protein S27;40S ribosomal protein S27-like	H0YMV8;Q71UM5;C9JLI6	RPS27L	0	975340	970200	0
Beta-2-syntrophin	Q13425;Q13425-2;H0YCS0	SNTB2	0	961020	2056100	0
Ankyrin repeat and MYND domain-containing protein 2	Q8IV38;G3VOG5	ANKMY2	0	949330	2376100	0
Oligosaccharyltransferase complex subunit OSTC	A0A087WUD3;Q9NRP0;Q9NRP0-2	OSTC	0	887330	1423500	0

## Supplements

Protein names	Protein IDs	Gene names	iBAQ (control)	iBAQ (DLC3α wt)	iBAQ (DLC3α K725E)	Q-value
Putative tRNA (cytidine(32)/guanosine(34)-2-O)-methyltransferase	Q9UET6-2;Q9UET6;B7Z4K4	FTSJ1	0	871730	3005600	0
Dolichyl-diphosphooligosaccharide-protein glycosyltransferase subunit STT3A	A0A0C4DH80;E9PN73;E9PI32;P46977	STT3A	0	843310	921370	0
Dynein light chain roadblock-type 1;Dynein light chain roadblock-type 2	B1AKR6;Q9NP97;H3BQ11;Q8TF09	DYNLRB1;DYNLRB2	0	810530	196490	0
MICOS complex subunit MIC60	Q16891-2;Q16891;B9A067;Q16891-4;Q16891-3;C9J406;H7C463	IMMT	0	806840	5817100	0
AP-2 complex subunit sigma	M0R1S0;M0QZ21;M0RON4;X6R390;MOQYZ2;P53680-2;P53680	AP2S1	0	786640	1453800	0
Junctophilin-1	Q9HDC5	JPH1	0	747780	2927200	0
ATPase family AAA domain-containing protein 3B	Q5T9A4;Q5T9A4-3	ATAD3B	0	726260	2171200	0
26S proteasome non-ATPase regulatory subunit 13	A0A087WUL9;Q9UNM6;J3KNQ3;Q9UNM6-2;E9PL38;H0YD73	PSMD13	0	714220	4130500	0
60S ribosomal protein L3	B5MCW2;G5E9G0;P39023;H7C422	RPL3	0	700710	908920	0
ATP synthase subunit O, mitochondrial	P48047;H7C0C1	ATP5O	0	698200	910870	0
Estradiol 17-beta-dehydrogenase 12	Q53GQ0	HSD17B12	0	683580	446910	0
ADP/ATP translocase 1	P12235;V9GYG0	SLC25A4	0	680080	279390	0
Leucine-rich repeat-containing protein 59	Q96AG4	LRRC59	0	666860	417970	0
TBC1 domain family member 4	O60343-2;O60343-3;O60343	TBC1D4	0	661560	1966600	0
Peptidyl-tRNA hydrolase 2, mitochondrial	J3KQ48;Q9Y3E5	PTRH2	0	619480	1040300	0
Chitobiosyldiphosphodolichol beta-mannosyltransferase	K7EPU3;Q9BT22	ALG1	0	614480	980630	0
Protein RER1	Q5T093;Q5T092;A0A0AMR06;Q5T091;Q9POH9;O15258	RER1	0	610770	1436100	0
Plakophilin-2	A0A087WXY2;B8QGS9;Q99959-2;Q99959	PKP2	0	594790	884980	0
Peptidyl-prolyl cis-trans isomerase FKBP8	Q14318;Q14318-2;U3KQ64;A0A0A0MTJ1;Q14318-3	FKBP8	0	583560	1431300	0
28S ribosomal protein S29, mitochondrial	V9GYF7;V9GZ61;V9GYW1;V9GYA7;P51398-2;P51398-3;P51398	DAP3	0	580610	698490	0
RNA-binding protein 14	Q96PK6	RBM14	0	566190	734340	0
Inhibitor of nuclear factor kappa-B kinase-interacting protein	Q70UQ0-4	IKBIP	0	565400	259960	0

## Supplements

Protein names	Protein IDs	Gene names	iBAQ (control)	iBAQ (DLC3α wt)	iBAQ (DLC3α K725E)	Q-value
Beta-1-syntrophin	Q13884;Q13884-2	SNTB1	0	564690	510580	0
Proteasome subunit beta type-5	P28074;P28074-3	PSMB5	0	552640	2577500	0
Sorting nexin-27	Q96L92-3;Q96L92;A0A0C4DFU6;Q96L92-2	SNX27	0	519990	295750	0
TAR DNA-binding protein 43	A0A087WX29;Q13148;K7EJM5;K7EN94;B1AKP7;G3V162;A0A087X260;A0A087WYY0;A0A087WXQ5;A0A087WV68;Q13148-4	TARDBP	0	516500	1287300	0
Mitochondrial import inner membrane translocase subunit Tim21	Q9BVV7	TIMM21	0	493140	1009600	0
Glutathione peroxidase;Probable glutathione peroxidase 8	E7ETY7;Q8TED1	GPX8	0	490490	793680	0
BAG family molecular chaperone regulator 5	Q9UL15;Q9UL15-2	BAG5	0	486020	2294300	0
Heat shock 70 kDa protein 4L	O95757;E9PDE8;D6RJ96	HSPA4L	0	482440	1379300	0
NADH dehydrogenase [ubiquinone] 1 alpha subcomplex subunit 5	F8WAS3;C9IZN5;A0A087X1G1;H7BYD0;Q16718-2;Q16718	NDUFA5	0	480150	605560	0
Mitochondrial thiamine pyrophosphate carrier	J3KSB1;J3KSI7;J3QL84;J3KS44;J3QLV3;J3KRY6;Q9HC21-2;Q9HC21	SLC25A19	0	478580	944660	0
Utrophin	P46939;P46939-2	UTRN	0	475550	721680	0
Diacylglycerol kinase;Diacylglycerol kinase epsilon	I3L112;P52429	DGKE	0	471390	1339300	0
Protein QIL1	K7EIR2;Q5XKP0	C19orf70;QIL1	0	469960	706180	0
Cyclin-dependent kinase inhibitor 2A, isoforms 1/2/3;Cyclin-dependent kinase 4 inhibitor B	K7ES20;K7ENC6;J3QRG6;A0A0A0MRI0;P42771-2;P42771;P42771-4;P42772	CDKN2A;CDKN2B	0	460270	855690	0
Voltage-dependent anion-selective channel protein 1	P21796	VDAC1	0	457810	1636200	0
Tetratricopeptide repeat protein 4	O95801	TTC4	0	453310	2041200	0
Mitochondrial import inner membrane translocase subunit TIM50	Q3ZCQ8;Q3ZCQ8-2;MOROC3;MOR2F8;MOR047;Q3ZCQ8-3	TIMM50	0	452720	1121000	0
Angiomotin-like protein 2	Q9Y2J4;Q9Y2J4-2;Q9Y2J4-4;Q9Y2J4-3	AMOTL2	0	449830	656520	0
Complex I assembly factor TIMMDC1, mitochondrial	Q9NPL8;C9JU35;G3XA94	TIMMDC1	0	449800	744860	0
Phosphatidylinositol 3-kinase regulatory subunit alpha	P27986;P27986-4;P27986-5;P27986-3;P27986-2	PIK3R1	0	448340	1602700	0

Supplements

Protein names	Protein IDs	Gene names	iBAQ (control)	iBAQ (DLC3α wt)	iBAQ (DLC3α K725E)	Q-value
Ras-related protein Rab-5C;Ras-related protein Rab-5B	P51148;P51148-2;K7EIP6;F8WCY6;F8WD79;F8VPW9;F8VSF8;F8VWZ7;F8VWU4;F8VVZ0;F8VUA5;F8VVK3;K7ERI8;K7ERQ8;P61020-2;P61020	RAB5C;RAB5A;RAB5B	0	446110	441160	0
F-box/WD repeat-containing protein 1A	B7Z3H4;Q9Y297-2;Q9Y297	BTRC	0	445990	1113400	0
Growth factor receptor-bound protein 2	P62993-2;P62993;J3KT38;J3QRL5	GRB2	0	445720	416640	0
NADH dehydrogenase [ubiquinone] iron-sulfur protein 7, mitochondrial	F5H5N1;F5GXJ1;O75251-2;O75251;A0A087WXF6;A0A087WTI3	NDUFS7	0	442870	105340	0
Ras-related C3 botulinum toxin substrate 1	P63000;P63000-2	RAC1	0	440230	615810	0
Membrane-associated progesterone receptor component 2	O15173;O15173-2	PGRMC2	0	439120	1013700	0
KN motif and ankyrin repeat domain-containing protein 2	Q63ZY3-3;Q63ZY3;Q63ZY3-2	KANK2	0	433170	1041300	0
Peroxiredoxin-5, mitochondrial	P30044-4;P30044-2;P30044-3;P30044	PRDX5	0	420830	590190	0
Casein kinase I isoform alpha	P48729;P48729-3;P48729-2;D6REM4	CSNK1A1	0	413460	100980	0
Proteasome subunit beta type-4	P28070	PSMB4	0	409340	1089700	0
Protein YIPF5	Q969M3;Q969M3-3;E5RGR9;E5RHH4;Q969M3-2	YIPF5	0	400070	2021100	0
Transmembrane protein 165	V9GY93;Q9HC07-2;Q9HC07;V9GYC8	TMEM165	0	398490	743160	0
Cytochrome c1, heme protein, mitochondrial	P08574	CYC1	0	387780	610550	0
Signal recognition particle receptor subunit beta	Q9Y5M8;H7C4H2	SRPRB	0	383310	1293100	0
Sodium/potassium-transporting ATPase subunit alpha-1;Sodium/potassium-transporting ATPase subunit alpha-3;Sodium/potassium-transporting ATPase subunit alpha-2	P05023-3;P05023-4;P05023;P05023-2;M0R116;B1AKY9;A0A0A0MT26;P13637;P50993;P13637-2;P13637-3	ATP1A1;ATP1A3;ATP1A2	0	376460	367830	0
Phosphatidylglycerophosphatase and protein-tyrosine phosphatase 1	Q8WUKO	PTPMT1	0	375300	698000	0
Probable tRNA N6-adenosine threonylcarbamoyltransferase	Q9NPF4	OSGEP	0	373160	891110	0
Mitochondrial carrier homolog 2	Q9Y6C9;E9PIE4	MTCH2	0	370090	957280	0
NADH-ubiquinone oxidoreductase 75 kDa subunit, mitochondrial	P28331;P28331-2;B4DJ81;P28331-3;P28331-4;P28331-5	NDUFS1	0	351440	769140	0

Supplements

Protein names	Protein IDs	Gene names	iBAQ (control)	iBAQ (DLC3α wt)	iBAQ (DLC3α K725E)	Q-value
Coatomer subunit delta	B0YIW6;P48444;Q6P1Q5	ARCN1	0	348430	410260	0
Multifunctional methyltransferase subunit TRM112-like protein	F5GYQ2;F5GX77;Q9UI30-2;Q9UI30	TRMT112	0	346200	389390	0
Activator of 90 kDa heat shock protein ATPase homolog 1	H0YJG7;O95433-2;O95433;G3V438;H0YJ63;H0YJU2	AHSA1	0	336090	2974600	0
Exportin-5	H0Y9I3;Q9HAV4	XPO5	0	330930	716850	0
Cytochrome c oxidase assembly protein COX11, mitochondrial	I3L4E7;B4DI26;Q9Y6N1-2;Q9Y6N1	COX11	0	329130	525910	0
Transmembrane protein 11, mitochondrial	P17152	TMEM11	0	318240	911280	0
Proteasome subunit alpha type-1;Proteasome subunit alpha type	P25786;P25786-2;B4DEV8;F5GX11	PSMA1	0	311310	1624900	0
Protein lin-7 homolog C;Protein lin-7 homolog B;Protein lin-7 homolog A	G3V1D4;Q9NUP9;H0YI92;H0YIA8;Q9HAP6;O14910	LIN7C;LIN7A;LIN7B	0	309430	345550	0
Dystrobrevin;Dystrobrevin beta	E9PEY4;E7EVB6;O60941-41-6;O60941-3;O60941-5;O60941-2;O60941-4;O60941-7;O60941	DTNB	0	307380	370990	0
Importin subunit alpha-1	P52292;J3QLL0;J3KS65	KPNA2;POU2F2	0	305100	566920	0
Aurora kinase A	O14965;A3KFJ0	AURKA	0	301920	315050	0
ATPase WRNIP1	Q96S55-3;Q96S55-2;Q96S55	WRNIP1	0	300130	733520	0
Obscurin-like protein 1	A6NN50;O75147-2;O75147-1;O75147-4;O75147;A8MSZ8	OBSL1	0	295990	892170	0
Cytochrome c oxidase protein 20 homolog	Q5RI15;Q5RI15-2	COX20	0	293020	473230	0
WD repeat-containing protein 92	Q96MX6-2;Q96MX6	WDR92	0	292900	650050	0
NADH dehydrogenase [ubiquinone] iron-sulfur protein 3, mitochondrial	O75489	NDUFS3	0	290290	591130	0
DNA-directed RNA polymerases I, II, and III subunit RPABC1	A0A0A0MQR7;P19388;A0A087WVN5;A0A087WWX0;A0A087WVZ9	POLR2E	0	283950	171820	0
Lysozyme C	F8VV32;A0A0B4J259;P61626	LYZ	0	283530	355750	0
Protein UXT	A0A0C4DFR8;Q9UBK9;S4R2Z4	UXT	0	280790	704430	0
L-aminoacidopate-semialdehyde dehydrogenase-phosphopantetheinyl transferase	Q9NRN7;Q9NRN7-2	AASDHPPT	0	274310	328720	0
Valine--tRNA ligase	A2ABF4;A0A0G2JIT9;P26640	VARS	0	260710	677690	0
Ras GTPase-activating-like protein IQGAP1	P46940;H0YLE8	IQGAP1	0	259640	521750	0
Tubulin beta-3 chain	A0A0B4J269;Q13509;Q13509-2	TUBB3	0	259430	553260	0

## Supplements

Protein names	Protein IDs	Gene names	iBAQ (control)	iBAQ (DLC3α wt)	iBAQ (DLC3α K725E)	Q-value
Cyclin-dependent kinase 4	F8VYH9;F8VTV8;F8VWX7;P11802;F8VXD2;F8VZZ0;F8VZ51;F8W1L8;P11802-2	CDK4	0	257680	782920	0
HCLS1-associated protein X-1	O00165-4;O00165-5;O00165;O00165-2;Q5VYD6;O00165-6;O00165-3	HAX1	0	254560	420210	0
Fatty aldehyde dehydrogenase	J3QRD1;P51648;P51648-2	ALDH3A2	0	254180	890830	0
Protein scribble homolog	AOA0G2JNZ2;AOA0G2JPP5;Q14160;Q14160-3;AOA0G2JMS7;Q14160-2	SCRIB	0	253010	381870	0
7-dehydrocholesterol reductase	E9PJ54;E9PM00;Q9UBM7	DHCR7	0	250640	172210	0
Surfeit locus protein 4	Q5T8U5;O15260-2;O15260;O15260-3	SURF4	0	246830	2034900	0
Microtubule-associated protein RP/EB family member 2	K7EL66;K7ERD8;Q15555-2;Q15555-4;Q15555-5;Q15555-3;Q15555	MAPRE2	0	230510	674100	0
Uncharacterized protein C19orf52	Q9BSF4;K7ENF5	C19orf52	0	230260	483810	0
Phosphatidate cytidyltransferase, mitochondrial	H7C1A2;AOA0G2JQ92;Q96BW9-2;Q96BW9-3;Q96BW9	TAMM41	0	228480	429510	0
NADH dehydrogenase [ubiquinone] iron-sulfur protein 2, mitochondrial	O75306-2;O75306	NDUFS2	0	225250	191000	0
Calcium-binding mitochondrial carrier protein Aralar1	O75746-2;O75746	SLC25A12	0	224400	603200	0
Putative eukaryotic translation initiation factor 2 subunit 3-like protein;Eukaryotic translation initiation factor 2 subunit 3	Q2VIR3;P41091;F8W810;Q2VIR3-2	EIF2S3L;EIF2S3	0	223980	725890	0
EKC/KEOPS complex subunit LAGE3	Q14657	LAGE3	0	222710	387180	0
Transportin-1	S4R398;Q92973-3;Q92973-2;Q92973;O14787-2	TNPO1	0	221200	981330	0
Alpha-1-syntrophin	Q13424-2;Q13424	SNTA1	0	220630	183420	0
Nuclear migration protein nudC	Q9Y266;AOA0A0MSU9	NUDC	0	219260	572220	0
Sphingosine-1-phosphate lyase 1	O95470;HOY3V8;H7BXL7	SGPL1	0	219160	382840	0
Dnal homolog subfamily A member 4	F5H170;Q8WW22-3;Q8WW22;Q8WW22-2	DNAJA4	0	212190	1883100	0
Ribonuclease P protein subunit p20	C9JYM0;O75817	POP7	0	207860	197600	0

Supplements

Protein names	Protein IDs	Gene names	iBAQ (control)	iBAQ (DLC3α wt)	iBAQ (DLC3α K725E)	Q-value
Serine/threonine-protein phosphatase 2A 55 kDa regulatory subunit B alpha isoform;Serine/threonine-protein phosphatase 2A 55 kDa regulatory subunit B delta isoform	P63151;P63151-2;E5RIY1;Q66LE6	PPP2R2A;PPP2R2D	0	205050	788210	0
Ubiquitin-like protein 4A	Q5HY81;P11441	UBL4A	0	200060	466460	0
Glycine--tRNA ligase	P41250	GARS	0	199120	324520	0
Spermidine synthase	P19623	SRM	0	197990	595380	0
28S ribosomal protein S25, mitochondrial	E7EPW2;P82663-3;P82663-2;P82663	MRPS25	0	197240	151540	0
Protein pelota homolog	Q9BRX2	PELO	0	196180	197920	0
Small nuclear ribonucleoprotein F	P62306;A0A0B4J254;F8W0W6	SNRPF	0	193470	1206200	0
tRNA (cytosine(34)-C(5))-methyltransferase	Q08J23-3;Q08J23-2;Q08J23	NSUN2	0	192420	255640	0
28S ribosomal protein S7, mitochondrial	J3QQS1;J3QLS3;Q9Y2R9;J3KSI8;J3QKW2	MRPS7	0	191410	255030	0
Glutamate-rich WD repeat-containing protein 1	Q9BQ67;M0QX71	GRWD1	0	184990	288600	0
FAS-associated factor 2	Q96CS3	FAF2	0	184050	895900	0
Ran GTPase-activating protein 1	P46060	RANGAP1	0	183300	450380	0
Vesicle transport through interaction with t-SNAREs homolog 1B	Q9UEU0;J3KMW2;G3V5I2;Q9UEU0-2	VTI1B	0	182940	158370	0
NADH dehydrogenase [ubiquinone] flavoprotein 1, mitochondrial	E9PQP1;E9PMX3;G3VOI5;P49821-2;P49821;E9PJL9;E9PLC6;E9PPRO;B4DE93	NDUFV1	0	179980	1129000	0
Lamin-B receptor	Q14739;C9JXK0	LBR	0	179600	374670	0
BRCA2 and CDKN1A-interacting protein	Q9P287-4;Q9P287-3;Q9P287;Q9P287-2	BCCIP	0	177510	694850	0
Regulator of microtubule dynamics protein 3	Q96TC7;H0YLG5;H0YMB1;Q96TC7-2	RMDN3	0	176390	714570	0
RNA-binding protein 4;RNA-binding protein 4B	E9PB51;Q9BWF3-4;Q9BQ04;Q9BWF3;E9PLB0;E9PM61;D6R9K7;U3KQD5;J3QRR5;Q9BWF3-3;Q9BWF3-2	RBM4;RBM4B	0	172310	164200	0
Cleft lip and palate transmembrane protein 1-like protein	G5E9Z2;Q96KA5-2;Q96KA5	CLPTM1L	0	171610	150990	0
Protein SCO2 homolog, mitochondrial	O43819;C9JBU1	SCO2	0	168390	823570	0
Mitochondrial glutamate carrier 1	Q9H936;A0A0D9SFA8;K4DIB0;K4DIA2;A0A0D9SG84;E9PI74;E9PQ36;K4DIB6;K4DIB3;K4DIB8;K4DIA8;A0A0D9SEI9;A0A0D9SFE1;E9PJH7	SLC25A22	0	166590	299350	0
Exportin-1	O14980	XPO1	0	165570	613310	0
Sideroflexin-4	Q6P4A7-2;Q6P4A7	SFXN4	0	165010	329790	0

Supplements

Protein names	Protein IDs	Gene names	iBAQ (control)	iBAQ (DLC3α wt)	iBAQ (DLC3α K725E)	Q-value
Probable ubiquitin carboxyl-terminal hydrolase FAF-X; Probable ubiquitin carboxyl-terminal hydrolase FAF-Y	Q93008-1; Q93008; O00507	USP9X; USP9Y	0	164910	546580	0
Transcription intermediary factor 1-beta	Q13263; Q13263-2; M0R0K9	TRIM28	0	157840	629290	0
Phosphatidylserine synthase 1	P48651; P48651-3; P48651-2	PTDSS1	0	155180	317100	0
Probable ATP-dependent RNA helicase DDX47	Q9H0S4-2; Q9H0S4	DDX47	0	155020	100240	0
Thioredoxin domain-containing protein 5	Q86UY0; Q8NBS9-2; Q8NBS9	TXNDC5	0	154670	142940	0
Golgi-associated PDZ and coiled-coil motif-containing protein	F5H1Y4; Q9HD26-2; Q9HD26; Q9HD26-3	GOPC	0	152700	434540	0
Dehydrogenase/reductase SDR family member 7B	J3KRS1; A0A0C4DGQ8; Q6IAN0	DHRS7B	0	150760	286500	0
Sarcoplasmic/endoplasmic reticulum calcium ATPase 2	P16615-5; P16615-2; P16615-3; P16615-4; H7C5W9	ATP2A2	0	147400	422920	0
Histone-lysine N-methyltransferase SMYD3	B0QZA0; B0QZ88; Q9H7B4-3; Q9H7B4	SMYD3	0	145250	263120	0
Mitotic spindle-associated MMXD complex subunit MIP18	Q9Y3D0; J3QLT9	FAM96B	0	138400	300970	0
Transferrin receptor protein 1; Transferrin receptor protein 1, serum form	F8WBE5; P02786	TFRC	0	134070	442810	0
PIH1 domain-containing protein 1	Q9NWS0; M0R2P8; M0R3A4; M0QXD5; M0QYA2	PIH1D1	0	133960	734790	0
Na(+)/H(+) exchange regulatory cofactor NHE-RF2	Q15599-2; Q15599	SLC9A3R2	0	132740	171930	0
Disks large homolog 1	C9IYP1; H7C166; B4E2H8; E7EQD7; A0A0C4DFT3; Q12959-8; Q12959-9; Q12959-5; Q12959-3; Q12959-6; Q12959-4; Q12959; Q12959-7; Q12959-2	DLG1	0	129340	194350	0
Saccharopine dehydrogenase-like oxidoreductase	Q8NBX0	SCCPDH	0	125390	314560	0
Protein-S-isoprenylcysteine O-methyltransferase	O60725	ICMT	0	122050	227470	0
A-kinase anchor protein 8-like	Q9ULX6-2; Q9ULX6; V9GZ50	AKAP8L	0	121580	250990	0
Uncharacterized protein C2orf47, mitochondrial	H7C0V0; Q8WWC4	C2orf47	0	120250	178680	0
Melanoma-associated antigen D1	Q9Y5V3; Q9Y5V3-2	MAGED1	0	118090	786480	0
Alpha-catulin	Q9UBT7-3; Q9UBT7-2; Q9UBT7; Q5JTO9	CTNNA1	0	112020	154300	0

Supplements

Protein names	Protein IDs	Gene names	iBAQ (control)	iBAQ (DLC3 $\alpha$ wt)	iBAQ (DLC3 $\alpha$ K725E)	Q-value
Vacuolar protein sorting-associated protein 4A;Vacuolar protein sorting-associated protein 4B;Fidgetin-like protein 1	I3L4J1;Q9UN37;O75351;Q6PIW4-2;Q6PIW4	VPS4A;VPS4B;FIGNL1	0	111390	192440	0
Mitotic checkpoint protein BUB3	J3QT28;O43684-2;O43684	BUB3	0	109390	428500	0
Nischarin	Q9Y2I1;Q9Y2I1-2	NISCH	0	109110	238450	0
Dystrobrevin alpha	Q9Y4J8-13;Q9Y4J8-2;Q9Y4J8-14;Q9Y4J8-15;Q9Y4J8;Q9Y4J8-12;Q9Y4J8-16;Q9Y4J8-5;Q9Y4J8-4;Q9Y4J8-3;MOQZ28;Q9Y4J8-6;Q9Y4J8-10;Q9Y4J8-11	DTNA	0	107780	150060	0
Serine/threonine-protein phosphatase;Serine/threonine-protein phosphatase PP1-beta catalytic subunit	C9J9S3;C9JP48;P62140;E7ETD8	PPP1CB	0	107570	189690	0
Proteasomal ubiquitin receptor ADRM1	Q16186;A0A087WX59	ADRM1	0	106910	907380	0
BTB/POZ domain-containing protein KCTD12	Q96CX2	KCTD12	0	104900	374390	0
Serine/threonine-protein kinase PLK1	P53350;I3L2H5	PLK1	0	102260	128290	0
Glucose-6-phosphate translocase	U3KPU7;U3KQS2;O43826;O43826-2	SLC37A4	0	101220	172910	0
Phosphatidylinositol 3-kinase regulatory subunit beta	O00459;E9PFP1	PIK3R2	0	100860	465030	0
Ubiquitin-associated domain-containing protein 2	Q8NBM4;Q8NBM4-3;Q8NBM4-2;X6R5E5;Q8NBM4-4	UBAC2	0	100840	691620	0
Stomatin-like protein 2, mitochondrial	Q9UJZ1-2;Q9UJZ1;F2Z2I8;A0A087WYB4	STOML2	0	100210	266470	0

## References

- Albrecht, D.E., and S.C. Froehner. 2002. Syntrophins and Dystrobrevins: Defining the Dystrophin Scaffold at Synapses. *Neurosignals*. 11:123-129.
- Alpy, F., and C. Tomasetto. 2005. Give lipids a START: the StAR-related lipid transfer (START) domain in mammals. *Journal of Cell Science*. 118:2791-2801.
- Anastas, J.N., T.L. Biechele, M. Robitaille, J. Muster, K.H. Allison, S. Angers, and R.T. Moon. 2012. A protein complex of SCRIB, NOS1AP and VANGL1 regulates cell polarity and migration, and is associated with breast cancer progression. *Oncogene*. 31:3696-3708.
- Asnagli, L., W.C. Vass, R. Quadri, P.M. Day, X. Qian, R. Braverman, A.G. Papageorge, and D.R. Lowy. 2010. E-cadherin negatively regulates neoplastic growth in non-small cell lung cancer: role of Rho GTPases. *Oncogene*. 29:2760-2771.
- Assémat, E., E. Bazellières, E. Pallesi-Pocachard, A. Le Bivic, and D. Masey-Harroche. 2008. Polarity complex proteins. *Biochimica et Biophysica Acta (BBA) - Biomembranes*. 1778:614-630.
- Audebert, S., C. Navarro, C. Nourry, S. Chasserot-Golaz, P. Lécine, Y. Bellaïche, J.-L. Dupont, R.T. Premont, C. Sempéré, J.-M. Strub, A. Van Dorselaer, N. Vitale, and J.-P. Borg. 2004. Mammalian Scribble Forms a Tight Complex with the  $\beta$ PIX Exchange Factor. *Current Biology*. 14:987-995.
- Barras, D., and C. Widmann. 2013. GAP-independent functions of DLC1 in metastasis. *Cancer and Metastasis Reviews*. 33:87-100.
- Baum, B., and M. Georgiou. 2011. Dynamics of adherens junctions in epithelial establishment, maintenance, and remodeling. *The Journal of Cell Biology*. 192:907-917.
- Bhattacharya, M., A. Sundaram, M. Kudo, J. Farmer, P. Ganesan, A. Khalifeh-Soltani, M. Arjomandi, K. Atabai, X. Huang, and D. Sheppard. 2014. IQGAP1-dependent scaffold suppresses RhoA and inhibits airway smooth muscle contraction. *The Journal of Clinical Investigation*. 124:4895-4898.
- Bilder, D., and N. Perrimon. 2000. Localization of apical epithelial determinants by the basolateral PDZ protein Scribble. *Nature*. 403:676-680.
- Bolte, S., and F.P. Cordelières. 2006. A guided tour into subcellular colocalization analysis in light microscopy. *Journal of Microscopy*. 224:213-232.
- Borchert, N., C. Dieterich, K. Krug, W. Schütz, S. Jung, A. Nordheim, R.J. Sommer, and B. Macek. 2010. Proteogenomics of *Pristionchus pacificus* reveals distinct proteome structure of nematode models. *Genome Research*. 20:837-846.
- Bos, J.L., H. Rehmann, and A. Wittinghofer. 2007. GEFs and GAPs: Critical Elements in the Control of Small G Proteins. *Cell*. 130:385.
- Bouchet, B.P., R.E. Gough, Y.-C. Ammon, D. van de Willige, H. Post, G. Jacquemet, A.F.M. Altelaar, A.J.R. Heck, B.T. Goult, and A. Akhmanova. 2016. Talin-KANK1 interaction controls the recruitment of cortical microtubule stabilizing complexes to focal adhesions. *eLife*. 5:e18124.
- Braun, A.C., J. Hendrick, S.A. Eisler, S. Schmid, A. Hausser, and M.A. Olayioye. 2015. The Rho-specific GAP protein DLC3 coordinates endocytic membrane trafficking. *Journal of Cell Science*. 128:1386-1399.
- Braun, A.C., and M.A. Olayioye. 2015. Rho regulation: DLC proteins in space and time. *Cellular Signalling*. 27:1643-1651.
- Bray, K., C. Brakebusch, and T. Vargo-Gogola. 2011. The Rho GTPase Cdc42 is required for primary mammary epithelial cell morphogenesis in vitro. *Small GTPases*. 2:247-258.
- Brodu, V., and J. Casanova. 2006. The RhoGAP crossveinless-c links tracheless and EGFR signaling to cell shape remodeling in *Drosophila* tracheal invagination. *Genes & Development*. 20:1817-1828.

- Brown, M.C., M.S. Curtis, and C.E. Turner. 1998. Paxillin LD motifs may define a new family of protein recognition domains. *Nat Struct Mol Biol.* 5:677-678.
- Bryant, D.M., A. Datta, A.E. Rodriguez-Fraticelli, J. Peränen, F. Martin-Belmonte, and K.E. Mostov. 2010. A molecular network for de novo generation of the apical surface and lumen. *Nature cell biology.* 12:1035-1045.
- Bryant, D.M., M.C. Kerr, L.A. Hammond, S.R. Joseph, K.E. Mostov, R.D. Teasdale, and J.L. Stow. 2007. EGF induces macropinocytosis and SNX1-modulated recycling of E-cadherin. *Journal of Cell Science.* 120:1818-1828.
- Bryant, D.M., J. Rognot, A. Datta, A.W. Overeem, M. Kim, W. Yu, X. Peng, D.J. Eastburn, A.J. Ewald, Z. Werb, and K.E. Mostov. 2014. A Molecular Switch for the Orientation of Epithelial Cell Polarization. *Developmental cell.* 31:171-187.
- Buchsbaum, R.J. 2007. Rho activation at a glance. *Journal of Cell Science.* 120:1149-1152.
- Buchsbaum, R.J., B.A. Connolly, and L.A. Feig. 2002. Interaction of Rac Exchange Factors Tiam1 and Ras-GRF1 with a Scaffold for the p38 Mitogen-Activated Protein Kinase Cascade. *Molecular and Cellular Biology.* 22:4073-4085.
- Buchsbaum, R.J., B.A. Connolly, and L.A. Feig. 2003. Regulation of p70 S6 Kinase by Complex Formation between the Rac Guanine Nucleotide Exchange Factor (Rac-GEF) Tiam1 and the Scaffold Spinophilin. *Journal of Biological Chemistry.* 278:18833-18841.
- Campa, C.C., E. Ciralo, A. Ghigo, G. Germeña, and E. Hirsch. 2015. Crossroads of PI3K and Rac pathways. *Small GTPases.* 6:71-80.
- Cao, X., T. Kaneko, J.S. Li, A.-D. Liu, C. Voss, and S.S.C. Li. 2015. A phosphorylation switch controls the spatiotemporal activation of Rho GTPases in directional cell migration. *Nature Communications.* 6:7721.
- Cao, X., C. Voss, B. Zhao, T. Kaneko, and S.S.-C. Li. 2012. Differential regulation of the activity of deleted in liver cancer 1 (DLC1) by tensins controls cell migration and transformation. *Proceedings of the National Academy of Sciences.* 109:1455-1460.
- Carr, H.S., C. Cai, K. Keinänen, and J.A. Frost. 2009. Interaction of the RhoA Exchange Factor Net1 with Discs Large Homolog 1 Protects It from Proteasome-mediated Degradation and Potentiates Net1 Activity. *The Journal of Biological Chemistry.* 284:24269-24280.
- Chan, L.-K., F.C.F. Ko, I.O.-L. Ng, and J.W.P. Yam. 2009. Deleted in Liver Cancer 1 (DLC1) Utilizes a Novel Binding Site for Tensin2 PTB Domain Interaction and Is Required for Tumor-Suppressive Function. *PLoS ONE.* 4:e5572.
- Chatterjee, S., L. Seifried, M.E. Feigin, D.L. Gibbons, C. Scuoppo, W. Lin, Z.H. Rizvi, E. Lind, D. Dissanayake, J. Kurie, P. Ohashi, and S.K. Muthuswamy. 2012. Dysregulation of Cell Polarity Proteins Synergize with Oncogenes or the Microenvironment to Induce Invasive Behavior in Epithelial Cells. *PLoS ONE.* 7:e34343.
- Chen, B., B. Zheng, M. DeRan, G.K. Jarugumilli, J. Fu, Y.S. Brooks, and X. Wu. 2016. ZDHHC7-mediated S-palmitoylation of Scribble regulates cell polarity. *Nat Chem Biol.* advance online publication.
- Ching, Y.-P., C.-M. Wong, S.-F. Chan, T.H.-Y. Leung, D.C.-H. Ng, D.-Y. Jin, and I.O.-L. Ng. 2003. Deleted in Liver Cancer (DLC) 2 Encodes a RhoGAP Protein with Growth Suppressor Function and Is Underexpressed in Hepatocellular Carcinoma. *Journal of Biological Chemistry.* 278:10824-10830.
- Citi, S., D. Guerrero, D. Spadaro, and J. Shah. 2014. Epithelial junctions and Rho family GTPases: the zonular signalosome. *Small GTPases.* 5:1-15.
- Courbard, J.-R., A. Djiane, J. Wu, and M. Mlodzik. 2009. The Apical/Basal-polarity determinant Scribble cooperates with the PCP core factor Stbm/Vang and functions as one of its effectors. *Developmental biology.* 333:67-77.

- Cox, J., and M. Mann. 2008. MaxQuant enables high peptide identification rates, individualized p.p.b.-range mass accuracies and proteome-wide protein quantification. *Nat Biotech.* 26:1367-1372.
- Cox, J., N. Neuhauser, A. Michalski, R.A. Scheltema, J.V. Olsen, and M. Mann. 2011. Andromeda: A Peptide Search Engine Integrated into the MaxQuant Environment. *Journal of Proteome Research.* 10:1794-1805.
- de Vreede, G., J.D. Schoenfeld, S.L. Windler, H. Morrison, H. Lu, and D. Bilder. 2014. The Scribble module regulates retromer-dependent endocytic trafficking during epithelial polarization. *Development (Cambridge, England).* 141:2796-2802.
- Denholm, B., S. Brown, R.P. Ray, M. Ruiz-Gómez, H. Skaer, and J.C.-G. Hombria. 2005. crossveinless-c is a RhoGAP required for actin reorganisation during morphogenesis. *Development.*
- Desclozeaux, M., J. Venturato, F.G. Wylie, J.G. Kay, S.R. Joseph, H.T. Le, and J.L. Stow. 2008. Active Rab11 and functional recycling endosome are required for E-cadherin trafficking and lumen formation during epithelial morphogenesis. *American Journal of Physiology - Cell Physiology.* 295:C545-C556.
- Dow, L.E., A.M. Brumby, R. Muratore, M.L. Coombe, K.A. Sedelies, J.A. Trapani, S.M. Russell, H.E. Richardson, and P.O. Humbert. 2003. hScrib is a functional homologue of the Drosophila tumour suppressor Scribble. *Oncogene.* 22:9225-9230.
- Dow, L.E., I.A. Elsum, C.L. King, K.M. Kinross, H.E. Richardson, and P.O. Humbert. 2008. Loss of human Scribble cooperates with H-Ras to promote cell invasion through deregulation of MAPK signalling. *Oncogene.* 27:5988-6001.
- Dow, L.E., J.S. Kauffman, J. Caddy, A.S. Peterson, S.M. Jane, S.M. Russell, and P.O. Humbert. 2006. The tumour-suppressor Scribble dictates cell polarity during directed epithelial migration: regulation of Rho GTPase recruitment to the leading edge. *Oncogene.* 26:2272-2282.
- Du, X., X. Qian, A. Papageorge, A.J. Schetter, W.C. Vass, X. Liu, R. Braverman, A.I. Robles, and D.R. Lowy. 2012. Functional Interaction of Tumor Suppressor DLC1 and Caveolin-1 in Cancer Cells. *Cancer Research.* 72:4405-4416.
- Durkin, M.E., M.R. Avner, C.-G. Huh, B.-Z. Yuan, S.S. Thorgeirsson, and N.C. Popescu. 2005. DLC-1, a Rho GTPase-activating protein with tumor suppressor function, is essential for embryonic development. *FEBS Letters.* 579:1191-1196.
- Durkin, M.E., V. Ullmannova, M. Guan, and N.C. Popescu. 2007a. Deleted in liver cancer 3 (DLC-3), a novel Rho GTPase-activating protein, is downregulated in cancer and inhibits tumor cell growth. *Oncogene.* 26:4580-4589.
- Durkin, M.E., B.-Z. Yuan, X. Zhou, D.B. Zimonjic, D.R. Lowy, S.S. Thorgeirsson, and N.C. Popescu. 2007b. DLC-1: a Rho GTPase-activating protein and tumour suppressor. *Journal of Cellular and Molecular Medicine.* 11:1185-1207.
- Eastburn, D.J., M.M. Zegers, and K.E. Mostov. 2012. Scrib regulates HGF-mediated epithelial morphogenesis and is stabilized by Sgt1-HSP90. *Journal of Cell Science.* 125:4147-4157.
- Ellenbroek, S.I.J., S. Iden, and J.G. Collard. 2012. Cell polarity proteins and cancer. *Seminars in Cancer Biology.* 22:208-215.
- Elsum, I.A., and P.O. Humbert. 2013. Localization, Not Important in All Tumor-Suppressing Properties: A Lesson Learnt from Scribble. *Cells Tissues Organs.* 198:1-11.
- Elsum, I.A., C. Martin, and P.O. Humbert. 2013. Scribble regulates an EMT polarity pathway through modulation of MAPK-ERK signaling to mediate junction formation. *Journal of Cell Science.* 126:3990-3999.
- Erlmann, P., S. Schmid, F.A. Horenkamp, M. Geyer, T.G. Pomorski, and M.A. Olayioye. 2009. DLC1 Activation Requires Lipid Interaction through a Polybasic Region Preceding the RhoGAP Domain. *Molecular Biology of the Cell.* 20:4400-4411.
- Etienne-Manneville, S., and A. Hall. 2001. Integrin-Mediated Activation of Cdc42 Controls Cell Polarity in Migrating Astrocytes through PKCzeta. *Cell.* 106:489-498.

- Etienne-Manneville, S., and A. Hall. 2002. Rho GTPases in cell biology. *Nature*. 420:629-635.
- Etienne-Manneville, S., J.-B. Manneville, S. Nicholls, M.A. Ferenczi, and A. Hall. 2005. Cdc42 and Par6–PKC $\zeta$  regulate the spatially localized association of Dlg1 and APC to control cell polarization. *The Journal of Cell Biology*. 170:895-901.
- Feigin, M.E., S.D. Akshinthala, K. Araki, A.Z. Rosenberg, L.B. Muthuswamy, B. Martin, B.D. Lehmann, H.K. Berman, J.A. Pietsenpol, R.D. Cardiff, and S.K. Muthuswamy. 2014. Mislocalization of the Cell Polarity Protein Scribble Promotes Mammary Tumorigenesis and Is Associated with Basal Breast Cancer. *Cancer Research*. 74:3180-3194.
- Fernandez-Borja, M., L. Janssen, D. Verwoerd, P. Hordijk, and J. Neefjes. 2005. RhoB regulates endosome transport by promoting actin assembly on endosomal membranes through Dia1. *Journal of Cell Science*. 118:2661-2670.
- Frank, S.R., J.H. Bell, M. Frödin, and S.H. Hansen. 2012. A  $\beta$ PIX-PAK2 complex confers protection against Scrib-dependent and cadherin-mediated apoptosis. *Current biology : CB*. 22:1747-1754.
- Gampel, A., P.J. Parker, and H. Mellor. 1999. Regulation of epidermal growth factor receptor traffic by the small GTPase RhoB. *Current Biology*. 9:955-958.
- García-Mata, R., and K. BurrIDGE. 2006. Catching a GEF by its tail. *Trends in Cell Biology*. 17:36-43.
- García-Mata, R., A.D. Dubash, L. Sharek, H.S. Carr, J.A. Frost, and K. BurrIDGE. 2007. The Nuclear RhoA Exchange Factor Net1 Interacts with Proteins of the Dlg Family, Affects Their Localization, and Influences Their Tumor Suppressor Activity. *Molecular and Cellular Biology*. 27:8683-8697.
- Gardioli, D., A. Zacchi, F. Petrera, G. Stanta, and L. Banks. 2006. Human discs large and scrib are localized at the same regions in colon mucosa and changes in their expression patterns are correlated with loss of tissue architecture during malignant progression. *International Journal of Cancer*. 119:1285-1290.
- Geiger, B., A. Bershadsky, R. Pankov, and K.M. Yamada. 2001. Transmembrane crosstalk between the extracellular matrix and the cytoskeleton. *Nat Rev Mol Cell Biol*. 2:793-805.
- Giallourakis, C., Z. Cao, T. Green, H. Wachtel, X. Xie, M. Lopez-Illasaca, M. Daly, J. Rioux, and R. Xavier. 2006. A molecular-properties-based approach to understanding PDZ domain proteins and PDZ ligands. *Genome Research*. 16:1056-1072.
- Godde, N.J., J.M. Sheridan, L.K. Smith, H.B. Pearson, K.L. Britt, R.C. Galea, L.L. Yates, J.E. Visvader, and P.O. Humbert. 2014. Scribble Modulates the MAPK/Fra1 Pathway to Disrupt Luminal and Ductal Integrity and Suppress Tumour Formation in the Mammary Gland. *PLoS Genet*. 10:e1004323.
- Goodison, S., J. Yuan, D. Sloan, R. Kim, C. Li, N.C. Popescu, and V. Urquidi. 2005. The RhoGAP Protein DLC-1 Functions as a Metastasis Suppressor in Breast Cancer Cells. *Cancer research*. 65:6042-6053.
- Halaoui, R., and L. McCaffrey. 2015. Rewiring cell polarity signaling in cancer. *Oncogene*. 34:939-950.
- Hall, A. 1998. Rho GTPases and the Actin Cytoskeleton. *Science*. 279:509-514.
- Hanahan, D., and R.A. Weinberg. 2000. The Hallmarks of Cancer. *Cell*. 100:57-70.
- Healy, K.D., L. Hodgson, T.-Y. Kim, A. Shutes, S. Maddileti, R.L. Juliano, K.M. Hahn, T.K. Harden, Y.-J. Bang, and C.J. Der. 2008. DLC-1 Suppresses Non-Small Cell Lung Cancer Growth and Invasion By RhoGAP-Dependent and Independent Mechanisms. *Molecular carcinogenesis*. 47:326-337.
- Heering, J., P. Erlmann, and M.A. Olayioye. 2009. Simultaneous loss of the DLC1 and PTEN tumor suppressors enhances breast cancer cell migration. *Experimental Cell Research*. 315:2505-2514.
- Hodge, R.G., and A.J. Ridley. 2016. Regulating Rho GTPases and their regulators. *Nat Rev Mol Cell Biol*. advance online publication.

- Holeiter, G., A. Bischoff, A.C. Braun, B. Huck, P. Erlmann, S. Schmid, R. Herr, T. Brummer, and M.A. Olayioye. 2012. The RhoGAP protein Deleted in Liver Cancer 3 (DLC3) is essential for adherens junctions integrity. *Oncogenesis*. 1:e13.
- Holeiter, G., J. Heering, P. Erlmann, S. Schmid, R. Jähne, and M.A. Olayioye. 2008. Deleted in Liver Cancer 1 Controls Cell Migration through a Dia1-Dependent Signaling Pathway. *Cancer Research*. 68:8743-8751.
- Homma, Y., and Y. Emori. 1995. A dual functional signal mediator showing RhoGAP and phospholipase C-delta stimulating activities. *The EMBO Journal*. 14:286-291.
- Humbert, P.O., N.A. Grzeschik, A.M. Brumby, R. Galea, I. Elsum, and H.E. Richardson. 2008. Control of tumorigenesis by the Scribble/Dlg/Lgl polarity module. *Oncogene*. 27:6888-6907.
- Hurd, T.W., S. Fan, C.-J. Liu, H.K. Kweon, K. Hakansson, and B. Margolis. 2003. Phosphorylation-Dependent Binding of 14-3-3 to the Polarity Protein Par3 Regulates Cell Polarity in Mammalian Epithelia. *Current Biology*. 13:2082-2090.
- Iden, S., and J.G. Collard. 2008. Crosstalk between small GTPases and polarity proteins in cell polarization. *Nat Rev Mol Cell Biol*. 9:846-859.
- Ikenoue, T., K. Inoki, B. Zhao, and K.-L. Guan. 2008. PTEN Acetylation Modulates Its Interaction with PDZ Domain. *Cancer Research*. 68:6908-6912.
- Itoh, M., S. Tsukita, Y. Yamazaki, and H. Sugimoto. 2012. Rho GTP exchange factor ARHGEF11 regulates the integrity of epithelial junctions by connecting ZO-1 and RhoA-Myosin II signaling. *Proceedings of the National Academy of Sciences of the United States of America*. 109:9905-9910.
- Jacquemet, G., and M.J. Humphries. 2013. IQGAP1 is a key node within the small GTPase network. *Small GTPases*. 4:199-207.
- Jaffe, A.B., and A. Hall. 2005. RHO GTPASES: Biochemistry and Biology. *Annual Review of Cell and Developmental Biology*. 21:247-269.
- Jaffe, A.B., A. Hall, and A. Schmidt. 2005. Association of CNK1 with Rho Guanine Nucleotide Exchange Factors Controls Signaling Specificity Downstream of Rho. *Current Biology*. 15:405-412.
- Jaffe, A.B., N. Kaji, J. Durgan, and A. Hall. 2008. Cdc42 controls spindle orientation to position the apical surface during epithelial morphogenesis. *The Journal of Cell Biology*. 183:625-633.
- Jaiswal, M., R. Dvorsky, E. Amin, S.L. Risse, E.K. Fansa, S.-C. Zhang, M.S. Taha, A.R. Gauhar, S. Nakhaei-Rad, C. Kordes, K.T. Koessmeier, I.C. Cirstea, M.A. Olayioye, D. Häussinger, and M.R. Ahmadian. 2014. Functional cross-talk between ras and rho pathways: a Ras-specific GTPase-activating protein (p120RasGAP) competitively inhibits the RhoGAP activity of deleted in liver cancer (DLC) tumor suppressor by masking the catalytic arginine finger. *The Journal of Biological Chemistry*. 289:6839-6849.
- Jiang, W., M. Betson, R. Mulloy, R. Foster, M. Lévy, E. Ligeti, and J. Settleman. 2008. p190A RhoGAP Is a Glycogen Synthase Kinase-3- $\beta$  Substrate Required for Polarized Cell Migration. *The Journal of Biological Chemistry*. 283:20978-20988.
- Kallay, L.M., A. McNickle, P.J. Brennwald, A.L. Hubbard, and L.T. Braiterman. 2006. Scribble associates with two polarity proteins, lgl2 and vangl2, via distinct molecular domains. *Journal of Cellular Biochemistry*. 99:647-664.
- Kawai, K., S.-y. Kitamura, K. Maehira, J.-i. Seike, and H. Yagisawa. 2010. START-GAP1/DLC1 is localized in focal adhesions through interaction with the PTB domain of tensin2. *Advances in Enzyme Regulation*. 50:202-215.
- Kawai, K., M. Kiyota, J. Seike, Y. Deki, and H. Yagisawa. 2007. START-GAP3/DLC3 is a GAP for RhoA and Cdc42 and is localized in focal adhesions regulating cell morphology. *Biochemical and Biophysical Research Communications*. 364:783-789.
- Kawai, K., J.-i. Seike, T. Iino, M. Kiyota, Y. Iwamae, H. Nishitani, and H. Yagisawa. 2009. START-GAP2/DLC2 is localized in focal adhesions via its N-terminal region. *Biochemical and Biophysical Research Communications*. 380:736-741.

- Kawai, K., M. Yamaga, Y. Iwamae, M. Kiyota, H. Kamata, H. Hirata, Y. Homma, and H. Yagisawa. 2004. A PLC $\delta$ 1-binding protein, p122RhoGAP, is localized in focal adhesions. *Biochemical Society Transactions*. 32:1107-1109.
- Khalil, B.D., S. Hanna, B.A. Saykali, S. El-Sitt, A. Nasrallah, D. Marston, M. El-Sabban, K.M. Hahn, M. Symons, and M. El-Sibai. 2014. The Regulation of RhoA at Focal Adhesions by StarD13 is Important for Astrocytoma Cell Motility. *Experimental cell research*. 321:109-122.
- Kim, E., and M. Sheng. 2004. PDZ domain proteins of synapses. *Nat Rev Neurosci*. 5:771-781.
- Kim, M., A. M. Shewan, A.J. Ewald, Z. Werb, and K.E. Mostov. 2015. p114RhoGEF governs cell motility and lumen formation during tubulogenesis through a ROCK–myosin-II pathway. *Journal of Cell Science*. 128:4317-4327.
- Kim, T.Y., K.D. Healy, C.J. Der, N. Sciaky, Y.-J. Bang, and R.L. Juliano. 2008. Effects of Structure of Rho GTPase-activating Protein DLC-1 on Cell Morphology and Migration. *The Journal of Biological Chemistry*. 283:32762-32770.
- Kim, T.Y., S. Jackson, Y. Xiong, T.G. Whitsett, J.R. Lobello, G.J. Weiss, N.L. Tran, Y.-J. Bang, and C.J. Der. 2013. CRL4A-FBXW5–mediated degradation of DLC1 Rho GTPase-activating protein tumor suppressor promotes non-small cell lung cancer cell growth. *Proceedings of the National Academy of Sciences of the United States of America*. 110:16868-16873.
- Klezovitch, O., T.E. Fernandez, S.J. Tapscott, and V. Vasioukhin. 2004. Loss of cell polarity causes severe brain dysplasia in Lgl1 knockout mice. *Genes & Development*. 18:559-571.
- Ko, F.C.F., Y.-S. Yeung, C.-M. Wong, L.-K. Chan, R.T.P. Poon, I. Oi-Lin Ng, and J.W.P. Yam. 2010. Deleted in liver cancer 1 isoforms are distinctly expressed in human tissues, functionally different and under differential transcriptional regulation in hepatocellular carcinoma. *Liver International*. 30:139-148.
- Lang, P., F. Gesbert, M. Delespine-Carmagnat, R. Stancou, M. Pouchelet, and J. Bertoglio. 1996. Protein kinase A phosphorylation of RhoA mediates the morphological and functional effects of cyclic AMP in cytotoxic lymphocytes. *The EMBO Journal*. 15:510-519.
- Laprise, P., S. Beronja, N.F. Silva-Gagliardi, M. Pellikka, A.M. Jensen, C.J. McGlade, and U. Tepass. 2006. The FERM Protein Yurt Is a Negative Regulatory Component of the Crumbs Complex that Controls Epithelial Polarity and Apical Membrane Size. *Developmental cell*. 11:363-374.
- Leung, T.H.-Y., Y.-P. Ching, J.W.P. Yam, C.-M. Wong, T.-O. Yau, D.-Y. Jin, and I.O.-L. Ng. 2005. Deleted in liver cancer 2 (DLC2) suppresses cell transformation by means of inhibition of RhoA activity. *Proceedings of the National Academy of Sciences of the United States of America*. 102:15207-15212.
- Li, G., X. Du, W.C. Vass, A.G. Papageorge, D.R. Lowy, and X. Qian. 2011. Full activity of the deleted in liver cancer 1 (DLC1) tumor suppressor depends on an LD-like motif that binds talin and focal adhesion kinase (FAK). *Proceedings of the National Academy of Sciences of the United States of America*. 108:17129-17134.
- Li, H., K.-L. Fung, D.-Y. Jin, S.S.M. Chung, Y.-P. Ching, I.O.-L. Ng, K.-H. Sze, B.C.B. Ko, and H. Sun. 2007. Solution structures, dynamics, and lipid-binding of the sterile  $\alpha$ -motif domain of the deleted in liver cancer 2. *Proteins: Structure, Function, and Bioinformatics*. 67:1154-1166.
- Liao, Y.-C., L. Si, R.W. deVere White, and S.H. Lo. 2007. The phosphotyrosine-independent interaction of DLC-1 and the SH2 domain of cten regulates focal adhesion localization and growth suppression activity of DLC-1. *The Journal of Cell Biology*. 176:43-49.
- Lin, Y., N.T. Chen, Y.P. Shih, Y.C. Liao, L. Xue, and S.H. Lo. 2010. DLC2 modulates angiogenic responses in vascular endothelial cells by regulating cell attachment and migration. *Oncogene*. 29:3010-3016.

- Lohia, M., Y. Qin, and I.G. Macara. 2012. The Scribble Polarity Protein Stabilizes E-Cadherin/p120-Catenin Binding and Blocks Retrieval of E-Cadherin to the Golgi. *PLoS ONE*. 7:e51130.
- Lukasik, D., E. Wilczek, A. Wasiutynski, and B. Gornicka. 2011. Deleted in liver cancer protein family in human malignancies (Review). *Oncology Letters*. 2:763-768.
- Mack, N.A., and M. Georgiou. 2014. The interdependence of the Rho GTPases and apicobasal cell polarity. *Small GTPases*. 5:e973768.
- Mack, N.A., A.P. Porter, H.J. Whalley, J.P. Schwarz, R.C. Jones, A.S. Syed, A. Bjartell, K.I. Anderson, and A. Malliri. 2012.  $\beta$ 2-syntrophin and Par-3 promote an apicobasal Rac activity gradient at cell-cell junctions by differentially regulating Tiam1 activity. *Nature cell biology*. 14:1169-1180.
- Marcos-Ramiro, B., D. García-Weber, S. Barroso, J. Feito, M.C. Ortega, E. Cernuda-Morollón, N. Reglero-Real, L. Fernández-Martín, M.C. Durán, M.A. Alonso, I. Correas, S. Cox, A.J. Ridley, and J. Millán. 2016. RhoB controls endothelial barrier recovery by inhibiting Rac1 trafficking to the cell border. *The Journal of Cell Biology*. 213:385-402.
- Marinissen, M.J., and J.S. Gutkind. 2005. Scaffold proteins dictate Rho GTPase-signaling specificity. *Trends in Biochemical Sciences*. 30:423-426.
- Mertens, A.E.E., T.P. Rygiel, C. Olivo, R. van der Kammen, and J.G. Collard. 2005. The Rac activator Tiam1 controls tight junction biogenesis in keratinocytes through binding to and activation of the Par polarity complex. *The Journal of Cell Biology*. 170:1029-1037.
- Möller, Y., M. Siegemund, S. Beyes, R. Herr, D. Lecis, D. Delia, R. Kontermann, T. Brummer, K. Pfizenmaier, and M.A. Olayioye. 2014. EGFR-Targeted TRAIL and a Smac Mimetic Synergize to Overcome Apoptosis Resistance in KRAS Mutant Colorectal Cancer Cells. *PLoS ONE*. 9:e107165.
- Montcouquiol, M., R.A. Rachel, P.J. Lanford, N.G. Copeland, N.A. Jenkins, and M.W. Kelley. 2003. Identification of Vangl2 and Scrb1 as planar polarity genes in mammals. *Nature*. 423:173-177.
- Muösch, A., D. Cohen, C. Yeaman, W.J. Nelson, E. Rodriguez-Boulan, and P.J. Brennwald. 2002. Mammalian Homolog of Drosophila Tumor Suppressor Lethal (2) Giant Larvae Interacts with Basolateral Exocytic Machinery in Madin-Darby Canine Kidney Cells. *Molecular Biology of the Cell*. 13:158-168.
- Murdoch, J.N., D.J. Henderson, K. Doudney, C. Gaston-Massuet, H.M. Phillips, C. Paternotte, R. Arkell, P. Stanier, and A.J. Copp. 2003. Disruption of scribble (Scrb1) causes severe neural tube defects in the circletail mouse. *Human Molecular Genetics*. 12:87-98.
- Nagaraja, G.M., and R.P. Kandpal. 2004. Chromosome 13q12 encoded Rho GTPase activating protein suppresses growth of breast carcinoma cells, and yeast two-hybrid screen shows its interaction with several proteins. *Biochemical and Biophysical Research Communications*. 313:654-665.
- Nagasaka, K., P. Massimi, D. Pim, V.K. Subbiah, C. Kranjec, S. Nakagawa, T. Yano, Y. Taketani, and L. Banks. 2010. The mechanism and implications of hScrib regulation of ERK. *Small GTPases*. 1:108-112.
- Nagase, T., N. Seki, K.-i. Ishikawa, A. Tanaka, and N. Nomura. 1996. Prediction of the Coding Sequences of Unidentified Human Genes. V. The Coding Sequences of 40 New Genes (KIAA0161-KIAA0200) Deduced by Analysis of cDNA Clones from Human Cell Line KG-1. *DNA Research*. 3:17-24.
- Nakagawa, S., and J.M. Huibregtse. 2000. Human Scribble (Vartul) Is Targeted for Ubiquitin-Mediated Degradation by the High-Risk Papillomavirus E6 Proteins and the E6AP Ubiquitin-Protein Ligase. *Molecular and Cellular Biology*. 20:8244-8253.
- Nakajima, H., and T. Tanoue. 2011. Lulu2 regulates the circumferential actomyosin tensile system in epithelial cells through p114RhoGEF. *The Journal of Cell Biology*. 195:245-261.

- Nakayama, M., T.M. Goto, M. Sugimoto, T. Nishimura, T. Shinagawa, S. Ohno, M. Amano, and K. Kaibuchi. 2008. Rho-Kinase Phosphorylates PAR-3 and Disrupts PAR Complex Formation. *Developmental Cell*. 14:205-215.
- Navarro, C., S. Nola, S. Audebert, M.-J. Santoni, J.-P. Arsanto, C. Ginestier, S. Marchetto, J. Jacquemier, D. Isnardon, A. Le Bivic, D. Birnbaum, and J.-P. Borg. 2005. Junctional recruitment of mammalian Scribble relies on E-cadherin engagement. *Oncogene*. 24:4330-4339.
- Nelson, W.J. 2009. Remodeling Epithelial Cell Organization: Transitions Between Front–Rear and Apical–Basal Polarity. *Cold Spring Harbor Perspectives in Biology*. 1:a000513.
- Ng, D.C.-H., S.-F. Chan, K.H. Kok, J.W.P. Yam, Y.-P. Ching, I.O.-I. Ng, and D.-Y. Jin. 2006. Mitochondrial targeting of growth suppressor protein DLC2 through the START domain. *FEBS Letters*. 580:191-198.
- Ngok, S.P., R. Geyer, A. Kourtidis, N. Mitin, R. Feathers, C. Der, and P.Z. Anastasiadis. 2013. TEM4 is a junctional Rho GEF required for cell–cell adhesion, monolayer integrity and barrier function. *Journal of Cell Science*. 126:3271-3277.
- Ngok, S.P., W.-H. Lin, and P.Z. Anastasiadis. 2014. Establishment of epithelial polarity – GEF who's minding the GAP? *Journal of Cell Science*. 127:3205-3215.
- Nishimura, T., and K. Kaibuchi. 2007. Numb Controls Integrin Endocytosis for Directional Cell Migration with aPKC and PAR-3. *Developmental Cell*. 13:15-28.
- Nishimura, T., T. Yamaguchi, K. Kato, M. Yoshizawa, Y.-i. Nabeshima, S. Ohno, M. Hoshino, and K. Kaibuchi. 2005. PAR-6-PAR-3 mediates Cdc42-induced Rac activation through the Rac GEFs STEF/Tiam1. *Nat Cell Biol*. 7:270-277.
- Nola, S., R. Daigaku, K. Smolarczyk, M. Carstens, B. Martin-Martin, G. Longmore, M. Bailly, and V.M.M. Braga. 2011. Ajuba is required for Rac activation and maintenance of E-cadherin adhesion. *The Journal of Cell Biology*. 195:855-871.
- Nola, S., M. Sebbagh, S. Marchetto, N. Osmani, C. Nourry, S. Audebert, C. Navarro, R. Rachel, M. Montcouquiol, N. Sans, S. Etienne-Manneville, J.-P. Borg, and M.-J. Santoni. 2008. Scrib regulates PAK activity during the cell migration process. *Human Molecular Genetics*. 17:3552-3565.
- Noll, B., J. Hendrick, and M.A. Olayioye. 2016. Rho-Signalgebung in der Tumorentstehung und -progression. *BIOspektrum*. 22:369-372.
- Noren, N.K., W.T. Arthur, and K. Burrige. 2003. Cadherin Engagement Inhibits RhoA via p190RhoGAP. *Journal of Biological Chemistry*. 278:13615-13618.
- Nourry, C., S.G.N. Grant, and J.-P. Borg. 2003. PDZ Domain Proteins: Plug and Play! *Science Signaling*. 2003:re7-re7.
- Orgaz, J.L., C. Herraiz, and V. Sanz-Moreno. 2014. Rho GTPases modulate malignant transformation of tumor cells. *Small GTPases*. 5:e29019.
- Osmani, N., N. Vitale, J.-P. Borg, and S. Etienne-Manneville. 2006. Scrib Controls Cdc42 Localization and Activity to Promote Cell Polarization during Astrocyte Migration. *Current Biology*. 16:2395-2405.
- Overeem, A.W., D.M. Bryant, and S.C.D. van Ijzendoorn. 2015. Mechanisms of apical-basal axis orientation and epithelial lumen positioning. *Trends in Cell Biology*. 25:476-485.
- P. Kandpal, R. 2006. Rho GTPase Activating Proteins in Cancer Phenotypes. *Current Protein and Peptide Science*. 7:355-365.
- Pagliarini, R.A., and T. Xu. 2003. A Genetic Screen in Drosophila for Metastatic Behavior. *Science*. 302:1227-1231.
- Palazzo, A.F., T.A. Cook, A.S. Alberts, and G.G. Gundersen. 2001. mDia mediates Rho-regulated formation and orientation of stable microtubules. *Nat Cell Biol*. 3:723-729.
- Pan, C.Q., M. Sudol, M. Sheetz, and B.C. Low. 2012. Modularity and functional plasticity of scaffold proteins as p(l)acemakers in cell signaling. *Cellular Signalling*. 24:2143-2165.

- Paszek, M.J., N. Zahir, K.R. Johnson, J.N. Lakins, G.I. Rozenberg, A. Gefen, C.A. Reinhart-King, S.S. Margulies, M. Dembo, D. Boettiger, D.A. Hammer, and V.M. Weaver. 2005. Tensional homeostasis and the malignant phenotype. *Cancer Cell*. 8:241-254.
- Pearson, H.B., P.A. Perez-Mancera, L.E. Dow, A. Ryan, P. Tennstedt, D. Bogani, I. Elsum, A. Greenfield, D.A. Tuveson, R. Simon, and P.O. Humbert. 2011. SCRIB expression is deregulated in human prostate cancer, and its deficiency in mice promotes prostate neoplasia. *The Journal of Clinical Investigation*. 121:4257-4267.
- Pegtel, D.M., S.I.J. Ellenbroek, A.E.E. Mertens, R.A. van der Kammen, J. de Rooij, and J.G. Collard. 2007. The Par-Tiam1 Complex Controls Persistent Migration by Stabilizing Microtubule-Dependent Front-Rear Polarity. *Current Biology*. 17:1623-1634.
- Piekny, A.J., and M. Glotzer. 2008. Anillin Is a Scaffold Protein That Links RhoA, Actin, and Myosin during Cytokinesis. *Current Biology*. 18:30-36.
- Priya, R., G.A. Gomez, S. Budnar, S. Verma, H.L. Cox, N.A. Hamilton, and A.S. Yap. 2015. Feedback regulation through myosin II confers robustness on RhoA signalling at E-cadherin junctions. *Nat Cell Biol*. 17:1282-1293.
- Qian, X., G. Li, H.K. Asmussen, L. Asnaghi, W.C. Vass, R. Braverman, K.M. Yamada, N.C. Popescu, A.G. Papageorge, and D.R. Lowy. 2007. Oncogenic inhibition by a deleted in liver cancer gene requires cooperation between tensin binding and Rho-specific GTPase-activating protein activities. *Proceedings of the National Academy of Sciences of the United States of America*. 104:9012-9017.
- Qiao, F., and J.U. Bowie. 2005. The Many Faces of SAM. *Science Signaling*. 2005:re7-re7.
- Qin, Y., C. Capaldo, B.M. Gumbiner, and I.G. Macara. 2005. The mammalian Scribble polarity protein regulates epithelial cell adhesion and migration through E-cadherin. *The Journal of Cell Biology*. 171:1061-1071.
- Quiros, M., and A. Nusrat. 2014. RhoGTPases, actomyosin signaling and regulation of the Epithelial Apical Junctional Complex. *Seminars in Cell & Developmental Biology*. 36:194-203.
- Raftopoulou, M., and A. Hall. 2004. Cell migration: Rho GTPases lead the way. *Developmental Biology*. 265:23-32.
- Ratheesh, A., G.A. Gomez, R. Priya, S. Verma, E.M. Kovacs, K. Jiang, N.H. Brown, A. Akhmanova, S.J. Stehbens, and A.S. Yap. 2012. Centralspindlin and  $\alpha$ -catenin regulate Rho signalling at the epithelial zonula adherens. *Nature cell biology*. 14:818-828.
- Ridley, A.J. 2006. Rho GTPases and actin dynamics in membrane protrusions and vesicle trafficking. *Trends in Cell Biology*. 16:522-529.
- Ridley, A.J., M.A. Schwartz, K. Burridge, R.A. Firtel, M.H. Ginsberg, G. Borisy, J.T. Parsons, and A.R. Horwitz. 2003. Cell Migration: Integrating Signals from Front to Back. *Science*. 302:1704-1709.
- Rolli-Derkinderen, M., G. Toumaniantz, P. Pacaud, and G. Loirand. 2010. RhoA Phosphorylation Induces Rac1 Release from Guanine Dissociation Inhibitor  $\alpha$  and Stimulation of Vascular Smooth Muscle Cell Migration. *Molecular and Cellular Biology*. 30:4786-4796.
- Sabbir, M.G., N. Wigle, S. Loewen, Y. Gu, C. Buse, G.G. Hicks, and M.R.A. Mowat. 2010. Identification and characterization of Dlc1 isoforms in the mouse and study of the biological function of a single gene trapped isoform. *BMC Biology*. 8:17-17.
- Sahai, E., and C.J. Marshall. 2002a. RHO-GTPases and cancer. *Nat Rev Cancer*. 2:133-142.
- Sahai, E., and C.J. Marshall. 2002b. ROCK and Dia have opposing effects on adherens junctions downstream of Rho. *Nat Cell Biol*. 4:408-415.
- Sakamori, R., S. Das, S. Yu, S. Feng, E. Stypulkowski, Y. Guan, V. Douard, W. Tang, R.P. Ferraris, A. Harada, C. Brakebusch, W. Guo, and N. Gao. 2012. Cdc42 and

- Rab8a are critical for intestinal stem cell division, survival, and differentiation in mice. *The Journal of Clinical Investigation*. 122:1052-1065.
- Scholz, R.-P., J. Regner, A. Theil, P. Erlmann, G. Holeiter, R. Jähne, S. Schmid, A. Hausser, and M.A. Olayioye. 2009. DLC1 interacts with 14-3-3 proteins to inhibit RhoGAP activity and block nucleocytoplasmic shuttling. *Journal of Cell Science*. 122:92-102.
- Schwanhausser, B., D. Busse, N. Li, G. Dittmar, J. Schuchhardt, J. Wolf, W. Chen, and M. Selbach. 2011. Global quantification of mammalian gene expression control. *Nature*. 473:337-342.
- Sheng, M., and C. Sala. 2001. PDZ domains and the organization of supramolecular complexes. *Annual Review of Neuroscience*. 24:1-29.
- Steinberg, F., M. Gallon, M. Winfield, E. Thomas, A.J. Bell, K.J. Heesom, J.M. Tavaré, and P.J. Cullen. 2013. A global analysis of SNX27-retromer assembly and cargo specificity reveals a function in glucose and metal ion transport. *Nature cell biology*. 15:461-471.
- Strand D, U.S., Corvi R, Hartenstein K, Schenkel H, Kalmes A, Merdes G, Neumann B, Krieg-Schneider F, Coy JF. 1995. A human homologue of the Drosophila tumour suppressor gene *l(2)gl* maps to 17p11.2-12 and codes for a cytoskeletal protein that associates with nonmuscle myosin II heavy chain. *Oncogene*. 11:291-301.
- Takeichi, M. 2014. Dynamic contacts: rearranging adherens junctions to drive epithelial remodelling. *Nat Rev Mol Cell Biol*. 15:397-410.
- Terry, S.J., C. Zihni, A. Elbediwy, E. Vitiello, I.V.L.C. San, M.S. Balda, and K. Matter. 2011. Spatially restricted activation of RhoA at epithelial junctions by p114RhoGEF drives junction formation and morphogenesis. *Nature cell biology*. 13:159-166.
- Tkachenko, E., M. Sabouri-Ghomi, O. Pertz, C. Kim, E. Gutierrez, M. Machacek, A. Groisman, G. Danuser, and M.H. Ginsberg. 2011. Protein Kinase A Governs a RhoA-RhoGDI Protrusion-Retraktion Pacemaker in Migrating Cells. *Nature cell biology*. 13:660-667.
- Toret, C.P., C. Collins, and W.J. Nelson. 2014. An Elmo–Dock complex locally controls Rho GTPases and actin remodeling during cadherin-mediated adhesion. *The Journal of Cell Biology*. 207:577-587.
- Tripathi, B.K., X. Qian, P. Mertins, D. Wang, A.G. Papageorge, S.A. Carr, and D.R. Lowy. 2014a. CDK5 is a major regulator of the tumor suppressor DLC1. *The Journal of Cell Biology*. 207:627-642.
- Tripathi, V., N.C. Popescu, and D.B. Zimonjic. 2012. DLC1 Interaction with  $\alpha$ -Catenin Stabilizes Adherens Junctions and Enhances DLC1 Antioncogenic Activity. *Molecular and Cellular Biology*. 32:2145-2159.
- Tripathi, V., N.C. Popescu, and D.B. Zimonjic. 2014b. DLC1 induces expression of E-cadherin in prostate cancer cells through Rho pathway and suppresses invasion. *Oncogene*. 33:724-733.
- Ullmannova, V., and N.C. Popescu. 2006. Expression profile of the tumor suppressor genes DLC-1 and DLC-2 in solid tumors. *International Journal of Oncology*. 29:1127-1132.
- Um, K., S. Niu, J.G. Duman, J. Cheng, Y.-K. Tu, B. Schwechter, F. Liu, L. Hiles, A. Narayanan, R.T. Ash, S. Mulherkar, K. Alpadi, S.M. Smirnakis, and K.F. Tolias. 2014. Dynamic Control of Excitatory Synapse Development by a Rac1 GEF/GAP Regulatory Complex. *Developmental cell*. 29:701-715.
- Valdes, J.L., J. Tang, M.I. McDermott, J.-C. Kuo, S.P. Zimmerman, S.M. Wincovitch, C.M. Waterman, S.L. Milgram, and M.P. Playford. 2011. Sorting Nexin 27 Protein Regulates Trafficking of a p21-activated Kinase (PAK) Interacting Exchange Factor ( $\beta$ -Pix)-G Protein-coupled Receptor Kinase Interacting Protein (GIT) Complex via a PDZ Domain Interaction. *The Journal of Biological Chemistry*. 286:39403-39416.
- Vaughan, L., C.-T. Tan, A. Chapman, D. Nonaka, N.A. Mack, D. Smith, R. Booton, Adam F.L. Hurlstone, and A. Malliri. 2015. HUWE1 Ubiquitylates and Degrades

- the RAC Activator TIAM1 Promoting Cell-Cell Adhesion Disassembly, Migration, and Invasion. *Cell Reports*. 10:88-102.
- Vega, F.M., and A.J. Ridley. 2008. Rho GTPases in cancer cell biology. *FEBS Letters*. 582:2093-2101.
- Vega, F.M., M. Thomas, N. Reymond, and A.J. Ridley. 2015. The Rho GTPase RhoB regulates cadherin expression and epithelial cell-cell interaction. *Cell Communication and Signaling*. 13:1-9.
- Vigil, D., J. Cherfils, K.L. Rossman, and C.J. Der. 2010. Ras superfamily GEFs and GAPs: validated and tractable targets for cancer therapy? *Nature reviews. Cancer*. 10:842-857.
- Vitiello, E., J.G. Ferreira, H. Maiato, M.S. Balda, and K. Matter. 2014. The tumour suppressor DLC2 ensures mitotic fidelity by coordinating spindle positioning and cell-cell adhesion. *Nature Communications*. 5:5826.
- Waghmare, I., and M. Kango-Singh. 2016. Loss of Cell Adhesion Increases Tumorigenic Potential of Polarity Deficient Scribble Mutant Cells. *PLoS ONE*. 11:e0158081.
- Wang, H.-R., Y. Zhang, B. Ozdamar, A.A. Ogunjimi, E. Alexandrova, G.H. Thomsen, and J.L. Wrana. 2003. Regulation of Cell Polarity and Protrusion Formation by Targeting RhoA for Degradation. *Science*. 302:1775-1779.
- Wells, C.D., J.P. Fawcett, A. Traweger, Y. Yamanaka, M. Goudreault, K. Elder, S. Kulkarni, G. Gish, C. Virag, C. Lim, K. Colwill, A. Starostine, P. Metalnikov, and T. Pawson. 2006. A Rich1/Amot Complex Regulates the Cdc42 GTPase and Apical-Polarity Proteins in Epithelial Cells. *Cell*. 125:535-548.
- White, C.D., H.H. Erdemir, and D.B. Sacks. 2012. IQGAP1 and Its Binding Proteins Control Diverse Biological Functions. *Cellular Signalling*. 24:826-834.
- Wildenberg, G.A., M.R. Dohn, R.H. Carnahan, M.A. Davis, N.A. Lobdell, J. Settleman, and A.B. Reynolds. 2006. p120-Catenin and p190RhoGAP Regulate Cell-Cell Adhesion by Coordinating Antagonism between Rac and Rho. *Cell*. 127:1027-1039.
- Wirtz, K.W.A. 2006. Phospholipid transfer proteins in perspective. *FEBS Letters*. 580:5436-5441.
- Wong, C.-M., J.M.-F. Lee, Y.-P. Ching, D.-Y. Jin, and I.O.-I. Ng. 2003. Genetic and Epigenetic Alterations of DLC-1 Gene in Hepatocellular Carcinoma. *Cancer Research*. 63:7646-7651.
- Wong, C.-M., J.W.-P. Yam, Y.-P. Ching, T.-O. Yau, T.H.-Y. Leung, D.-Y. Jin, and I.O.-L. Ng. 2005. Rho GTPase-Activating Protein Deleted in Liver Cancer Suppresses Cell Proliferation and Invasion in Hepatocellular Carcinoma. *Cancer Research*. 65:8861-8868.
- Wong, C.C.-L., C.-M. Wong, F.C.-F. Ko, L.-K. Chan, Y.-P. Ching, J.W.-P. Yam, and I.O.-I. Ng. 2008. Deleted in Liver Cancer 1 (DLC1) Negatively Regulates Rho/ROCK/MLC Pathway in Hepatocellular Carcinoma. *PLoS ONE*. 3:e2779.
- Xu, K., A. Sacharidou, S. Fu, D.C. Chong, B. Skaug, Z.J. Chen, G.E. Davis, and O. Cleaver. 2011. Blood vessel tubulogenesis requires Rasip1 regulation of GTPase signaling. *Developmental cell*. 20:526-539.
- Xue, W., A. Krasnitz, R. Lucito, R. Sordella, L. VanAelst, C. Cordon-Cardo, S. Singer, F. Kuehnel, M. Wigler, S. Powers, L. Zender, and S.W. Lowe. 2008. DLC1 is a chromosome 8p tumor suppressor whose loss promotes hepatocellular carcinoma. *Genes & Development*. 22:1439-1444.
- Yam, J.W.P., F.C.F. Ko, C.-Y. Chan, D.-Y. Jin, and I.O.-L. Ng. 2006. Interaction of Deleted in Liver Cancer 1 with Tensin2 in Caveolae and Implications in Tumor Suppression. *Cancer Research*. 66:8367-8372.
- Yamada, S., and W.J. Nelson. 2007. Localized zones of Rho and Rac activities drive initiation and expansion of epithelial cell-cell adhesion. *The Journal of Cell Biology*. 178:517-527.

- Yang, X.-Y., M. Guan, D. Vigil, C.J. Der, D.R. Lowy, and N.C. Popescu. 2009. p120Ras-GAP binds the DLC1 Rho-GAP tumor suppressor protein and inhibits its RhoA GTPase and growth suppressing activities. *Oncogene*. 28:1401-1409.
- Yau, T.O., T.H.Y. Leung, S. Lam, O.F. Cheung, E.K.K. Tung, P.L. Khong, A. Lam, S. Chung, and I.O.L. Ng. 2009. Deleted in Liver Cancer 2 (DLC2) Was Dispensable for Development and Its Deficiency Did Not Aggravate Hepatocarcinogenesis. *PLoS ONE*. 4:e6566.
- Yoshihara, K., J. Ikenouchi, Y. Izumi, M. Akashi, S. Tsukita, and M. Furuse. 2011. Phosphorylation state regulates the localization of Scribble at adherens junctions and its association with E-cadherin–catenin complexes. *Experimental Cell Research*. 317:413-422.
- Yu, W., A.M. Shewan, P. Brakeman, D.J. Eastburn, A. Datta, D.M. Bryant, Q.-W. Fan, W.A. Weiss, M.M.P. Zegers, and K.E. Mostov. 2008. Involvement of RhoA, ROCK I and myosin II in inverted orientation of epithelial polarity. *EMBO Reports*. 9:923-929.
- Yuan, B.-Z., A.M. Jefferson, L. Millicchia, N.C. Popescu, and S.H. Reynolds. 2007. Morphological changes and nuclear translocation of DLC1 tumor suppressor protein precede apoptosis in human non-small cell lung carcinoma cells. *Experimental Cell Research*. 313:3868-3880.
- Yuan, B.-Z., M.J. Miller, C.L. Keck, D.B. Zimonjic, S.S. Thorgeirsson, and N.C. Popescu. 1998. Cloning, Characterization, and Chromosomal Localization of a Gene Frequently Deleted in Human Liver Cancer (DLC-1) Homologous to Rat RhoGAP. *Cancer Research*. 58:2196-2199.
- Yuan, B.-Z., X. Zhou, M.E. Durkin, D.B. Zimonjic, K. Gumundsdottir, J.E. Eyfjord, S.S. Thorgeirsson, and N.C. Popescu. 2003. DLC-1 gene inhibits human breast cancer cell growth and in vivo tumorigenicity. *Oncogene*. 22:445-450.
- Zaidel-Bar, R., M. Cohen, L. Addadi, and B. Geiger. 2004. Hierarchical assembly of cell–matrix adhesion complexes. *Biochemical Society Transactions*. 32:416-420.
- Zarbalis, K., S.R. May, Y. Shen, M. Ekker, J.L.R. Rubenstein, and A.S. Peterson. 2004. A Focused and Efficient Genetic Screening Strategy in the Mouse: Identification of Mutations That Disrupt Cortical Development. *PLoS Biology*. 2:e219.
- Zeitler, J., C.P. Hsu, H. Dionne, and D. Bilder. 2004. Domains controlling cell polarity and proliferation in the Drosophila tumor suppressor Scribble. *The Journal of Cell Biology*. 167:1137-1146.
- Zhan, L., A. Rosenberg, K.C. Bergami, M. Yu, Z. Xuan, A.B. Jaffe, C. Allred, and S.K. Muthuswamy. 2008. Deregulation of Scribble promotes mammary tumorigenesis and reveals a role for cell polarity in carcinoma. *Cell*. 135:865-878.
- Zhong, D., J. Zhang, S. Yang, U.J.K. Soh, J.P. Buschdorf, Y.T. Zhou, D. Yang, and B.C. Low. 2009. The SAM domain of the RhoGAP DLC1 binds EF1A1 to regulate cell migration. *Journal of Cell Science*. 122:414-424.
- Zihni, C., M.S. Balda, and K. Matter. 2014. Signalling at tight junctions during epithelial differentiation and microbial pathogenesis. *Journal of Cell Science*. 127:3401-3413.
- Zumbrunn, J., K. Kinoshita, A.A. Hyman, and I.S. Näthke. 2001. Binding of the adenomatous polyposis coli protein to microtubules increases microtubule stability and is regulated by GSK3 beta phosphorylation. *Current Biology*. 11:44-49.

## Publications

### This work was published in part in the following publication:

Hendrick, J., M. Franz-Wachtel, Y. Moeller, S. Schmid, B. Macek, and M.A. Olayioye. 2016. The polarity protein Scribble positions DLC3 at adherens junctions to regulate Rho signaling. *Journal of Cell Science*. DOI:10.1242/jcs.190074

Hendrick, J., and M.A. Olayioye. (in preparation)  
invited commentary article for publication in *Small GTPases*.

### Other publications:

Moeller, Y., M. Morkel, J. Schmid, S. Beyes, J. Hendrick, M. Strotbek, P. Riemer, S. Schmid, L.C. Schmitt, R. Kontermann, T. Mürdter, M. Schwab, C. Sers, and M.A. Olayioye. 2016. Oncogenic Ras triggers hyperproliferation and impairs polarized colonic morphogenesis by autocrine ErbB3 signaling. *Oncotarget*. 7(33):53526-53539.

Noll, B., J. Hendrick, and M.A. Olayioye. 2016. Rho-Signalgebung in der Tumorentstehung und -progression. *BIOspektrum*. 22:369-372.

Braun, A.C., J. Hendrick, S.A. Eisler, S. Schmid, A. Hausser, and M.A. Olayioye. 2015. The Rho-specific GAP protein DLC3 coordinates endocytic membrane trafficking. *Journal of Cell Science*. 128:1386-1399.

### Posters and conference participations:

2015      Hendrick, J., Y. Moeller, A.C. Braun, S. Schmid, M. Franz-Wachtel, B. Macek and M.A. Olayioye. The RhoGAP protein DLC3 interacts with the basolateral Scribble complex and regulates epithelial cell polarity.

- Poster at the Beatson International Cancer Conference “Control of Cell Polarity and Movement in Cancer” in Glasgow, UK

Hendrick, J. A DLC3 protein interaction network regulating cell junction stability and cell polarity.

- Talk at the annual PhD workshop “Molecular Mechanisms and Therapeutic Approaches in Cancer and Inflammatory Diseases“ in Konstanz, Germany

2014

Hendrick, J. Identification and characterization of the DLC3 interactome.

- Talk at the annual PhD workshop “Molecular Mechanisms and Therapeutic Approaches in Cancer and Inflammatory Diseases“ in Freudenstadt, Germany

Braun AC, J. Hendrick, S.A. Eisler, S. Schmid, A. Hausser and M.A. Olayioye. Membrane recycling is regulated by the DLC3 tumor suppressor protein via localized RhoA signaling.

- Poster at the EMBO Workshop “Signaling to and from Endomembranes” in Konstanz, Germany

2013

Braun AC, J. Hendrick, S.A. Eisler, S. Schmid, A. Hausser and M.A. Olayioye. The Rho-specific GAP protein DLC3 coordinates endocytic membrane trafficking.

- Poster at the Invadosome Meeting “Cell Migration and Invasion in Physiology and Pathology” in Nijmegen, The Netherlands

## Acknowledgements

I would like to express my gratitude to the following people for their support and assistance during my PhD thesis.

First of all, I wish to express my deep thanks to my supervisor Professor Dr. Monilola Olayioye for the chance to work on this interesting research project, for her excellent scientific guidance and the continuous support throughout my PhD. I like to thank her for sharing her great ideas and scientific knowledge with me and for being a wonderful teacher. Her encouraging advice and our inspiring discussions were of inestimable value for the accomplishment of this thesis.

I would especially like to thank Professor Dr. Thomas Kufer for kindly taking over the second opinion of this thesis and Professor Dr. Roland Kontermann for accepting the obligation to act as chair of my doctoral defence.

I would also like to thank Professor Dr. Klaus Pfizenmaier and Professor Dr. Markus Morrison for giving me the opportunity to do this research at the IZI and for their interest and scientific advice during seminars. Moreover, I wish to thank Dr. Angelika Hausser for her helpful input, valuable ideas and the inspiring discussions during the Lab meetings.

My special thanks go to Yvonne Möller and Simone Schmid for their experimental support and to Dr. Stephan Eisler for his help at the microscope. I would also like to thank our cooperation partners Professor Dr. Boris Macek and Dr. Mirita Franz-Wachtel from the Proteome Center Tübingen who performed the mass spectrometry analysis.

I would like to thank all the people from the MoLab and the Hausser Lab I was working with during my PhD, for stimulating discussions, knowledge exchange and their help in many issues. Thank you for the excellent working environment and the great time in and outside the lab! My thanks are also expressed to all other colleagues at the IZI for the nice and supportive atmosphere.

Finally, I would especially like to thank my family and my friends who encouraged and supported me during my entire studies. Most importantly, I would like to give my biggest thanks to Patrick for his love and attendance on my way towards the PhD.

## Eidesstattliche Erklärung

Hiermit erkläre ich, Janina Hendrick, dass ich die vorliegende Arbeit selbständig angefertigt habe. Es wurden nur die in der Arbeit ausdrücklich benannten Quellen und Hilfsmittel benutzt. Wörtlich oder sinngemäß übernommenes Gedankengut habe ich als solches kenntlich gemacht.

I hereby assure that I performed this work independently without further help or other materials than stated. Passages and ideas from other sources have been clearly indicated.

---

Datum, Ort

---

Unterschrift